

**Obesity-associated systemic and intrinsic IR dysregulates B cell metabolism and function**

by

Mengyi Zhu

A thesis submitted in partial fulfillment of the requirements for the degree of

Master of Science

In

Immunology

Department of Medical Microbiology and Immunology  
University of Alberta

© Mengyi Zhu, 2024

## **Abstract**

Obesity and associated insulin resistance (IR) represent a significant global health burden. Emerging evidence suggests that obesity is accompanied by impaired adaptive immunity. B cells contribute significantly to adaptive immunity, and the dysregulation of B cell function in obese individuals has been demonstrated. Insulin is a crucial hormone governing glucose homeostasis, which is essential for cell survival, growth, activation, and function. Our laboratory previously observed that B cells can express the insulin receptor (InsR), and diet-induced obesity (DIO) impaired insulin signaling in B cells. However, the specific role of insulin signaling and IR in B cells remains unknown. Therefore, my research aims to elucidate the impact of insulin signaling and IR on the regulation of B cell activation and function during both a healthy state and diet-induced obesity.

Here, I present my findings that the activation and disruption of insulin signaling may have no effect on the activation of B cells but regulated the metabolism in B cells stimulated with LPS or CpG. Several studies have mentioned that vaccinations for overweight or obese individuals may be less effective than lean individuals. Thus, to determine whether and how obesity-associated IR regulates B cell-mediated immunity under vaccination, I utilized an OVA/CFA-induced primary immunization model. I observed that obesity-induced IR altered the antibody production by B cells and impaired the antigen-specific germinal center reaction. To further isolate the effect of IR specifically on B cells, by using a mouse model with genetic InsR ablation in B cells, I observed

that B cell-intrinsic IR dampened the antigen-specific germinal center reaction and altered antibody production by B cells during OVA/CFA-induced primary immune responses. These changes may be associated with the loss of help from CD4<sup>+</sup> T cells and T<sub>FH</sub> cells, as well as impaired metabolism in B cells.

Next, to assess the role of B cell-intrinsic IR in B cell-mediated memory responses, I employed an OVA/CFA/IFA-induced prime/boost protocol in B cell-specific InsR-deficient mice. I observed that B cell-intrinsic IR negatively regulated the re-entry of memory B cells into the germinal center and the differentiation of plasma cells from memory B cells upon re-exposure to the same antigen. Prompted by the clinical observations that obese individuals are at an increased risk of severe respiratory infections, including H1N1, I subjected mice with InsR ablation in B cells to intranasal infection with the H1N1/PR8 influenza virus. I observed that B cell-intrinsic IR impaired the B cell-mediated anti-viral immunity by impairing virus-specific germinal center reaction, altering antibody production, and weakening immune-dominant T cell responses.

Altogether, my findings highlight the significant role of insulin signaling and IR in modulating B cells functionality. Conducting further investigations to better understand the mechanisms by which insulin signaling and IR modulate B cell-mediated immunity will be important to decipher whether the insulin signaling pathway can be manipulated to bolster protective immunity in individuals with IR.

## **Preface**

This thesis is composed of original work by Mengyi Zhu. The research project, of which this thesis is a part, received research ethics approval from the University of Alberta Research Ethics Board, Project Name “The impact of obesity and insulin resistance on immune function”, No. AUP00003251, approved August 6, 2019.

## **Acknowledgements**

First and foremost, I would like to express my deepest gratitude to my supervisor, Dr. Sue Tsai, for her invaluable guidance, unwavering support, and constant encouragement throughout my Master's degree. Thank you for all the time and dedication you have put into helping me throughout the past four years. Your extensive knowledge, insightful feedback, and patient mentorship have been instrumental in shaping this work. As an international student, the difficulties and challenges I have had to endure are relatively greater and have led me to hover on the brink of giving up several times. I am sure that without your help, I would not have been able to persevere until now and face all the challenges and setbacks. Words cannot fully express my gratitude to you, thank you for providing me with the opportunity to study in this lab and for never considering giving up on me no matter what challenges arose. This project would not have been possible without your dedication. Thank you for believing in me and for being an inspiring mentor.

I would like to thank my committee members Dr. Hanne Ostergaard and Dr. Catherine Field for their valuable input and constructive feedback. Thank you to my defense committee members Dr. Hanne Ostergaard, Dr. Catherine Field, and Dr. Robert Ingham.

I am also grateful for all my friends and colleagues in the Tsai-Clemente lab. To Dr. Masoud Akbari, I am deeply grateful to you for your technical and emotional support throughout these four years. To Amir Reza Hematyar Naghneh, thank you for always selflessly caring for my mice when I was busy. It is you who have reminded me countless times of the importance of caring for my mental health. To Kasia Dzierlega, Megan Lee and Aklima Akter, thank you for accompanying me through those dark times, I will never forget our time crying together in the office. To Yueyi Huang, thank you for letting me feel the understanding and support from fellow countrymen. Thank you to Paulo José Basso, Erin Stranchan, Luisa Soares, Adrian Schcolnik Cabrera, Amro M. Soliman,

Blake Roberts, Derek Parker, and Kevin Chu for all help and creating an amazing environment to work in.

I would also like to thank my friends and family for being there for me throughout this experience. To my best friend Jiarui Zhang, thank you for all your love, support, and encouragement. You are always the first person I turn to when I encounter difficulties. To my parents, Yingjuan Zhu and Jiangang Li, thank you for your unconditional love and support, I would not have the courage to explore the world and pursue my dream without your support. To my partner, Bosheng Liang, thank you for your love and unwavering care, which allows me to focus on my research without worrying about anything. Finally, I would like to express gratitude to a non-human member. To my cat Yituo Zhu, thank you for listening to my complaints about everything so patiently and keeping me company during those sleepless nights.

## Table of Contents

<b>Abstract</b> .....	<b>ii</b>
<b>Preface</b> .....	<b>iv</b>
<b>Acknowledgements</b> .....	<b>v</b>
<b>List of tables</b> .....	<b>xi</b>
<b>List of figures</b> .....	<b>xii</b>
<b>List of abbreviation</b> .....	<b>xv</b>
<b>Chapter 1: Introduction</b> .....	<b>1</b>
<b>1.1 Obesity and insulin resistance</b> .....	<b>1</b>
1.1.1 <i>Obesity</i> .....	1
1.1.2 <i>Obesity induces adipocyte hypertrophy in white adipose tissue</i> .....	2
1.1.3 <i>Immune cell composition of VAT in homeostasis and obesity</i> .....	3
1.1.4 <i>Insulin signaling</i> .....	10
1.1.5 <i>Development of obesity-associated insulin resistance</i> .....	15
<b>1.2 B cell differentiation and function</b> .....	<b>20</b>
1.2.1 <i>Development and differentiation of B cells</i> .....	20
1.2.2 <i>Development of B cell-mediated memory responses</i> .....	25
1.2.3 <i>Function of B cells</i> .....	28
<b>1.3 Metabolic signaling in B cells</b> .....	<b>30</b>
1.3.1 <i>Dynamic changes in metabolic activity during B cell differentiation and activation</i> .....	33
1.3.2 <i>Insulin signaling and B cell metabolism</i> .....	36
<b>1.4 Hypotheses and objectives of study</b> .....	<b>37</b>
<b>Chapter 2: Methods and Materials</b> .....	<b>39</b>
<b>2.1 Mice</b> .....	<b>39</b>
<b>2.2 Diet-induced obesity (DIO) model</b> .....	<b>39</b>
<b>2.3 Intraperitoneal glucose tolerance test (IPGTT) and insulin tolerance test (ITT)</b> .....	<b>40</b>

<b>2.4</b>	<b>OVA/CFA immunization</b> .....	<b>40</b>
<b>2.5</b>	<b>OVA/CFA/IFA recall model</b> .....	<b>41</b>
<b>2.6</b>	<b>Influenza virus infection</b> .....	<b>41</b>
<b>2.7</b>	<b>Serum and BAL collection</b> .....	<b>42</b>
<b>2.8</b>	<b>Tissue isolation and Digestion</b> .....	<b>42</b>
<b>2.9</b>	<b>Flow cytometry</b> .....	<b>43</b>
<b>2.10</b>	<b>B cell isolation</b> .....	<b>44</b>
<b>2.11</b>	<b>Phospho-flow cytometry assay</b> .....	<b>44</b>
<b>2.12</b>	<b>OVA/influenza- specific Ig ELISA assay</b> .....	<b>44</b>
<b>2.13</b>	<b>Seahorse metabolic flux assay</b> .....	<b>45</b>
<b>2.14</b>	<b>Statistical analysis</b> .....	<b>48</b>
<b>2.15</b>	<b>Table of reagents and software</b> .....	<b>48</b>
<b>Chapter 3: The impact of insulin signaling and IR on B cell activation and metabolism.</b>		<b>53</b>
<b>3.1</b>	<b>Introduction</b> .....	<b>53</b>
<b>3.2</b>	<b>Results</b> .....	<b>53</b>
3.2.1	<i>DIO induced IR in B cells</i> .....	53
3.2.2	<i>Insulin stimulation and B cell-intrinsic IR did not affect LPS- and CpG-stimulated B cell activation in vitro</i> .....	58
3.2.3	<i>Insulin stimulation regulated glycolytic and oxidative metabolism in LPS- and CpG-stimulated B cells</i> .....	64
3.2.4	<i>DIO-induced IR regulated glycolytic and oxidative metabolism in LPS- and CpG-stimulated B cells</i> .....	71
3.2.5	<i>B cell-intrinsic IR regulated glycolytic and oxidative metabolism in LPS- and CpG-stimulated B cells</i> .....	77
<b>3.3</b>	<b>Discussion</b> .....	<b>83</b>

<b>Chapter 4: The role of IR on B cell-mediated adaptive immunity elicited by vaccination and influenza virus infection .....</b>	<b>87</b>
<b>4.1 Introduction .....</b>	<b>87</b>
<b>4.2 Results .....</b>	<b>88</b>
4.2.1 <i>DIO induced IR impaired OVA/CFA-induced GC reaction during OVA/CFA-induced primary immune responses.....</i>	88
4.2.2 <i>B cell-intrinsic IR altered the B cell antibody production and GC reaction during OVA/CFA-induced primary immune response.....</i>	92
4.2.3 <i>The negative impact of B cell-intrinsic IR on GC reaction may result from the deficiency in help from CD4<sup>+</sup> T cells and T<sub>FH</sub> cells .....</i>	97
4.2.4 <i>B cell-intrinsic IR regulated glycolytic and oxidative metabolism in B cells during OVA/CFA-induced primary immune response.....</i>	100
4.2.5 <i>B cell-intrinsic IR impaired B cell-mediated memory responses to OVA/IFA secondary immunization .....</i>	103
4.2.6 <i>B cell-intrinsic IR impaired B cell-mediated anti-viral immunity by altering antibody production and impairing the GC reaction.....</i>	107
4.2.7 <i>The impairment in GC reaction upon H1N1/PR8 influenza infection may result from the loss of help from CD4<sup>+</sup> T cells and T<sub>FH</sub> cells .....</i>	113
4.2.8 <i>B cell-intrinsic IR impaired immune dominant T cell responses upon H1N1/PR8 influenza virus infection.....</i>	118
<b>4.3 Discussion.....</b>	<b>126</b>
<b>4.4 Contributions.....</b>	<b>130</b>
<b>Chapter 5: Discussion.....</b>	<b>131</b>
<b>5.1 Conclusion.....</b>	<b>131</b>
5.1.1 <i>The impact of insulin signaling and IR on B cell activation and metabolism.....</i>	131
5.1.2 <i>The role of IR on B cell-mediated adaptive immunity elicited by vaccine and infection.....</i>	133

**5.2 Significance .....135**  
**Reference.....136**

**List of tables**

Table 2.1 List of antibodies used for flow cytometry .....48

Table 2.2 List of reagents .....51

Table 2.3 List of commercial assays and kits used. ....52

Table 2.4 List of software used for data analysis.....52

## List of figures

Figure 1.1 Comparison of immune cell composition in lean and obese adipose tissue .....	9
Figure 1.2 Schematic of insulin signaling .....	13
Figure 1.3 Schematic of the mechanisms underlying obesity-associated IR .....	18
Figure 1.4 Illustration of the development and differentiation process of B cells .....	23
Figure 1.5 Illustration of B cell-mediated memory responses .....	26
Figure 1.6 Illustration of metabolic pathways supporting B cell activation and function .....	31
Figure 1.7 Illustration of changes in metabolic activity during different B cell activation and differentiation stages .....	35
Figure 2.1 Schematic diagram of the principle of the Seahorse metabolic flux assay .....	47
Figure 3.1 Insulin induced the activation of insulin signaling in B cells .....	55
Figure 3.2 HFD-feeding induced IR. ....	56
Figure 3.3 DIO induced IR in B cells.....	57
Figure 3.4 Insulin stimulation did not impact LPS- and CpG-stimulated B cell activation <i>in vitro</i> .....	61
Figure 3.5 B cell-intrinsic IR did not impact LPS-stimulated B cell activation <i>in vitro</i> .....	62
Figure 3.6 B cell-intrinsic IR did not impact CpG-stimulated B cell activation <i>in vitro</i> .....	63
Figure 3.7 Insulin stimulation regulated glycolytic and oxidative metabolism in LPS-stimulated B cells.....	68
Figure 3.8 Insulin stimulation regulated glycolytic and oxidative metabolism in CpG-stimulated B cells.....	70
Figure 3.9 DIO-induced IR regulated glycolytic and oxidative metabolism in LPS-stimulated B cells.....	73
Figure 3.10 DIO-induced IR regulated glycolytic and oxidative metabolism in CpG-stimulated B cells.....	76

Figure 3.11 B cell-intrinsic IR regulated glycolytic and oxidative metabolism in LPS-stimulated B cells..... 79

Figure 3.12 B cell-intrinsic IR regulated glycolytic and oxidative metabolism in CpG-stimulated B cells..... 81

Figure 4.1 DIO-induced IR altered antibody production by B cells during OVA/CFA-induced primary immune response ..... 89

Figure 4.2 DIO-induced IR impaired OVA/CFA-induced GC reaction during primary immune response ..... 90

Figure 4.3 B cell-intrinsic IR altered antibody production by B cells during OVA/CFA-induced primary immune response ..... 94

Figure 4.4 B cell-intrinsic IR impaired OVA/CFA-induced primary GC reaction..... 95

Figure 4.5 The negative impact of B cell-intrinsic IR on OVA/CFA-induced primary GC reaction may result from the deficiency in help from CD4<sup>+</sup> T cells and T<sub>FH</sub> cells ..... 98

Figure 4.6 B cell-intrinsic IR regulated B cell glycolytic and oxidative metabolism during OVA/CFA-induced primary immune response..... 102

Figure 4.7 B cell-intrinsic IR altered antibody production by B cells during the OVA/IFA secondary challenge ..... 104

Figure 4.8 B cell-intrinsic IR impaired B cell-mediated memory responses during the OVA/IFA secondary challenge ..... 106

Figure 4.9 B cell-intrinsic IR increased H1N1/PR8 influenza virus-induced disease severity.... 109

Figure 4.10 B cell-intrinsic IR altered antibody production by B cells upon H1N1/PR8 influenza virus infection..... 111

Figure 4.11 B cell-intrinsic IR impaired GC reaction upon H1N1/PR8 influenza virus infection ..... 112

Figure 4.12 B cell-specific InsR-deficient mice showed reduced influenza-specific CD4<sup>+</sup> T cells upon influenza virus infection..... 114

Figure 4.13 B cell-specific InsR-deficient mice showed reduced influenza-specific T<sub>FH</sub> cells upon influenza virus infection..... 116

Figure 4.14 B cell-specific InsR-deficient mice showed reduced influenza-specific CD8<sup>+</sup> T cells upon influenza virus infection..... 120

Figure 4.15 TNF $\alpha$ - and IFN $\gamma$ -producing CD4<sup>+</sup> T cells in H1N1/PR8 influenza-infected mice ..122

Figure 4.16 TNF $\alpha$ - and IFN $\gamma$ -producing CD8<sup>+</sup> T cells in H1N1/PR8 influenza-infected mice ..124

## List of abbreviation

<b>Abbreviation</b>	<b>Full Description</b>
2-DG	2-Deoxy-D-Glucose
$\alpha$ -KG	$\alpha$ -ketoglutarate
ACK	Ammonium-Chloride-Potassium
ADCC	Antibody dependent cellular cytotoxicity
ADP	Adenosine diphosphate
AGCs	Amino acid glutamine channels
AKT	Protein kinase B
ALN	Axillary lymph node
AMPK	Adenosine monophosphate-activated protein kinase
APC	Antigen presenting cell
AT	Adipose tissue
ATM	Adipose tissue resident macrophage
ATP	Adenosine triphosphate
Bad	B cell lymphoma-2-associated death promoter
BAFF	B cell activating factor
BAT	Brown adipose tissue
Bcl	B-cell lymphoma
BCR	B cell receptor
BM	Bone marrow
BMI	Body mass index
CD1c	Blood dendritic cell antigen 1
CD11c	Alpha integrin X

CD163	Scavenger receptor cysteine-rich type 1 protein
CD301	Macrophage galactose/N-acetyl galactosamine specific lectin
CD40L	CD40 ligand
CD66b	Carcinoembryonic antigen-related cell adhesion molecule 8
cDC	Conventional dendritic cell
CFA	Complete Freund's adjuvant
CMV	Cytomegalovirus
CoQ	Coenzyme Q
CPG	Cytidine monophosphate guanosine oligodeoxynucleotides
CPT1	Carnitine palmitoyl transferase 1
c-Raf	Raf proto-oncogene serine/threonine-protein kinase
Cyt C	Cytochrome c
D	Diversity
DC	Dendritic cell
DIO	Diet induced obesity
DZ	Dark zone
EBF1	Early B cell factor 1
ECAR	Extracellular acidification rate
eIF4E-BP1	Eukaryotic initiation factor 4E-binding protein 1
ER	Endoplasmic reticulum
Erk	Extracellular signal related kinase
F4/80	EGF -like module-containing mucin-like hormone receptor-like 1
FABP	Flavin adenine dinucleotide, reduced form
FADH <sub>2</sub>	Fatty acid-binding protein
FAO	Fatty acid oxidation

FATP	Fatty acid transport protein
FCCP	Carbonyl cyanide-4 (trifluoromethoxy) phenylhydrazone
FDC	Follicular dendritic cell
FFA	Free fatty acid
FO	Follicular
FoxO	Forkhead box O
GC	Germinal center
GCs	Glutamine channels
GDH	Glutamate dehydrogenase
GM-CSF	Granulocyte macrophage colony-stimulating factor
Grb2	Growth factor receptor-bound protein 2
Gsk-3	Glycogen synthase kinase 3
HFD	High fat diet
HIV	Human Immunodeficiency Virus
HSC	Hematopoietic stem cell
ICOS	Inducible T cell co-stimulator
IFA	Incomplete Freund's adjuvant
IFN- $\gamma$	Interferon gamma
IGFR	Insulin-like growth factor receptor
IgH	Immunoglobulin heavy chain
IKK	Inhibitor of nuclear factor- $\kappa$ B kinase- $\beta$
IL-1Ra	Interleukin 1 receptor antagonist
InsR	Insulin receptor
IPGTT	Intraperitoneal glucose tolerance test
IR	Insulin resistance

IRF3	Interferon regulatory factor
IRS	Insulin receptor substrate
ITT	Insulin tolerance test
J	Joining
JAK	Janus kinase
JNK	c-Jun N-terminal kinase
KO	Knockout
LPS	Lipopolysaccharides
LZ	Light zone
MAPK	Mitogen-activated protein kinase
MBC	Memory B cell
MFI	Mean fluorescence intensity
MHC	Major histocompatibility complex
mLN	Mediastinal lymph node
MPC	Mitochondrial pyruvate carrier
MPO	Myeloperoxidase
MST1	Mammalian sterile 20-like kinase 1
MTORC	Mammalian target of rapamycin complex
MyD88	Myeloid differentiation primary response 88
MZ	Marginal zone
NADH	Nicotinamide adenine dinucleotide, reduced form
NCD	Normal chow diet
NF- $\kappa$ B	Nuclear factor- $\kappa$ B
NK	Natural killer

OCR	Oxygen consumption rate
OVA	Ovalbumin
OXPHOS	Oxidative phosphorylation
Pax5	Paired Box 5
PBMC	Peripheral blood mononuclear cell
PDK1	3-Phosphoinositide dependent protein kinase 1
PI3K	Phosphoinositide-3-kinase
PIP2	Phosphatidylinositol 4,5-bisphosphate
PIP3	Phosphatidylinositol 3,4,5-triphosphate
PKC	Protein kinase C
PMA	Phorbol myristate acetate
PPAR- $\gamma$	Peroxisome proliferator-activated receptor gamma
PR8	H1N1/Puerto Rico/8/34
PRR	Pattern recognition receptor
PH	Pleckstrin homology
RAG-1	Recombination activating gene 1
Ras	Rat sarcoma
Rbp-4	Retinol binding protein 4
ROS	Reactive oxygen species
RTK	Receptor tyrosine kinase
S6K	Ribosomal S6 kinase
S6RP	S6 ribosomal protein
SAT	Subcutaneous adipose tissue
Ser	Serine
SLC1A5	L-type amino acid transporter

SLC38A2	Sodium-coupled neutral amino acid transporter 2
SOCS	Suppressor of cytokine signaling
STAT	Signal transducer and activator of transcription
T2D	Type 2 diabetes
TCA	Tricarboxylic acid
T <sub>FH</sub>	T follicular helper
TGF- $\beta$	Transforming growth factor beta
Th	T helper
TLR	Toll like receptor
TNF $\alpha$	Tumor necrosis factor alpha
Treg	Regulatory T
TRIF	TIR-domain-containing adapter-inducing Interferon- $\beta$
UCP1	Uncoupling protein 1
ULK1	Unc-51 like autophagy activating kinase 1
V	Variable
VAT	Visceral adipose tissue
WAT	White adipose tissue
WB	Western blotting
WHO	World health organization
WT	Wildtype

## **Chapter 1: Introduction**

### **1.1 Obesity and insulin resistance**

Current evidence suggests that obesity is associated with a range of comorbidities, including diabetes<sup>1, 2</sup>, respiratory infections<sup>3, 4</sup>, cardiovascular diseases<sup>5-8</sup>, obstructive sleep apnea<sup>9-11</sup>, stroke<sup>12-15</sup>, and cancers<sup>16</sup>. All these obesity-associated comorbidities increase the risk of mortality in individuals. However, the mechanisms by which obesity promotes the onset and progression of these comorbidities remain unclear. Obesity is considered as a major risk factor for developing IR<sup>17-20</sup>. Within the context of obesity, adipose tissue (AT) releases elevated levels of non-esterified fatty acids, glycerol, hormones, adipokines, and pro-inflammatory cytokines, all of which contribute to IR<sup>17</sup>. Thus, a deeper comprehension of the relationship between obesity and IR provides new insights into investigating precise mechanisms and developing novel therapeutic strategies for obesity-associated life-threatening comorbidities.

#### **1.1.1 Obesity**

Obesity has emerged as a significant global health epidemic in the 21<sup>st</sup> century<sup>21</sup>. It is typically quantified by a body mass index (BMI) of  $\geq 30$  kg/m<sup>2</sup>, which is calculated by dividing the body weight of an individual in kilograms by the height in meters squared<sup>22</sup>. According to the World Health Organization (WHO), the global prevalence of obesity has nearly doubled since 1990<sup>23</sup>. Around 890 million adults and 160 million children and adolescents were classified as obese in 2022<sup>23</sup>. Obesity has been reported as a major risk factor for many life-threatening diseases<sup>3-16</sup>. Hence, investigating the role of obesity in the onset and progression of these diseases is of crucial scientific importance. However, the etiology of obesity is complex and multifaceted, encompassing a combination of genetic, environmental, behavioral, and socioeconomic factors<sup>24, 25</sup>. Therefore, the interdisciplinary and multifaceted nature of obesity suggests that research related to obesity-associated diseases can be hindered by various impediments. For example, behavioral factors such

as diet and physical activity are influenced by socioeconomic status, cultural norms, and access to resources, making it difficult to standardize interventions across different populations<sup>24, 25</sup>. Additionally, clinical trials of obesity-associated diseases can be hindered by high costs, long timelines, and rigorous safety and efficacy testing requirements<sup>24, 25</sup>. In terms of immunology, obesity can be characterized by a low-grade chronic inflammation condition in the AT, which results from an abnormal or excessive accumulation of fat<sup>26, 27</sup>. Meanwhile, it induces adipocyte hypertrophy, disrupts metabolic homeostasis, and alters immune cell composition, leading to a phenotypic shift towards a pro-inflammatory state<sup>28-31</sup>. Given the escalating prevalence and significant impact of obesity on public health, elucidating the mechanisms underlying obesity-induced metabolic dysregulation and immune system dysfunction is imperative for the development of effective therapeutic strategies.

### ***1.1.2 Obesity induces adipocyte hypertrophy in white adipose tissue***

AT, also known as fatty tissue, is a connective tissue that is mainly composed of lipid-filled cells called adipocytes, surrounded by collagen fibers, fibroblasts, blood vascular components, and immune cells<sup>32</sup>. It is traditionally viewed as a critical regulator of systemic energy homeostasis by acting as a caloric reservoir<sup>33</sup>. More recently, AT has emerged to be recognized as a dynamic and multifunctional organ with implications for metabolic, endocrine, and immune homeostasis. Anatomically, AT is broadly classified into two main types with different functions: white adipose tissue (WAT) and brown adipose tissue (BAT)<sup>34, 35</sup>. BAT is predominantly located in discrete depots, including the interscapular, cervical, and axillary regions in humans. It specializes in energy dissipation through non-shivering thermogenesis, which is mediated by uncoupling protein 1 (UCP1)<sup>36-38</sup>. An increasing number of studies have found that lean individuals typically have a greater relative amount of BAT compared with individuals with higher BMI<sup>39, 40</sup>. Moreover, activating BAT and the browning of WAT can protect against obesity and obesity-related metabolic diseases<sup>41-43</sup>. Conversely, under conditions of energy surplus, WAT can expand through the enlargement of existing adipocytes, become dysfunctional and develop a low-grade

inflammatory state<sup>44</sup>. WAT is distributed throughout the whole body in depots such as the subcutaneous, visceral, and muscle, and serves as the primary site for excess energy storage in the form of triglycerides<sup>45</sup>. WAT is increasingly recognized as a dynamic endocrine organ that plays a crucial role in regulating systemic metabolism<sup>45</sup>. It is enriched with adipokines, which are bioactive molecules secreted by adipocytes, and play a critical role in regulating various processes, including energy and appetite regulation, lipid and glucose metabolism, endothelial cell function, inflammation, angiogenesis, blood pressure, and insulin sensitivity<sup>46</sup>.

WAT can be further categorized into subcutaneous adipose tissue (SAT) and visceral adipose tissue (VAT)<sup>47</sup>. SAT is located beneath the skin, primarily in the abdominal, gluteal, and femoral regions of the body. SAT represents the largest depot of AT in humans, and plays a crucial role in energy homeostasis, thermal insulation, and mechanical cushioning<sup>48</sup>. Unlike SAT, which is situated beneath the skin, VAT is located deep within the abdominal cavity, surrounding internal organs such as the liver, pancreas, and intestines<sup>48</sup>. VAT plays a pivotal role in metabolic regulation<sup>48-50</sup>. It acts as a dynamic reservoir of energy and actively secretes adipokines, cytokines, and other bioactive molecules that influence systemic metabolism, inflammation, and insulin sensitivity<sup>48-50</sup>. Additionally, VAT interacts extensively with the immune system, impacting immune responses<sup>51</sup>.

### ***1.1.3 Immune cell composition of VAT in homeostasis and obesity***

In obese individuals, VAT undergoes changes in cellular composition and immune cell infiltration, leading to a state of chronic low-grade inflammation<sup>51</sup>. This inflammatory milieu is characterized by the accumulation and activation of various immune cell populations within the VAT microenvironment, including macrophages, dendritic cells (DCs), natural killer (NK) cells, mast cells, neutrophils, eosinophils, T cells, and B cells (**Figure 1.1**).

Under homeostatic conditions, innate immune cells within the VAT typically exhibit an anti-inflammatory phenotype, which shifts towards a pro-inflammatory state in obese conditions<sup>52</sup>.

Macrophages represent the largest subpopulation of immune cells in AT, comprising approximately 40%-50% of the total cell population<sup>53</sup>. The number of AT-resident macrophages (ATMs) has been reported to increase significantly in obese rodents and humans<sup>53, 54</sup>, indicating that obesity is accompanied by the infiltration of macrophages into AT. Moreover, obesity also alters the polarization and function of ATMs. Macrophages can be generally divided into two subpopulation types based on the expression of different antigens and cytokines. In lean individuals, ATMs predominantly exhibit an anti-inflammatory M2 phenotype (F4/80<sup>+</sup>CD206<sup>+</sup>CD163<sup>+</sup>), secreting anti-inflammatory IL-10 and TGF- $\beta$ <sup>55</sup>. Conversely, obesity leads to an increase in the expression of pro-inflammatory adipokines and cytokines, resulting in a shift from the anti-inflammatory M2 phenotype to the pro-inflammatory M1 phenotype (F4/80<sup>+</sup>CD80<sup>+</sup>CD11c<sup>+</sup>)<sup>56</sup>. Several studies have demonstrated a positive correlation between the abundance of M1 phenotype ATMs and IR<sup>57-59</sup>. Additionally, the ablation of these cells mitigated IR and reduced the local and systemic production of pro-inflammatory factors<sup>58</sup>.

Although macrophages are capable of presenting antigens to effector lymphoid cells, DCs are considered as the primary antigen-presenting cells (APCs) that bridge innate to adaptive immunity<sup>60</sup>. In addition, DCs also produce an array of cytokines involved in the maturation and activation of adaptive immune cells, including IL-2 and IL-15<sup>61</sup>. Recent studies have shown that the expression of DC antigens CD1c, CD11c, and CD83 was elevated in the SAT of high fat diet (HFD)-induced obese murine models and obese humans<sup>62</sup>. Moreover, DCs from obese individuals were reported to induce the differentiation of T helper 17 (Th17) cells *in vitro*<sup>62</sup>. However, the number of conventional type 1 dendritic cells (cDC1s), which are important for the differentiation of regulatory T (Treg) cells, showed a significant decrease in obese individuals<sup>62</sup>. The resulting imbalance between anti-inflammatory Treg cells and pro-inflammatory Th17 cells leads to the polarization of ATMs towards the M1 phenotype and promotes a pro-inflammatory condition in obese individuals.

Mast cells, neutrophils, and eosinophils all contain granules in their cytoplasm<sup>63</sup>. Mast cells are abundant in barriers such as skin and mucosa, secrete a broad spectrum of inflammatory mediators, and function as first-line responders to invading pathogens<sup>64</sup>. The number of mast cells has been reported to be significantly elevated in the AT of obese mice and humans, together with the secretion of pro-inflammatory cytokines such as TNF- $\alpha$ , IL-1 $\beta$ , and IFN- $\gamma$ <sup>65</sup>. In addition, mast cells have been shown to negatively regulate insulin sensitivity under DIO conditions by releasing inflammatory mediators such as TNF- $\alpha$ , IL-6, and IL-1 $\beta$ , which contribute to chronic inflammation and metabolic dysfunction<sup>65, 66</sup>. Neutrophils are considered as the primary effectors of acute inflammatory reactions<sup>67</sup>. In obese individuals, neutrophils are among the earliest immune cells recruited into AT<sup>68</sup>. A 20-fold increase in AT neutrophils was observed as early as three days after the initiation of a HFD<sup>68</sup>. Moreover, in obese individuals, the plasma concentration of major neutrophil activating component myeloperoxidase (MPO) and the expression level of the neutrophil activation marker CD66b were increased compared with lean controls, suggesting that obesity also enhanced the activation of neutrophils<sup>69</sup>. Additionally, one study has reported that neutrophils mediated IR in mice fed a HFD by secreting elastase<sup>70</sup>. Eosinophils are key mediators of Th2 immunity and produce a vast array of anti-inflammatory cytokines, including IL-4, IL-10, IL-13, and TGF- $\beta$ <sup>71</sup>. In obese individuals, the number of AT-resident eosinophils was decreased<sup>72</sup>. Emerging studies have reported that AT-resident eosinophils are the major producers of IL-4 and IL-13, which are considered as central drivers of M2 macrophage differentiation in AT and are positively correlated with insulin sensitivity<sup>73</sup>. Therefore, the decrease in AT-resident eosinophils in obese individuals could contribute to IR.

NK cells are a subset of innate lymphocytes that differ from classical T and B lymphocytes and play an important role in early host protection<sup>74</sup>. NK cells rapidly respond to infected or transformed cells by producing lytic molecules such as perforin and Granzyme B, as well as cytokines including IFN- $\gamma$ , TNF- $\alpha$ , IL-6 and GM-CSF<sup>74</sup>. Recently, several studies have highlighted an important role of NK cells in AT homeostasis and the initiation of IR. Wensveen *et al.* demonstrated that NK cells rapidly produced IFN- $\gamma$  and promoted the recruitment of ATMs into

AT in HFD-fed animals<sup>75</sup>. These infiltrating macrophages produced increased levels of the pro-inflammatory cytokine IL-1 $\beta$ , which subsequently activated the c-Jun N-terminal kinase (JNK) and inhibitor of nuclear factor- $\kappa$ B kinase- $\beta$  (IKK) pathways<sup>75</sup>. The activation of both pathways induced the expression of pro-inflammatory cytokines and has been extensively implicated in IR and the pathogenesis of Type 2 diabetes (T2D)<sup>75</sup>. Subsequent studies conducted by Lee *et al.* provided further evidence of the pathogenic role of NK cells in IR<sup>76</sup>. Their results demonstrated that feeding a HFD increased NK cell numbers and their production of pro-inflammatory cytokines, which led to decreased insulin sensitivity<sup>76</sup>. The effects could be reversed in *E4bp4*<sup>-/-</sup> mice by genetically depleting NK cells<sup>76</sup>.

In terms of the adaptive immune system, *RAG-I*-deficient DIO mice, which lack mature B and T cells, have been reported to develop IR, suggesting that adaptive immune cells are not required for the initiation of obesity-associated IR<sup>77</sup>. However, other studies have shown that when present, adaptive immune cells play an important role in regulating IR during the development of obesity. T cells play a major role in adaptive immunity by shifting from naïve to several effector states. In AT, T cells constitute the second largest immune cell population, and HFD-induced obesity triggers the accumulation of T cells in AT compared with lean mice<sup>78</sup>. Moreover, treatment with anti-CD3 T cell-depleting antibody has been reported to reverse IR in DIO mice<sup>79</sup>. T cells can be classified into two different subtypes based on the expression of co-receptors CD4 or CD8. CD4<sup>+</sup> T cells recognize antigens presented by APCs and help direct other immune cells to sites of infection. CD4<sup>+</sup> T cells can be further classified into pro-inflammatory Th1 and Th17 cells, as well as anti-inflammatory Th2 and Treg cells. Recent studies have revealed that the frequency of Th1 cells was increased in DIO mice<sup>80</sup>, and the depletion of IFN- $\gamma$ , which is important for the differentiation of Th1 cells, improved obesity-induced IR<sup>80</sup>. Both findings suggest that a Th1 response supports the progression of obesity and IR. Th17 cells mainly secrete IL-17 and play a role in mediating inflammation in autoimmune diseases. The accumulation of Th17 cells has also been observed in the VAT under obese states<sup>81</sup>. Conversely, the accumulation of Th2 cells in AT protects against IR. The adoptive transfer of CD4<sup>+</sup> T cells from Th2 cell-deficient (*Stat6*<sup>-/-</sup>) mice into *RAG-I*-deficient

DIO mice did not reverse IR<sup>77</sup>. In addition, the frequency of Th2 cells in human SAT, VAT, and blood has been demonstrated to be inversely correlated with IR<sup>82</sup>. Treg cells play an important role in self-tolerance and mitigate inflammation by suppressing autoreactive T cells and inflammatory macrophages. In DIO mice, the number of Treg cells decreased dramatically<sup>83</sup>, and the induction of Treg cells with IL-2 in DIO mice improved insulin sensitivity<sup>77</sup>. Altogether, CD4<sup>+</sup> T cells tend to differentiate into pro-inflammatory subtypes in the context of obesity, contributing to chronic inflammatory conditions. CD8<sup>+</sup> T cells function to kill infected or foreign cells by releasing perforin and Granzyme B. Obesity increases the frequency of CD8<sup>+</sup> T cells in VAT and induces the secretion of IFN- $\gamma$  and Granzyme B<sup>84</sup>. Genetic and immunological depletion of CD8<sup>+</sup> T cells effectively alleviated AT inflammation and systemic IR in mice, and these effects could be reversed by the adoptive transfer of CD8<sup>+</sup> T cells<sup>85</sup>. All these data indicate that CD8<sup>+</sup> T cells contribute to the maintenance of AT inflammation and IR in obesity.

Similar to T cells, B cells play an important role in maintaining glucose homeostasis. B cells are broadly classified as B1 and B2 cells. B1 cells are considered to arise from the fetal liver during embryonic development and are primarily found in the pleural and peritoneal cavities<sup>86</sup>. B1 cells are also present in the mucosal tissues of the respiratory and gastrointestinal tracts<sup>86</sup>. B2 cells, also known as conventional B cells, are predominantly found in secondary organs such as spleens and lymph nodes, where they encounter antigens and differentiate into plasma cells or memory B cells (MBCs). Additionally, regulatory B (Breg) cells are a special subset of B2 cells that suppress immune-mediated inflammatory responses and facilitate the resolution of inflammation through the production of regulatory cytokines such as IL-10, IL-35 and TGF- $\beta$ <sup>87</sup>. At steady state, lean AT is predominantly enriched with IL-10-producing B1 cells and Breg cells<sup>88</sup>. However, obesity triggers a greater infiltration of B2 cells into VAT, particularly class-switched mature IgG<sup>+</sup> plasma cells<sup>89</sup>. These B2 cells, through IgG and cytokine production, interact with other immune cell types and accelerate the development of AT inflammation and IR<sup>90</sup>. Furthermore, B cell-knockout (KO) DIO mice showed improved insulin sensitivity and glucose tolerance compared with wildtype (WT)

DIO mice<sup>89, 90</sup>, supporting that B cells contribute significantly to the progression of obesity-associated IR.

Overall, the infiltration of pro-inflammatory immune cells combined with the reduction of anti-inflammatory immune cells in obese AT result in a shift towards a pro-inflammation state, which drives metabolic dysfunction and IR.

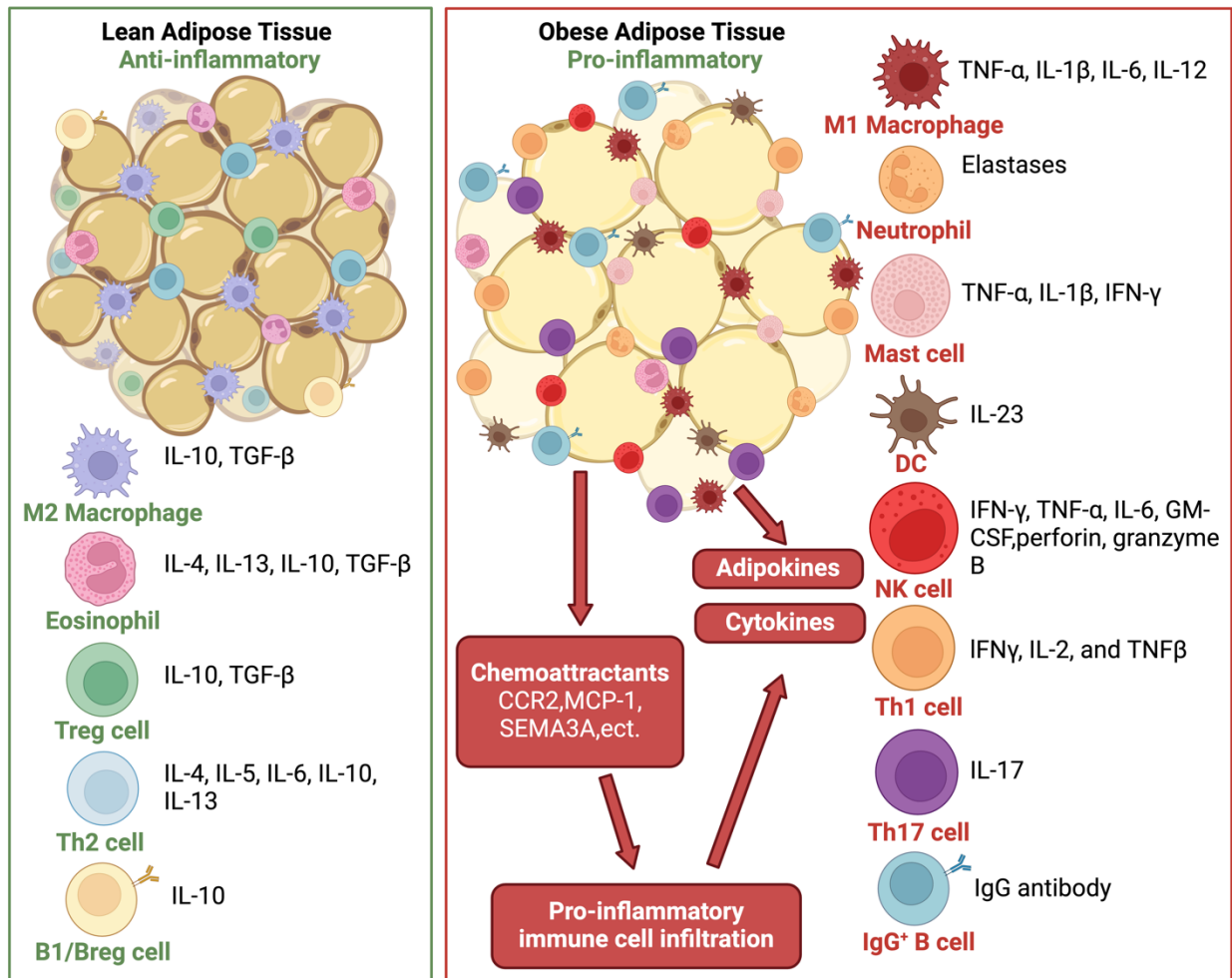


**Figure 1.1 Comparison of immune cell composition in lean and obese adipose tissue.** Lean adipose tissue is enriched with anti-inflammatory regulatory immune cells, including M2 macrophages, eosinophils, Treg cells, Th2 cells, B1 cells, and Breg cells. Conversely, obese adipose tissue contains hypertrophic adipocytes that secrete large amounts of adipokines, cytokines, and chemo-attractants, promoting the infiltration of pro-inflammatory immune cells such as M1 macrophages, neutrophils, mast cells, DCs, NK cells, Th1 cells, Th17 cells and IgG<sup>+</sup> B cells. Abbreviations are as follows: Treg: Regulatory T; Th: T helper; Breg: Regulatory B; DC: Dendritic cell; NK: Natural killer; Ig: Immunoglobulin; GM-CSF: Granulocyte macrophage colony stimulating factor; IFN- $\gamma$ : Interferon gamma; TNF- $\alpha$ : Tumor necrosis factor alpha; TGF- $\beta$ : Transforming growth factor beta. Figure drawn in BioRender.com.

#### **1.1.4 Insulin signaling**

Insulin is a hormone secreted by the  $\beta$ -cells in the pancreatic islets in response to elevated blood glucose level<sup>91</sup>. It maintains glucose homeostasis by facilitating cellular glucose uptake and regulating the metabolism of carbohydrates, lipids, and proteins, thereby modulating cell growth, proliferation, and differentiation<sup>91</sup>. IR reflects a state where cells fail to respond effectively to insulin signaling, resulting in impaired glucose metabolism and hyperinsulinemia<sup>92</sup>. Insulin exerts its effects through the InsR on target cell membranes, which leads to the phosphorylation of insulin receptor substrates (IRS) and the subsequent activation of two primary signaling pathways: the phosphoinositide-3-kinase (PI3K) / protein kinase B (AKT) pathway and the mitogen-activated protein kinase (MAPK) pathway (**Figure 1.2**)<sup>93</sup>.

The regulatory role of insulin in energy metabolism and cellular function is predominately mediated by the PI3K/AKT pathway<sup>94</sup>. Once bound to insulin, InsR, a receptor tyrosine kinase (RTK), is activated and undergoes self-phosphorylation, which can then recruit IRS and trigger their tyrosine phosphorylation<sup>93</sup>. The phosphorylated IRS then displays binding sites for numerous signaling partners, including PI3K<sup>93</sup>. After binding to IRS, PI3K is activated and then converts phosphatidylinositol 4,5-bisphosphate (PIP2) into phosphatidylinositol 3,4,5-triphosphate (PIP3) at the inner surface of the plasma membrane, which then activates 3-phosphoinositide dependent protein kinase-1 (PDK1) <sup>93</sup>. PDK1 has a pleckstrin homology (PH) domain, which has a high affinity for PIP3. The presence of PIP3 at the membrane causes PDK1 to translocate from the cytosol to the membrane and bind to PIP3. Upon binding, PDK1 undergoes a conformational change that allows it to adopt an active form<sup>93</sup>. PDK1 then activates AKT, which plays an important role in mediating several cellular functions<sup>95</sup>. The main function of insulin signaling is to regulate glucose metabolism. Activated AKT promotes glucose uptake into cells by enhancing the translocation of glucose transporters (GLUT) to the cell membrane, thereby maintaining glucose homeostasis<sup>95</sup>. Moreover, the activation of AKT induces the synthesis of glycogen by inhibiting glycogen synthase kinase 3 (GSK-3)<sup>95</sup>. Activated AKT also regulates cell survival by inhibiting

several pro-apoptotic factors, including B cell lymphoma-2-associated death (Bad) promotor, Forkhead box O (FoxO) transcription factors, GSK-3, and Mammalian Sterile 20-like kinase 1 (MST1)<sup>95</sup>. Finally, the activation of AKT leads to the phosphorylation and activation of the mammalian target of rapamycin complex 1 (mTORC1), which promotes cell growth, protein synthesis and lipid synthesis<sup>96, 97</sup>.

mTORC1 serves several functions within insulin signaling, influencing cellular response to nutrient availability and growth factors. Specifically, mTORC1 stimulates protein synthesis by phosphorylating and activating downstream elements such as ribosomal S6 kinase (S6K) and eukaryotic initiation factor 4E-binding protein 1 (eIF4E-BP1), all of which promote translation initiation and elongation, leading to increased synthesis of proteins necessary for cell growth and function<sup>97</sup>. Moreover, the activation of mTORC1 also contributes to the lipid synthesis by upregulating the expression of lipogenic enzymes and transcription factors involved in lipid metabolism, thereby supporting cell growth and membrane biogenesis<sup>97</sup>. The activation of mTORC1 supports cell growth and survival by negatively regulating autophagy, a process of cellular degradation and recycling. Activated mTORC1 inhibits Unc-51 like autophagy activating kinase 1 (ULK1), a key initiator of autophagy, thereby suppressing the breakdown of cellular components<sup>97</sup>. Additionally, mTORC1 exerts feedback regulation in insulin signaling through S6K-mediated phosphorylation of IRS, nutrient sensing mechanisms, and cross-talk with other signaling pathways, helping maintain cellular homeostasis and regulate insulin sensitivity in response to various nutrient and hormonal conditions<sup>97</sup>.

The mammalian target of rapamycin complex 2 (mTORC2) is another key protein complex involved in insulin signaling. mTORC2 phosphorylates AKT at the Serine 473 (Ser473) site, stabilizes AKT, and enhances its activity, which contributes to the downstream effects of insulin signaling, including glucose uptake, glycogen synthesis, and cell survival<sup>98</sup>. Similar to mTORC1, mTORC2 participates in feedback regulation by influencing the activity of other kinases and phosphatases involved in insulin signaling, thereby affecting the overall responsiveness of cells to

insulin<sup>98</sup>. Additionally, mTORC2 integrates with mTORC1 to ensure a balanced cellular response to nutrient and growth factor signals, contributing to overall metabolic homeostasis and cellular function<sup>98</sup>.

The MAPK pathway is another important component of the insulin signaling pathway. It is activated when IRS proteins recruit and bind to growth factor receptor-bound protein 2 (Grb2), leading to the activation of Rat sarcoma (Ras) protein and the subsequent activation of the MAPK cascade<sup>93</sup>. Firstly, activated Ras recruits the rapidly accelerated fibrosarcoma (Raf) proto-oncogene serine/threonine-protein kinase (c-Raf), which phosphorylates and activates mitogen-activated protein kinase (MEK)<sup>93</sup>. MEK subsequently phosphorylates extracellular signal regulated kinase (Erk) and promotes its translocation to the nucleus, where it is phosphorylated and transcriptional activated by transcription factors, ultimately regulating gene expression related to cell growth, differentiation, and metabolism<sup>93</sup>. In addition, the MAPK pathway can cross-talk with the PI3K/AKT pathway downstream of insulin signaling, influencing cell proliferation, survival, and differentiation<sup>93</sup>. Similar to the PI3K/AKT pathway, the MAPK pathway also participates in the feedback regulation, modulating insulin sensitivity by phosphorylating IRS proteins and contributing to IR in metabolic disorders<sup>93</sup>.

Altogether, the interplay between the PI3K/AKT and MAPK pathways in insulin signaling ensures precise control of cellular responses to insulin and adaption to changing metabolic conditions.

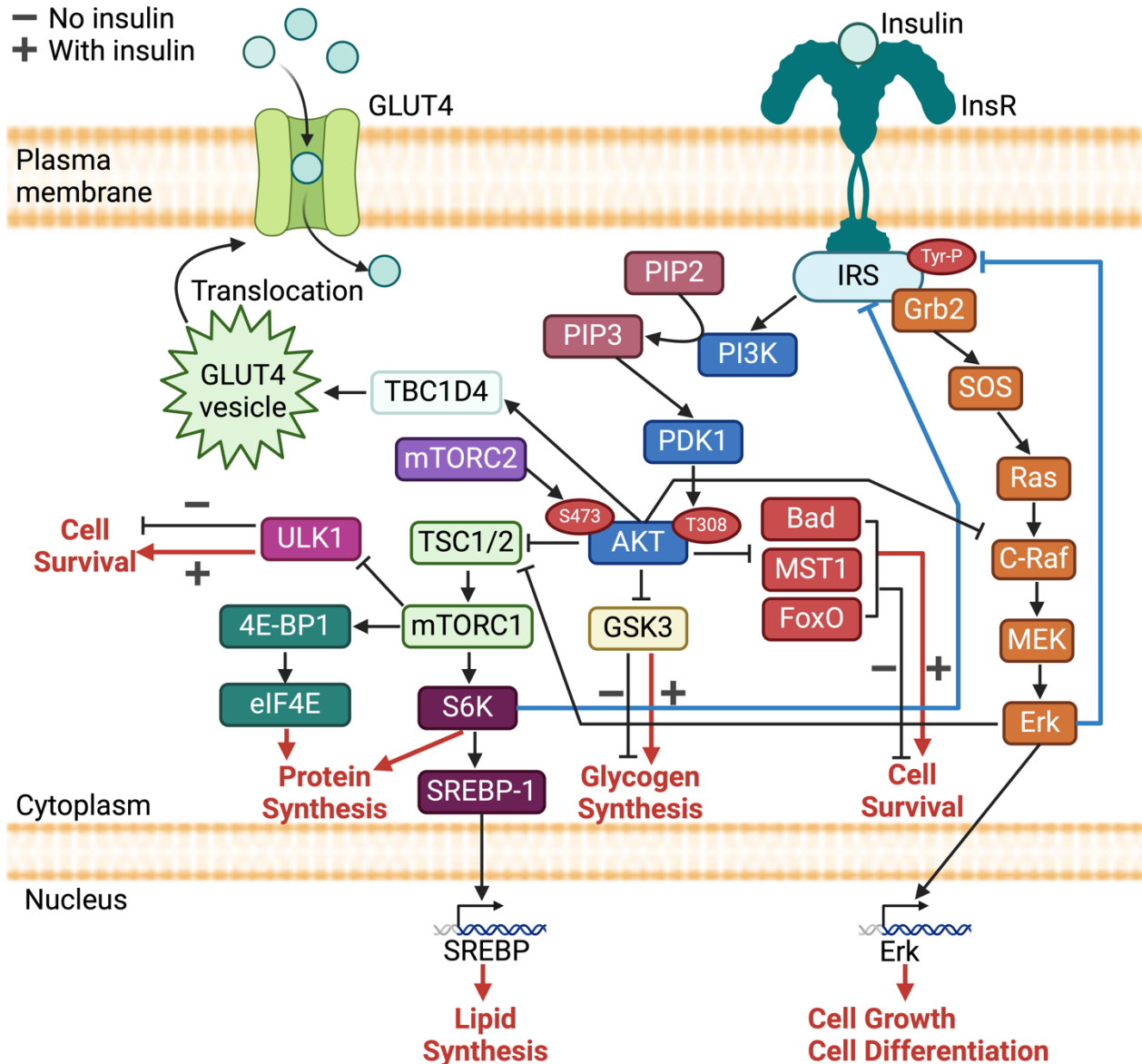


**Figure 1.2 Schematic of insulin signaling.** The insulin signaling cascade is initiated when insulin binds to InsR, triggering InsR self-phosphorylation as well as IRS recruitment and phosphorylation. Downstream signaling through the PI3K/AKT pathway promotes protein synthesis, lipid synthesis, glycogen synthesis, and glucose uptake, while inhibiting autophagy. Downstream signaling through the MAPK pathway promotes cell growth and differentiation. Abbreviations are as follows: InsR: Insulin receptor; IRS: Insulin receptor substrate; Ser: Serine; Grb2: Growth factor receptor-bound protein 2; SOS: Son of Sevenless; Ras: Rat sarcoma; Raf: Rapidly accelerated fibrosarcoma; C-Raf: Raf proto-oncogene serine/threonine-protein kinase; MEK: Mitogen-activated protein

kinase; Erk: Extracellular signal-regulated kinase; PI3K: Phosphoinositide 3-kinase; PDK1: 3-phosphoinositide-dependent kinase-1; AKT: Protein kinase B; GSK3: Glycogen synthase kinase 3; Bad: B cell lymphoma-2-associated death promotor; MST1: Mammalian sterile 20-like kinase 1; FoxO: Forkhead box O; TBC1D4: TBC1 Domain Family Member 4; GLUT1: Glucose transporter 1; TSC1/2: Tuberous sclerosis complex 1/2; mTORC1: Mammalian target of rapamycin complex 1; mTORC2: Mammalian target of rapamycin complex 2; S6K: Ribosomal protein S6 kinase; SREBP-1: Sterol regulatory element-binding protein 1; ULK1: Unc-51 like autophagy activating kinase 1; 4E-BP1: Eukaryotic translation initiation factor 4E-binding protein 1; eIF4E: Eukaryotic translation initiation factor 4E. Drawn in BioRender.com.

### ***1.1.5 Development of obesity-associated insulin resistance***

IR can be defined as an inadequate response to the physiological effects of circulating insulin in target tissues, primarily involving the liver, muscles, and AT<sup>91</sup>. The impairment in glucose uptake leads to elevated blood glucose levels. To compensate for IR, more insulin will be produced by the  $\beta$  cells and then circulate in the blood, resulting in elevated blood insulin levels, known as hyperinsulinemia. Prolonged IR will disrupt glucose homeostasis and induce  $\beta$ -cell stress, ultimately culminating in the development of T2D<sup>1, 2</sup>. Obesity is often accompanied by low-grade chronic inflammation and IR. Various complex mechanisms contribute to the development of obesity-associated IR, including the accumulation of adipokines, cytokines, lipopolysaccharides (LPS), dysfunctional lipid metabolism, and mitochondrial dysfunction (**Figure 1.3**).

Adipokines are a diverse group of bioactive proteins secreted by adipocytes and play crucial roles in regulating various physiological processes, including metabolism, inflammation and insulin sensitivity<sup>46</sup>. In obesity, the secretion of various adipokines is altered, contributing to the metabolic and inflammatory complications associated with IR. Leptin is a hormone produced by AT that regulates energy balance by suppressing appetite and increasing energy expenditure<sup>46</sup>. Several studies have shown that leptin levels were positively correlated with BMI and IR parameters<sup>99, 100</sup>. Leptin signaling enhances insulin signaling by promoting the phosphorylation of IRS proteins, which facilitates the activation of downstream signaling pathways<sup>101</sup>. However, despite high leptin levels, obese individuals often develop leptin resistance, for which, body does not respond effectively to leptin signals. Leptin resistance in obese individuals contributes to overeating and further weight gain, which exacerbates IR<sup>100, 102</sup>. Moreover, resistin, another adipokine implicated in promoting IR by impairing the phosphorylation of IRS proteins and increasing inflammation, was increased in obese individuals<sup>103, 104</sup>. Adiponectin is an adipokine that exhibits anti-inflammatory properties. It primarily utilizes the adenosine monophosphate-activated protein kinase (AMPK) signaling pathway and peroxisome proliferator-activated receptor gamma (PPAR- $\gamma$ ) signaling pathway to enhance insulin sensitivity and regulate glucose and lipid

metabolism<sup>46</sup>. The level of adiponectin in obese individuals has been reported to be significantly reduced, leading to decreased insulin sensitivity and increased risk of T2D<sup>105, 106</sup>. The most recent adipokines to emerge as a contributor to obesity-associated IR is retinol-binding protein 4 (RBP4). RBP4 is highly expressed in the liver and AT, and its circulating levels were positively correlated with obesity and IR in rodents<sup>107</sup>. The binding of RBP4 to its receptor activates the Janus kinase (JAK)/STAT5/ suppressor of cytokine signaling 3 (SOCS3) pathways<sup>108</sup>. The SOCS3 protein can bind to IRS proteins, block their phosphorylation, and promote their degradation, thereby inhibiting insulin signaling<sup>109</sup>. Overall, the changes in adipokine profiles create a pro-inflammatory environment and disrupt normal insulin signaling, leading to IR and metabolic dysregulation.

In addition to adipokines, adipocytes and infiltrated immune cells secrete a large number of cytokines including TNF- $\alpha$ , IFN- $\gamma$ , IL-6, and IL-1 $\beta$ . TNF- $\alpha$  and IL-1 $\beta$  inhibit insulin signaling by activating the JNK and IKK pathways<sup>110, 111</sup>. The activation of both pathways promotes the phosphorylation of IRS proteins on serine residues (Ser307) instead of tyrosine residues, thereby inhibiting the ability of IRS proteins to transmit the insulin signaling effectively<sup>111, 112</sup>. Moreover, TNF- $\alpha$  and IL-1 $\beta$  also mediate increased production of reactive oxygen species (ROS)<sup>113, 114</sup>, reduce the expression of InsR on the cell surface<sup>115-117</sup>, inhibit the secretion of adiponectin<sup>118</sup>, and increase circulating free fatty acids (FFA)<sup>119</sup>. Collectively, these changes contribute to IR. IFN- $\gamma$  and IL-6 are pro-inflammatory cytokines whose levels increase under obese conditions and can impair insulin signaling. These two cytokines both activate the JAK/STAT pathway to activate transcription factors, such as STAT1 for IFN- $\gamma$  and STAT3 for IL-6, leading to the induction of the pro-inflammatory genes and exacerbating IR<sup>120</sup>. Moreover, both IFN- $\gamma$  and IL-6 promote the expression of SOCS proteins, particularly SOCS3, which inhibits insulin signaling by binding to IRS proteins, blocking their phosphorylation, and promoting their degradation<sup>109</sup>.

The accumulation of LPS is another factor contributing to IR in obese individuals. Elevated LPS levels, which occur due to increased gut permeability and gut dysbiosis under obese conditions<sup>121, 122</sup>, activate Toll-like receptor 4 (TLR4) on various cells. This activation triggers two

main pathways: the myeloid differentiation primary response 88 (MyD88)-dependent NF- $\kappa$ B signaling pathway and the TIR-domain-containing adapter-inducing Interferon- $\beta$  (TRIF)-dependent interferon regulatory factor 3 (IRF3) pathway. Both pathways lead to the induction of the pro-inflammatory cytokines, which exacerbate inflammation and interfere with insulin signaling pathways, ultimately contributing to IR<sup>123</sup>.

Obesity is also associated with the dysregulation of lipid metabolism. The level of circulating FFA increased under obese conditions<sup>124, 125</sup>. FFA can bind to pattern recognition receptors (PRR) and activate protein kinases such as protein kinase C (PKC), JNK, and IKK<sup>124, 125</sup>. The activation of these kinases impairs insulin signaling by increasing the inhibitory serine phosphorylation of IRS proteins<sup>126</sup>. Moreover, the disruption of the lipid metabolism can lead to the accumulation of lipid intermediates such as diacylglycerols and ceramides within cells<sup>127</sup>. Similar to FFA, these lipid derivatives interfere with insulin signaling also by activating serine kinases like JNK and IKK, further impairing the function of IRS proteins and contributing to IR<sup>127</sup>.

Mitochondrial dysfunction and IR are closely linked. Mitochondria are the primary cellular organelles responsible for adenosine triphosphate (ATP) production, energy expenditure, and generation and disposal of ROS<sup>128</sup>. However, within the context of obesity and IR, changes in mitochondrial dynamics have been observed, including increased fission and decreased fusion, resulting in fragmented mitochondria<sup>129, 130</sup>. Fragmentation leads to impaired function of mitochondria, causing mitochondrial dysfunction characterized by impaired ATP production, increased ROS production, and altered lipid and glucose metabolism<sup>129, 130</sup>. The energy deficit hinders glucose uptake and utilization in insulin-sensitive tissues. The generation of excessive ROS induce oxidative stress, triggering inflammatory response and oxidative damage to cellular components, including proteins and lipids<sup>129</sup>.

Altogether, the mechanisms by which obesity contributes to IR are complex, with multiple factors collectively creating a pro-inflammatory environment and disrupting insulin signaling.

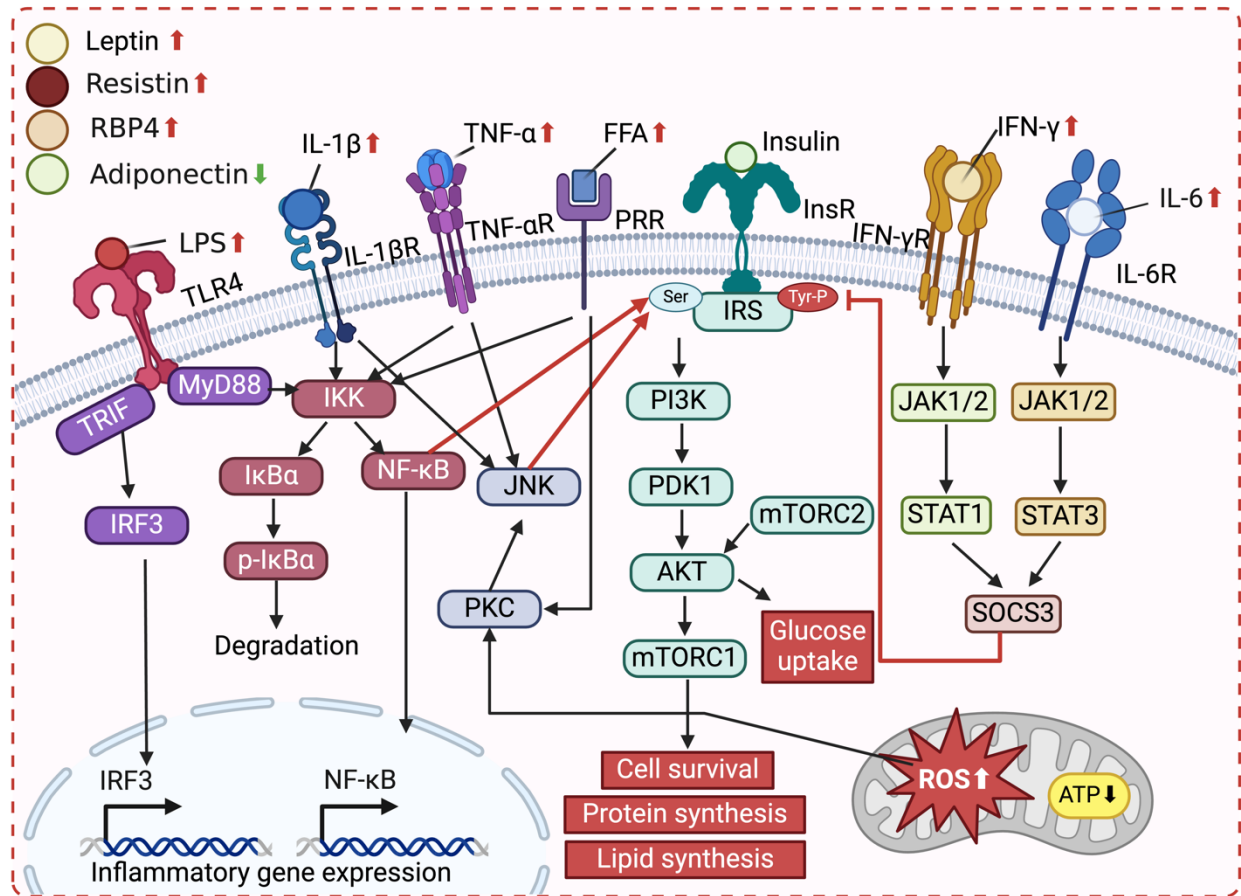


**Figure 1.3 Schematic of the mechanisms underlying obesity-associated IR.** Obesity alters the secretion of adipokines, leading to chronic inflammation. Under obese conditions, hypertrophic adipocytes and AT-infiltrated immune cells produce pro-inflammatory cytokines that dampen insulin signaling. TNF- $\alpha$  and IL-1 $\beta$  both activate the JNK and IKK pathways, inducing the expression of pro-inflammatory cytokines and promoting the serine phosphorylation of IRS proteins, thereby inhibiting insulin signaling. IFN- $\gamma$  and IL-6 activate the JAK/STAT pathway and promote the expression of SOCS3, which inhibits the tyrosine phosphorylation of IRS proteins. The accumulation of FFA in obesity leads to the activation of protein kinases such as PKC, JNK, and IKK, ultimately resulting in IR. Elevated levels of LPS in the bloodstream activate the MyD88-dependent NF- $\kappa$ B pathway and the TRIF-dependent IRF3 pathway, impairing insulin signaling by exacerbating inflammation and inhibiting the tyrosine phosphorylation of IRS proteins. Obesity is also associated with mitochondrial dysfunction, which leads to increased generation of ROS and decreased ATP production, further contributing to IR. Abbreviations are as follows: JAK: Janus

kinase; STAT: Signal transducer and activator of transcription; SOCS: Suppressor of cytokine signaling protein; IFN- $\gamma$ : Interferon gamma; Tyr: Tyrosine; Ser: Serine; IRS: Insulin receptor substrate; InsR: Insulin receptor; PI3K: Phosphoinositide 3-kinase; PDK1: 3-phosphoinositide-dependent kinase-1; AKT: Protein kinase B; mTORC: Mammalian target of rapamycin complex; FFA: Free fatty acids; PRR: Pattern recognition receptor; TNF- $\alpha$ : Tumor necrosis factor-alpha; IKK: Inhibitor of nuclear factor- $\kappa$ B kinase- $\beta$ ; NF- $\kappa$ B: Nuclear factor- $\kappa$ B; I $\kappa$ B $\alpha$ : Inhibitor of  $\kappa$ B alpha; LPS: Lipopolysaccharides; TLR4: Toll-like receptor 4; TRIF: TIR-domain-containing adapter-inducing Interferon- $\beta$ ; MyD88: Myeloid differentiation primary response 88; IRF3: Interferon regulatory factor 3; ATP: Adenosine triphosphate; ROS: Reactive oxygen species; JNK: c-Jun N-terminal kinase; PKC: Protein kinase C. Drawn in BioRender.com.

## 1.2 B cell differentiation and function

Obesity is accompanied by impaired adaptive immune responses elicited by vaccination and infection<sup>131-133</sup>. Genetically obese and DIO mice both showed impaired anti-viral immunity and increased mortality<sup>134-136</sup>. B cells produce antibodies and cytokines, serve as APCs, and participate in long-lasting immunological memory<sup>137, 138</sup>. Under obese conditions, B cells show alterations in recruitment and function<sup>89, 90</sup>, which contribute to dampened adaptive immunity.

### 1.2.1 Development and differentiation of B cells

B cells are critical components of the adaptive immune system. B cell development is a tightly regulated and sequential process that occurs primarily in the bone marrow (BM) and involves several distinct stages (**Figure 1.4**). The development of B cells begins with hematopoietic stem cells (HSCs) residing in the BM<sup>139</sup>. These multipotent stem cells have the potential to differentiate into various blood cell lineages, including B cells<sup>140</sup>. Under the influence of specific cytokines and transcription factors such as IL-7 and Early B cell factor 1 (EBF1), HSCs commit to the B cell lineage and become pro-B cells<sup>139, 141-143</sup>. At this stage, the genetic rearrangement of immunoglobulin heavy chain (*IgH*) genes occurs through a process known as *V(D)J* recombination, which involves the random assembly of Variable (*V*), Diversity (*D*), and Joining (*J*) gene segments to create a diverse repertoire of B cell receptors (BCRs)<sup>139, 144</sup>. After successful rearrangement of the *IgH* genes, pro-B cells transition into the pre-B cell stage. Pre-B cells express a functional pre-BCR complex on their surface, consisting of a successfully rearranged heavy chain paired with surrogate light chains<sup>139</sup>. The pre-BCR functions as a sensor to test the assembly and signaling capability of the heavy chain. If the heavy chain is structurally functional, signaling through the pre-BCR initiates a survival and proliferation response, leading to clonal expansion of pre-B cells bearing the same heavy chain<sup>139</sup>. Subsequently, surviving pre-B cells will undergo further maturation in the BM, during which the rearrangement of immunoglobulin light chain (*IgL*) genes occurs<sup>139</sup>. The newly rearranged light chain then pairs with the assembled heavy chain to form a

complete BCR, which is expressed on the surface of the immature B cells<sup>139</sup>. Initially, immature B cells express immunoglobulin M (IgM) BCRs and must undergo central tolerance mechanisms to ensure their BCRs do not strongly bind to self-antigens, thus preventing autoimmunity<sup>139, 145</sup>. Those immature B cells that fail selection will become anergic or undergo apoptosis<sup>145, 146</sup>.

Once immature B cells pass central tolerance in the BM, they will migrate to secondary lymphoid organs such as spleens and lymph nodes, where they encounter foreign antigens and complete their maturation process (**Figure 1.4**). Upon entering the secondary lymphoid organs, immature B cells will undergo further differentiation into transitional B cells and start to produce cell surface IgD molecules together with IgM molecules<sup>147</sup>. Subsequently, transitional B cells will encounter self-antigens and undergo the peripheral tolerance process<sup>146</sup>. Those who encounter self-antigens in the absence of appropriate co-stimulatory signals can become functionally inert or anergic, and those with high-affinity BCRs for self-antigens may undergo apoptosis to eliminate potentially harmful autoreactive B cells<sup>146</sup>. Moreover, transitional B cells with low-affinity BCRs for self-antigens in the spleens can further migrate to the marginal zone (MZ) and differentiate into MZ B cells with the help of stromal cells and MZ macrophages<sup>148</sup>. MZ B cells typically differentiate into short-lived plasma cells that rapidly produce low-affinity antibodies following activation<sup>148</sup>. Other transitional B cells will migrate to the follicle zone and differentiate into follicular (FO) B cells<sup>149</sup>. Upon antigen stimulation, antigen-activated FO B cells and CD4<sup>+</sup> T cells migrate towards the interface between B and T cell zones, respectively. The migration is driven by a network of chemokines and adhesion molecules that facilitate the precise positioning of these cells in proximity to one another, leading to the establishment of stable B cell : CD4<sup>+</sup> T cell interactions, further enabling B cells to receive helper signals from cognate CD4<sup>+</sup> T cells and undergo clonal expansion<sup>139, 149, 150</sup>. Some of the proliferating B cells with low-affinity BCRs cannot interact effectively with cognate helper T cells, and differentiate into short-lived plasma cells and germinal center (GC)-independent memory B cells (MBCs) in a process termed extrafollicular reaction<sup>139</sup>. Others with high-affinity BCRs receive several signals from T<sub>FH</sub> cells, including co-stimulatory signals such as CD40 ligand (CD40L) and inducible T-cell costimulatory

(ICOS), and cytokine signals such as IL-4, IL-5, IL-21, IFN- $\gamma$ , and TGF- $\beta$ <sup>139</sup>. These signals function together with the BCR signals to promote the class-switch recombination of proliferated B cells and help the entry of these B cells into GC<sup>139</sup>.

GC is a transitory specialized structure within secondary lymphoid organs, where B cells undergo several critical processes to enhance their ability to produce high-affinity antibodies<sup>151</sup> (**Figure 1.4**). GC is divided into two main zones named dark zone (DZ) and light zone (LZ), which have distinct functions and cellular components, contributing to the overall process of plasma cells and MBCs development<sup>139, 149, 151</sup>. Upon entering the GC, B cells first migrate into the DZ and undergo rapid proliferation, which is necessary to generate a large pool of antigen-specific B cells that can be subjected to subsequent selection processes<sup>139, 149, 151</sup>. During the proliferation, the *Ig* genes of B cells undergo somatic hypermutation, during which random point mutations are inserted into the variable region of the BCR genes to produce a diverse array of BCRs, some of which may have higher affinity for the antigens<sup>139, 144</sup>. Subsequently, the mutated B cells migrate to the LZ where they undergo the selection based on the affinity of their BCRs for the antigens presented by FDCs<sup>139, 149, 151</sup>. B cells with high-affinity BCRs can bind to the antigen more effectively and will be selected for survival, while B cells with low-affinity BCRs may undergo apoptosis or anergy<sup>152</sup>. In addition to FDCs, T<sub>FH</sub> cells within LZ also interact with B cells, providing essential survival and differentiation signals through cytokines and cell surface molecules<sup>139, 149, 151</sup>. The interaction between GC B cells and T<sub>FH</sub> cells within LZ, along with the help from FDCs, promotes the selection and differentiation of B cells into plasma cells and MBCs. The affinity-matured GC B cells can either re-enter the GC cycle<sup>139, 149, 151</sup>, or exit the GC as long-lived plasma cells or GC-dependent MBCs, which together mediate long-lasting humoral immunity<sup>139, 149, 151</sup>.

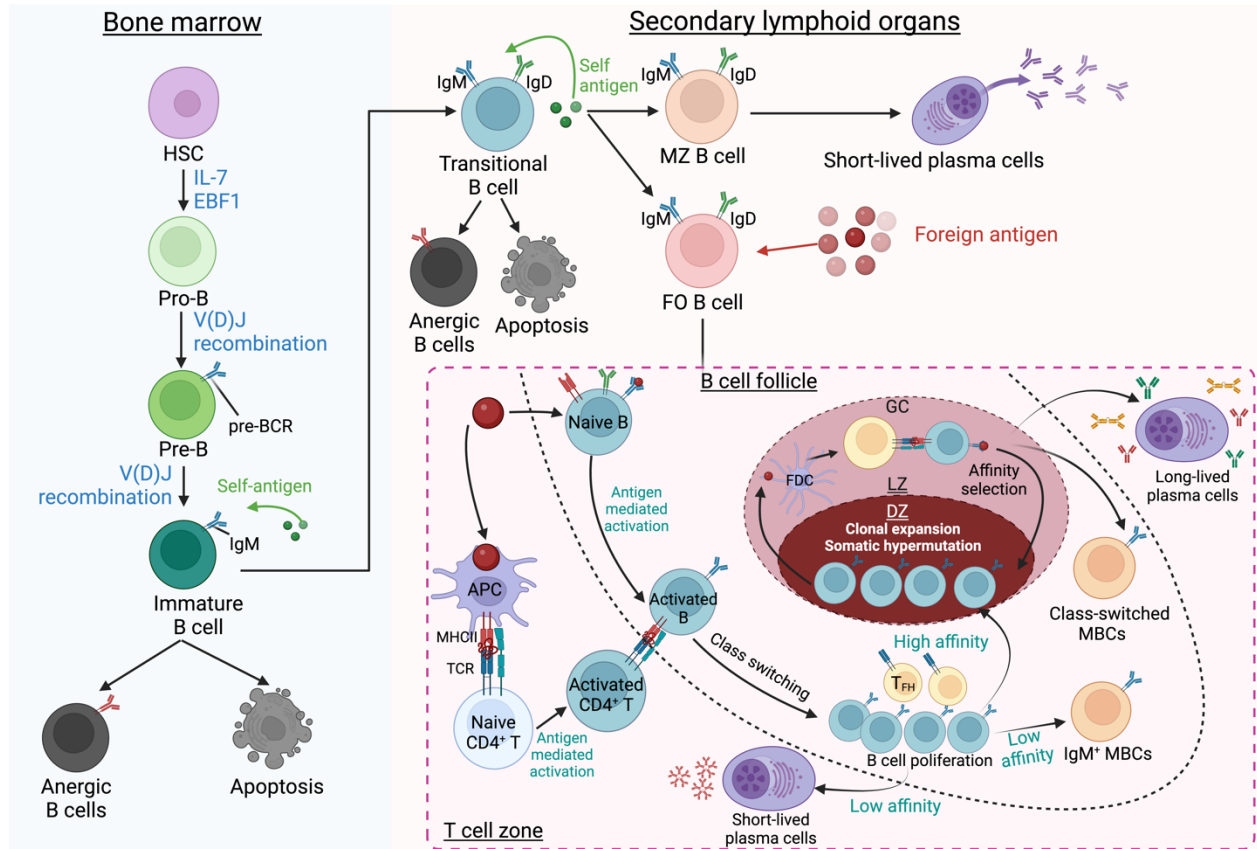


**Figure 1.4 Illustration of the development and differentiation process of B cells.** The development of B cells begins with HSCs residing in the bone marrow, which differentiate into pro-B cells under the influence of IL-7 and EBF1 and further differentiate into pre-B cells after undergoing *V(D)J* recombination. The pre-B cells will differentiate into immature B cells and express IgM BCR molecules. Immature B cells then undergo positive selection, surviving cells migrate into secondary lymphoid organs and differentiate into transitional B cells, which will undergo another round of positive selection to prevent autoimmune responses. Surviving transitional B cells in the spleens can then migrate into the MZ and differentiate into MZ B cells that rapidly differentiate into short-lived plasma cells. Other transitional B cells in secondary lymphoid organs migrate into the follicle, differentiate into FO B cells, and encounter foreign antigens to undergo subsequent maturation. Upon encountering foreign antigens, FO naïve B cells and naïve CD4<sup>+</sup> T cells will undergo antigen-mediated activation and migrate towards the interface between B and T cell zones, respectively, which leads to the establishment of stable B cell: CD4<sup>+</sup>

T cell interactions. Activated B cells then proliferate rapidly and enter GC with the help of T<sub>FH</sub> cells. In contrast, those B cells with low-affinity BCRs cannot interact effectively with cognate T<sub>FH</sub> cells and differentiate into short-lived plasma cells and GC-independent MBCs. After entering GC, B cells undergo clonal expansion and somatic hypermutation in the DZ, and affinity selection with the help of FDCs and T<sub>FH</sub> cells in the LZ, ultimately differentiating into long-lived plasma cells and class-switched MBCs. Abbreviations are as follows: HSC: Hematopoietic stem cells; EBF1: Early B cell factor 1; V(D)J: Variable, Diversity, Joining; BCR: B cell receptor; Ig: Immunoglobulin; MZ: Marginal zone; FO: Follicular; APC: Antigen presenting cell; MHC II: Class II major histocompatibility complex; TCR: T cell receptor; T<sub>FH</sub>: T follicular helper; LZ: Light zone; DZ: Dark zone; FDC: Follicular dendritic cell; GC: Germinal center; MBC: Memory B cell. Drawn in BioRender.com.

### ***1.2.2 Development of B cell-mediated memory responses***

The secondary immune response is an enhanced and more efficient reaction to an antigen that the immune system has previously encountered<sup>153</sup>. It is a key component of successful vaccination strategies<sup>154</sup>, providing long-term immunity and protection against infectious diseases. The secondary immune response is driven by memory B cells and memory T cells generated during the primary immune responses. This section will focus on B cell-mediated memory responses (**Figure 1.5**).

Compared with primary immune responses, secondary immune responses have key features including quicker onset, greater magnitude, and higher specificity<sup>155</sup>. Memory B cells can be activated within hours to a few days after re-exposure to the antigen<sup>156</sup>. Additionally, the number of antibodies produced during the memory response is larger than in the primary response, and the affinity of antibodies is higher due to the somatic hypermutation and affinity maturation during the GC reaction in the primary response<sup>155</sup>. Finally, memory B cells are highly specific to the antigen that initiated the primary response, ensuring a more precise and effective targeting of the antigen<sup>155</sup>.

As will be discussed later, activated B cells receiving insufficient co-stimulatory signals from T<sub>FH</sub> cells will differentiate into IgM<sup>+</sup> MBCs. In contrast, other activated B cells get help from T<sub>FH</sub> cells and enter the GC, ultimately differentiating into class-switched MBCs. During the secondary immune response, IgM<sup>+</sup> MBCs exposed to the same antigen frequently re-enter the GC and undergo a GC reaction similar to that during the primary immune response<sup>157, 158</sup>. Simultaneously, some of them rapidly differentiate into short-lived plasma cells and produce IgM antibodies<sup>157</sup>. Unlike IgM<sup>+</sup> MBCs, class-switched MBCs rapidly differentiate into long-lived plasma cells after re-exposure to the same antigen and produce different types of high-affinity antibodies, including IgA, IgG, and IgE<sup>157</sup>.

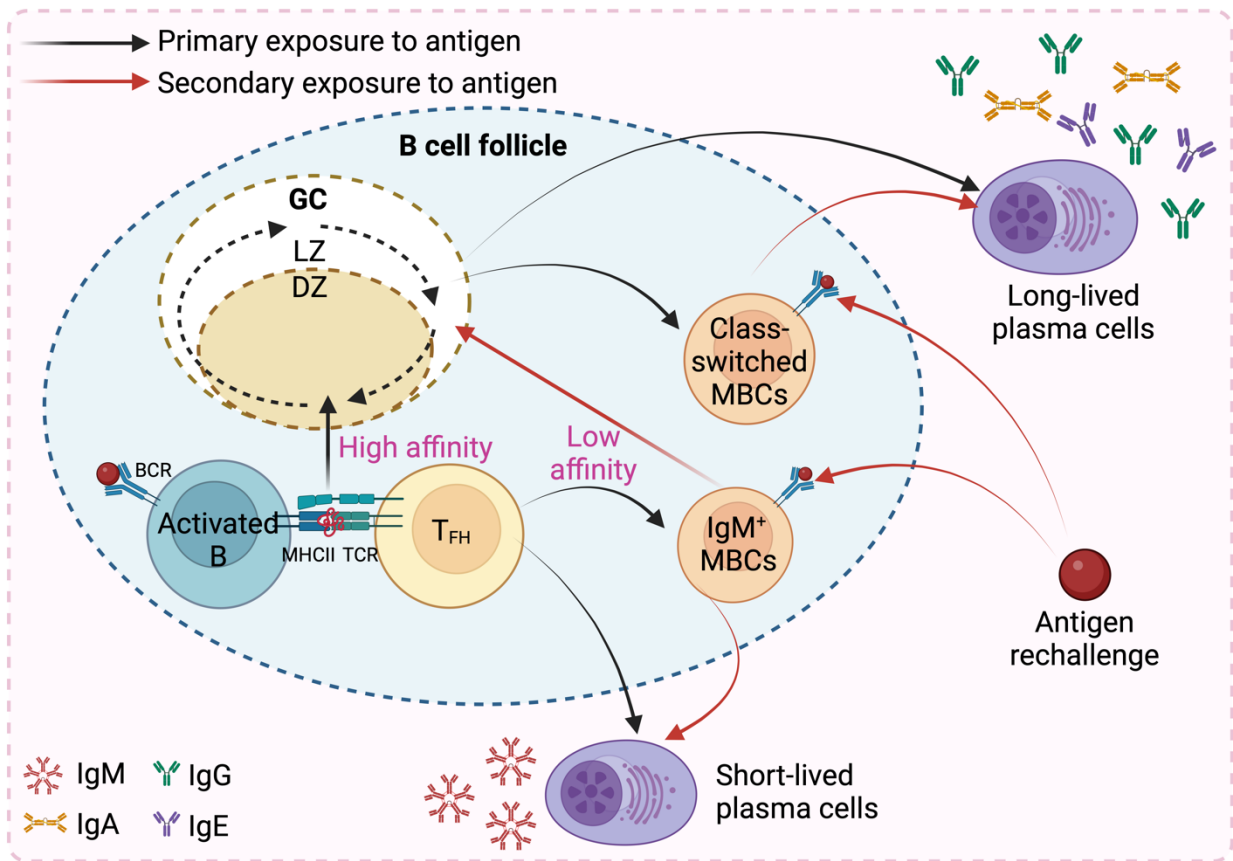
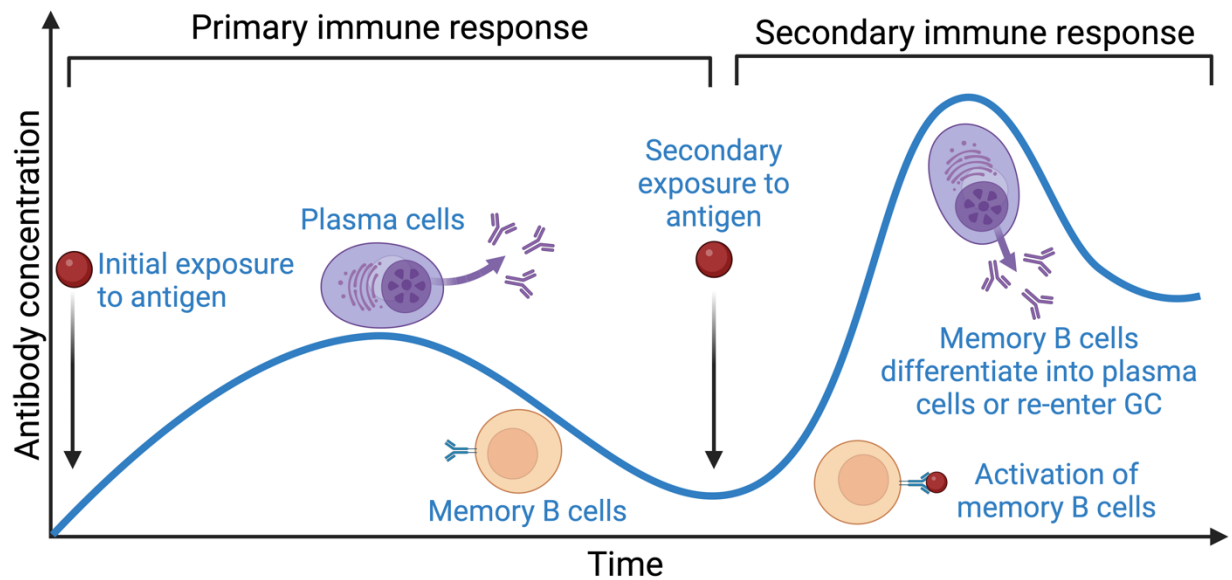


**Figure 1.5 Illustration of B cell-mediated memory responses.** The B cell-mediated memory response is quicker, stronger, and highly specific compared with the primary immune response. Upon re-exposure to the same antigen, IgM<sup>+</sup> MBCs frequently re-enter the GC and undergo another round of GC reaction. Some of these cells rapidly differentiate into short-lived plasma cells and

produce IgM antibodies. Class-switched MBCs rapidly differentiate into long-lived plasma cells and produce large amounts of high-affinity IgA, IgG, and IgE antibodies. Abbreviations are as follows: MBC: Memory B cell; MHC II: Class II major histocompatibility complex; BCR: B cell receptor; TCR: T cell receptor; T<sub>FH</sub>: T follicular helper; GC: Germinal center; LZ: Light zone; DZ: Dark zone; Ig: Immunoglobulin. Drawn in BioRender.com.

### 1.2.3 *Function of B cells*

B cells contribute significantly to adaptive immunity via antibody production, cytokine secretion, long-lasting immune memory generation, and modulation of other immune cells<sup>137, 138</sup>. The main function of B cells is to differentiate into plasma cells and produce large amounts of high-affinity antibodies. Those antibodies perform a wide range of functions essential for immune defense, including neutralizing pathogens and toxins, enhancing phagocytosis through opsonization, activating the complement system, and mediating antibody-dependent cellular cytotoxicity (ADCC)<sup>159, 160</sup>. Moreover, antibodies exist in different classes or isotypes due to genetic rearrangements during B cell development and maturation, with each class of antibodies having specific roles tailored to different aspects of the immune response<sup>161</sup>. For example, IgM is the first antibody produced during the initial immune response, while IgG provides long-term immunity against pathogens and is the most abundant in the bloodstream<sup>161</sup>. IgA is crucial for mucosal immunity, and IgE is involved in allergic responses and parasite defense<sup>161</sup>. Altogether, these antibodies play a pivotal role in the immediate and long-term protection of the body from infections and diseases.

In addition to antibodies, B cells can also produce a variety of cytokines that play important roles in regulating immune responses, interacting with other immune cells, and modulating inflammation<sup>162</sup>. Among these cytokines, IL-10 and TGF- $\beta$  have potent anti-inflammatory properties, suppressing the activity of pro-inflammatory immune cells to prevent excessive inflammation<sup>162</sup>. B cells can also produce pro-inflammatory cytokines, including IL-6, TNF- $\alpha$ , and IL-17, resulting in inflammatory conditions and stimulating immune responses<sup>162</sup>.

B cells contribute significantly to long-lasting memory immune responses. After an initial infection or vaccination, some activated B cells differentiate into MBCs instead of plasma cells<sup>163</sup>. MBCs persist long-term in the secondary lymphoid organs as well as in the bone marrow<sup>163</sup>. These MBCs are primed to respond quickly upon re-exposure to the same antigen. They can undergo

rapid proliferation and differentiation into plasma cells, producing high affinity and specific antibodies against the antigen<sup>163</sup>. The presence of MBCs ensures that the immune system can mount a more rapid and robust response to subsequent infections by the same pathogen, which is the basis for the effectiveness of vaccines.

Lastly, like conventional APCs such as DCs and macrophages, B cells participate in antigen presentation, which can occur through direct or cross presentation<sup>164-166</sup>. B cells express BCRs on their surface, which are membrane-bound antibodies that recognize and bind to specific antigens<sup>164-166</sup>. Once the BCR binds to an antigen, the antigen is internalized, processed, and presented on the surface of B cells by MHC class II molecules<sup>164-166</sup>. The MHC-peptide complex on B cells interacts with TCRs on cognate CD4<sup>+</sup> and CD8<sup>+</sup> T cells, leading to their activation<sup>167-169</sup>. The activated T cells, in turn, secrete cytokines and provide additional signals that enhance B cell proliferation, differentiation, and antibody production<sup>167-169</sup>.

Taken together, B cells are indispensable for maintaining the ability of the adaptive immune system to recognize, respond to, and remember specific pathogens. Their multifaceted roles include producing antibodies, secreting cytokines to regulate immune responses, forming long-term memory immunity, and presenting antigens to T cells. Through these diverse functions, B cells ensure a highly specific, effective, and adaptable immune response, providing both immediate defense against infections and long-lasting immunity.

### 1.3 Metabolic signaling in B cells

Through the different stages of B cell differentiation and activation, several metabolic pathways function to supply energy and building blocks, including the glycolysis, fatty acid oxidation (FAO), glutaminolysis, and oxidative phosphorylation (OXPHOS) pathways<sup>170</sup> (**Figure 1.6**). Glycolysis is the process by which glucose is broken down into pyruvate, generating ATP and NADH in the cytosol<sup>171</sup>. The glycolysis pathway provides quick energy and intermediates for other metabolic processes such as OXPHOS<sup>171</sup>. FAO involves the breakdown of fatty acids into acetyl-CoA units, which then enter the tricarboxylic acid (TCA) cycle and contribute to ATP production via OXPHOS<sup>172</sup>. Moreover, glutaminolysis is the catabolism of glutamine to produce glutamate and subsequently  $\alpha$ -ketoglutarate ( $\alpha$ -KG), which can enter the TCA cycle and contribute to ATP production via OXPHOS<sup>173</sup>. OXPHOS occurs in the mitochondria, where the electrons from NADH and FADH<sub>2</sub> are transferred through the electron transport chain, driving the production of ATP through the chemiosmotic gradient<sup>174</sup>. OXPHOS pathway is the primary source of ATP in aerobic organisms. It can generate approximately 30-34 ATP molecules from the complete oxidation of one molecule of glucose, which is much higher than the glycolysis pathway<sup>174</sup>. All these pathways are intricately regulated and interconnected, ensuring that B cells meet their energy demands and maintain metabolic flexibility under various physiological conditions. Dysregulated metabolism in B cells may contribute to the impaired adaptive immunity observed in obese individuals.

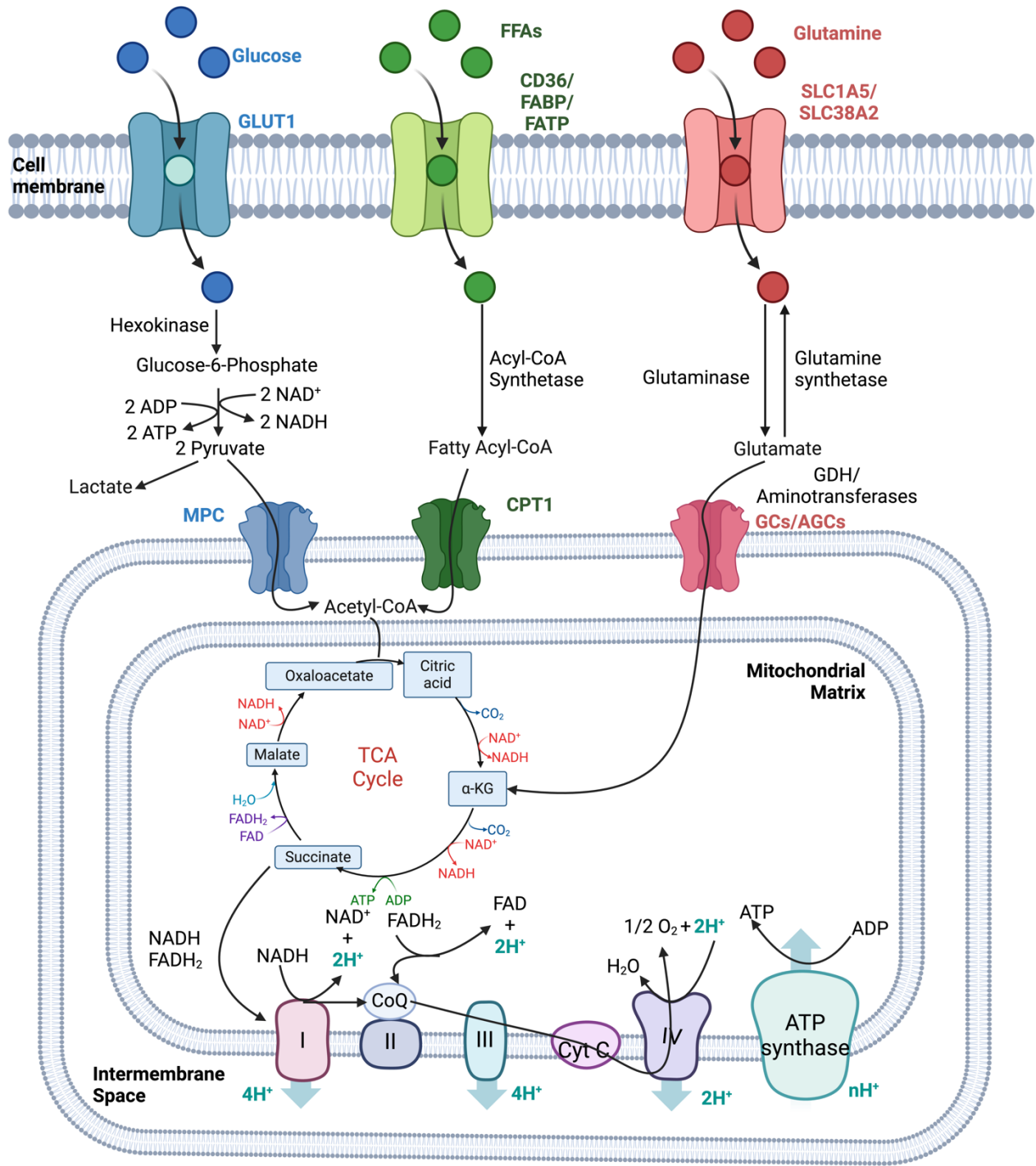


**Figure 1.6 Illustration of metabolic pathways supporting B cell activation and function.**

Glycolysis, FAO, and glutaminolysis pathways work together to generate energy and provide intermediates such as Acetyl-CoA and  $\alpha$ -KG for the TCA cycle. NADH, FADH<sub>2</sub>, and oxygen produced by the TCA cycle are then utilized in the OXPHOS pathway to produce ATP efficiently.

The OXPHOS pathway occurs in the mitochondria and produces a large amount of ATP to support B cell activation and function. Abbreviations are as follows: FFA: Free fatty acid; GLUT1: Glucose transporter 1; FABP: Fatty acid-binding protein; FATP: Fatty acid transport protein; SLC1A5: L-type amino acid transporter; SLC38A2: Sodium-coupled neutral amino acid transporter 2; ADP: Adenosine diphosphate; ATP: adenosine triphosphate; NADH: Nicotinamide adenine dinucleotide, reduced form; MPC: Mitochondrial pyruvate carrier; CPT1: Carnitine palmitoyl transferase 1; GDH: Glutamate dehydrogenase; GCs: Glutamine channels; AGCs: Amino acid glutamine channels; TCA: Tricarboxylic acid cycle; FADH<sub>2</sub>: Flavin adenine dinucleotide, reduced form;  $\alpha$ -KG:  $\alpha$ -ketoglutarate; Cyt C: Cytochrome c; CoQ: Coenzyme Q. Drawn in BioRender.com.

### ***1.3.1 Dynamic changes in metabolic activity during B cell differentiation and activation***

The metabolic signaling of B cells is a complex and dynamic process essential for their proliferation, activation, differentiation, and function (**Figure 1.7**). During the quiescent state, resting B cells primarily rely on the OXPHOS pathway for ATP production<sup>170</sup>. Resting B cells maintain a balance between energy production and minimal biosynthetic activity, preserving resources for rapid activation upon encountering an antigen<sup>170</sup>.

Upon encountering the antigen, activated B cells rapidly upregulate the glucose uptake and glycolysis pathway, even in the presence of oxygen<sup>170</sup>. Glycolysis is crucial for generating not only the ATP, but also the building blocks for nucleotides, amino acids, and lipids, which are essential for rapid cell division<sup>171</sup>. Specifically, the formed intermediates, such as glucose-6-phosphate, can be diverted into the pentose phosphate pathway, that produces ribose-5-phosphate that is a key precursor for the synthesis of nucleotides and nucleic acids<sup>171</sup>. Moreover, several glycolytic intermediates serve as precursors for amino acid synthesis, including 3-phosphoglycerate and phosphoenolpyruvate<sup>171</sup>. Additionally, pyruvate, the end product of glycolysis can be converted into acetyl-CoA via the pyruvate dehydrogenase complex, and acetyl-CoA is a key precursor for fatty acid synthesis and the production of lipids<sup>171</sup>. Furthermore, glycolysis plays an important role in maintaining redox balance through the generation of NADH and its subsequent oxidation to NAD<sup>+</sup>, enabling continuous metabolic flux and protecting the cell from oxidative damage<sup>171</sup>. Thus, this shift to aerobic glycolysis provides metabolic intermediates necessary for cell growth and proliferation. At the same time, activated B cells upregulate the mitochondrial content and OXPHOS pathway to provide a quick supply of ATP, further supporting the activation of B cells<sup>170</sup>. Subsequently, activated B cells enter the DZ of GC to undergo clonal expansion, these cells exhibit increased glycolytic activity and highly activate the OXPHOS pathway to allow for rapid ATP production<sup>170</sup>. The rapid production of ATP is crucial for supporting the energy and biosynthetic needs of highly proliferating B cells. Next, proliferated B cells enter the LZ of GC and undergo further differentiation with the help of FDCs and T<sub>FH</sub> cells. Unlike the highly glycolytic DZ B cells,

LZ B cells exhibit a more balanced use of glycolysis and OXPHOS, ensuring efficient energy production while maintaining the flexibility to shift metabolism based on cellular needs<sup>170</sup>.

Following the differentiation in the GC, B cells exit GC as plasma cells or MBCs, which have different functions and metabolic needs. Plasma cells exhibit high rates of protein synthesis to produce large quantities of antibodies. This process requires increased glucose uptake, glycolytic metabolism, and mitochondrial biogenesis to meet the heightened energy and biosynthetic demands<sup>170</sup>. Plasma cells rely on both glycolysis and OXPHOS pathways to generate ATP and necessary substrates for antibody production<sup>170</sup>. MBCs provide long-term immunity and revert to a more quiescent metabolic state like resting B cells<sup>170</sup>. They primarily rely on the OXPHOS and FAO pathways for energy, ensuring their long-term survival and readiness for rapid response upon re-exposure to the antigen<sup>170</sup>.

Overall, B cells undergo dynamic metabolic changes to support their activation, proliferation, differentiation, and function. This metabolic flexibility allows B cells to adapt to various physiological conditions and immune challenges, playing a crucial role in maintaining immune homeostasis and protecting against infections.

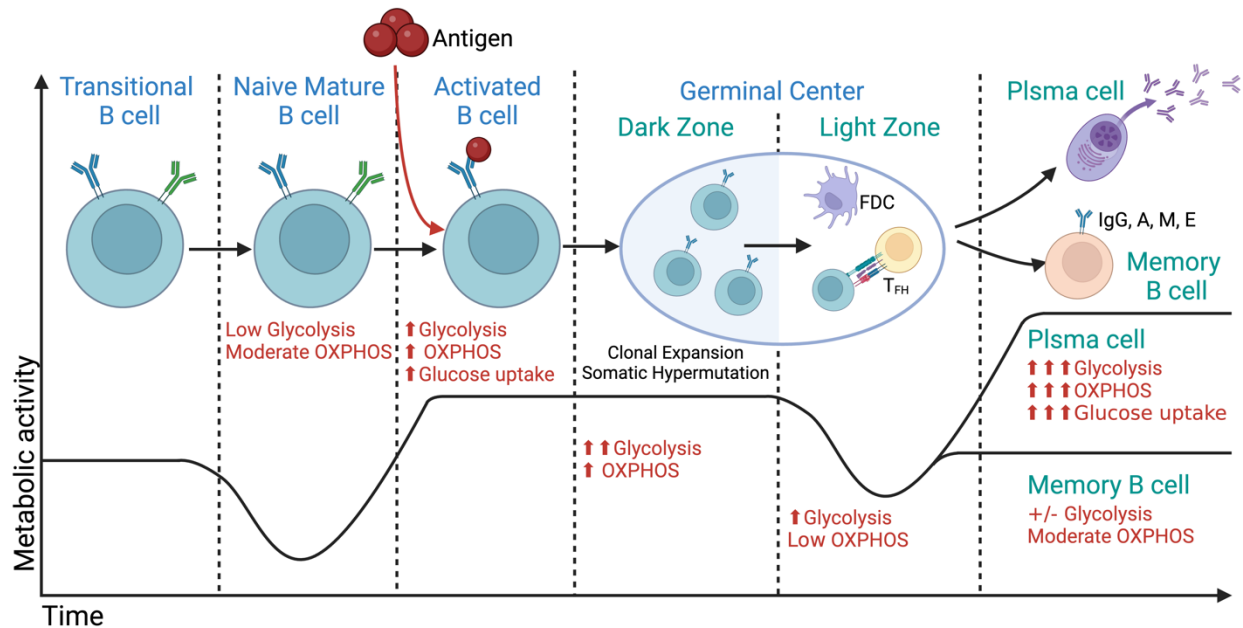


**Figure 1.7 Illustration of changes in metabolic activity during different B cell activation and differentiation stages.** During the quiescent state, resting B cells primarily rely on the OXPHOS pathway for ATP production. Upon encountering the antigens, activated B cells rapidly upregulate the glycolysis and OXPHOS pathways, leading to the rapid production of building blocks and ATP. DZ B cells exhibit increased glycolytic activity to support the energy needs of highly proliferating B cells. LZ B cells exhibit a more balanced use of the glycolysis and OXPHOS pathways. Plasma cells exhibit high rates of glycolysis pathway together with OXPHOS pathway to support antibody production. MBCs are more like resting B cells, primarily rely on the OXPHOS pathway to ensure long-term survival and readiness for rapid response upon re-exposure to the antigen. Abbreviations are as follows: Ig: Immunoglobulin; MBC: Memory B cell; OXPHOS: Oxidative phosphorylation; FDC: Follicular dendritic cell; T<sub>FH</sub>: T follicular helper. Drawn in BioRender.com. Adapted from “Akkaya, *et al.*, *Curr Opin Immunol.* **2019.**”.

### 1.3.2 *Insulin signaling and B cell metabolism*

Insulin is an essential hormone for maintaining glucose homeostasis in insulin-dependent tissues and cells<sup>91</sup>. The immune cells also rely on insulin for their metabolic needs, such as macrophages<sup>175, 176</sup>, DCs<sup>177</sup>, neutrophils<sup>178</sup>, and T cells<sup>179, 180</sup>. Recent studies demonstrated that all development stages of B cells express *Insr*<sup>181</sup>. However, the role of insulin signaling in B cells remains unknown.

InsR is a tyrosine kinase that can bind to its ligands and undergo auto-phosphorylation, further leading to the activation of the PI3K/AKT and Ras/Raf-MAPK pathways. Both pathways are important for supporting cell growth, survival and metabolism<sup>182</sup>. The activation and differentiation of B cells rely on the balance between the glycolysis, OXPHOS, and FAO pathways, which is tightly regulated by the signaling networks, including the PI3K/AKT pathway, mTOR pathway, and cytokines. The PI3K/AKT pathway is a critical downstream effector of insulin signaling, which enhances glucose uptake and glycolysis by regulating GLUT and glycolytic enzymes<sup>183</sup>. It also promotes cell survival, growth, and proliferation by regulating various metabolic enzymes and transporters<sup>183</sup>. The mTOR pathway is one of the downstream signaling pathways activated by AKT. The activation of the mTOR pathway promotes anabolic processes, including protein synthesis, lipid biosynthesis, and nucleotide production, supporting B cell growth and proliferation<sup>184</sup>. The disruption of the mTOR pathway can have broad effects on B cell development and function, including impaired early development, reduced maturation and selection, defective activation and proliferation, and compromised antibody production and memory formation<sup>185-188</sup>. Maintaining proper mTOR signaling is crucial for a fully functional B cell response.

In parallel to insulin signaling, cytokines produced due to insulin signaling, especially in conditions of IR, have important effects on B cell metabolism as well<sup>189</sup>. Pro-inflammatory cytokines like IL-6 and TNF- $\alpha$  can upregulate glycolysis, OXPHOS, and lipid synthesis to support the energy and biosynthetic needs of activated B cells<sup>189</sup>. These cytokines also influence amino

acid and nucleotide metabolism, ensuring B cells have the necessary resources for proliferation, differentiation, and antibody production<sup>189</sup>. However, chronic inflammation and altered cytokine environments can disrupt the metabolic balance, potentially impairing B cell function and contributing to immune dysregulation<sup>190</sup>.

Altogether, all findings suggest that insulin signaling has the potential to regulate B cell activation, differentiation, and function through regulating metabolism. Understanding these metabolic pathways is crucial for developing therapeutic strategies to modulate B cell function in metabolic diseases and autoimmune disorders.

#### **1.4 Hypotheses and objectives of study**

It is well established that obesity predisposes to IR. Obesity induces adipocyte hypertrophy and changes in immune cell composition with phenotypic activation towards a pro-inflammatory state<sup>191</sup>. These obese conditions confer a significant risk of life-threatening diseases<sup>1-16</sup>. Emerging evidence suggests that obesity is accompanied by impaired adaptive immune response elicited by vaccination<sup>131, 132, 192, 193</sup> and infection<sup>133, 194</sup>. Genetically or DIO mice both showed impaired anti-viral immunity and increased mortality<sup>134-136</sup>. B cells contribute significantly to adaptive immunity via antibody production, cytokine secretion, long-lasting immune memory generation, and modulation of other immune cells<sup>137, 138</sup>. Through the different stages of B cell development and activation, metabolic pathways, including glycolysis, OXPHOS, and FAO pathways, function together to supply needed energy and building blocks<sup>170</sup>. All these metabolic pathways can be regulated by insulin signaling. Insulin is an essential hormone for maintaining glucose homeostasis in insulin-dependent tissues and cells<sup>91</sup>, and many immune cells<sup>175-180</sup>, while the role of insulin signaling in B cells remains undetermined. Current studies have demonstrated that all development stages of B cells can express *Insr*<sup>181</sup>. Moreover, our lab previously observed that insulin activated insulin signaling in B cells, and DIO impaired insulin signaling in B cells. Based on all previous studies, I hypothesized that obesity impairs B cell activation and function in response to vaccines

and infection by dysregulating the engagement of metabolic pathways downstream of the insulin signaling pathway. By using a DIO mouse model and mice with B cell-specific InsR ablation, I will address the specific aims:

1. Define the impact of insulin signaling and IR on B cell activation and metabolism.
2. Understand how B cell IR modulates B cell-mediated adaptive immunity elicited by vaccination and infection.

## Chapter 2: Methods and Materials

### 2.1 Mice

All mice used in my studies were generated by intercrossing breeders obtained from the Jackson Laboratories. Genetically manipulated mice were generated as described below. Mouse genotypes were confirmed by PCR and gel electrophoresis. All mice were bred and housed in a specific pathogen-free, temperature-controlled, and 12-hour light and dark cycle environment at the University of Alberta Health Sciences Laboratory Animal Services mouse barrier facility. All mice used in comparative studies were matched for gender and age, and littermates were used as a control if possible. Unless specified, mice were fed a normal chow diet (NCD, 4% kcal from fat). All experiment procedures were approved by the Animal Care committee at the University of Alberta.

**CD19 Cre<sup>+/-</sup> InsR<sup>fl/fl</sup> mouse model:** B cell-specific InsR conditional knockout mice (CD19 Cre<sup>+/-</sup> InsR<sup>fl/fl</sup>) were generated by crossing C57BL/6 mice with an *Insr* transgene with exon 4 flanked by *loxP* sites (InsR<sup>fl/fl</sup>, strain number: 006955) with mice carrying the *Cre* recombinase gene inserted into the endogenous B lymphocyte antigen (*CD19*) locus (strain number: 006785). The CD19 promoter drives Cre-mediated recombination during the early stage (pro-B stage) and throughout B cell development and differentiation. Our lab previously documented >90% *Insr* ablation.

**Mb1 Cre<sup>+/-</sup> InsR<sup>fl/fl</sup> mouse model:** B cell-specific InsR conditional knockout mice (MB1 Cre<sup>+/-</sup> InsR<sup>fl/fl</sup>) were generated by crossing C57BL/6 mice with an *Insr* transgene with exon 4 flanked by *loxP* sites (InsR<sup>fl/fl</sup>, strain number: 006955) with mice carrying the *Cre* recombinase gene inserted into the endogenous *mb1* locus (strain number: 020505). The *mb1* gene encodes the Ig- $\alpha$  signaling subunit of the BCR and is expressed exclusively in B cells beginning at the very early pre-pro-B stage in the BM<sup>195</sup>. Our lab previously documented >90% *Insr* ablation.

### 2.2 Diet-induced obesity (DIO) model

Previous data from the Tsai lab showed that 16 weeks of HFD-feeding induced the impairment of insulin signaling in B cells. However, in the University of Alberta Health Sciences Laboratory Animal Services mouse barrier facility, initial studies using a DIO model did not cause IR in the mice until past 20 weeks of feeding, which may be related to the differences in microbiota. Thus, 6 weeks old male C57BL/6 mice were fed a high fat diet (HFD, 60% kcal from fat) for 20 weeks. Another set of mice were fed a NCD for 20 weeks as controls. Intraperitoneal glucose tolerance tests and insulin tolerance tests were performed following 20 weeks of feeding to assess the development of glucose intolerance and insulin resistance (see below).

### **2.3 Intraperitoneal glucose tolerance test (IPGTT) and insulin tolerance test (ITT)**

**IPGTT:** Mice were fasted overnight for 16 hours. Body weights were measured to calculate the dosage required to inject 1.5g glucose/kg body weight. The mice were anesthetized with inhalation of isoflurane in a biosafety cabinet (BSC). The tail vein was gently punctured with a 25-gauge needle, and a baseline blood glucose reading was acquired using a glucometer. Mice were intraperitoneally injected with prepared glucose solution, and blood glucose levels were measured at 10-, 20-, 30-, 60-, 90-, and 120-minutes post-injection.

**ITT:** Mice were fasted for 4 hours. Body weights were measured to calculate the dosage required to inject 0.75U insulin/kg body weight. The mice were anesthetized with inhalation of isoflurane in a biosafety cabinet (BSC). The tail vein was gently punctured with a 25-gauge needle, and a baseline blood glucose reading was acquired using glucometer. Mice were intraperitoneally injected with insulin solution, and blood glucose levels were measured at 10-, 20-, 30-, 60-, 90-, and 120-minutes post-injection.

### **2.4 OVA/CFA immunization**

Before injection, ovalbumin (OVA) protein was dissolved in PBS at 2 mg/mL concentration emulsified in complete Freund's adjuvant (CFA) to a 1:1 ratio and loaded into insulin syringes with

a 25-gauge needle. Female mice aged 10-15 weeks were used in the experiment. Mice were immunized subcutaneously with 50  $\mu$ L of OVA/CFA emulsion in both sides of the mammary gland area at the hairline level. Mice were euthanized 14 days post-immunization, spleens and draining axillary lymph nodes (ALNs) were collected for processing and flow cytometric analysis, sera were collected for OVA-specific Ig ELISA.

## **2.5 OVA/CFA/IFA recall model**

Before injection, ovalbumin (OVA) protein was dissolved in PBS at 2 mg/mL concentration emulsified in CFA or incomplete Freund's adjuvant (IFA) to a 1:1 ratio and loaded into insulin syringes with a 25-gauge needle. Female mice aged 10-15 weeks were used in the experiment. Mice were immunized subcutaneously with 50  $\mu$ L of OVA/CFA emulsion in both sides of the mammary gland area at day 0 and boosted with 50  $\mu$ L of OVA/IFA emulsion in both sides of the mammary gland area at day 42. Mice were euthanized 6 days after the secondary challenge, spleens and draining ALNs were collected for processing and flow cytometric analysis, sera were collected every 7 days for OVA-specific Ig ELISA.

## **2.6 Influenza virus infection**

Influenza virus A/Puerto Rico/8/34 (H1N1/PR8) virus was kindly provided by Dr. Kevin Kane at the Department of Microbiology and Immunology at the University of Alberta and stored at -80°C. Male mice aged 16-18 weeks were used in the experiment. Before use, the stock virus (10240 HAU/mL) was diluted in PBS at 7.31 HAU/mL concentration, and 25  $\mu$ L of diluted virus or PBS (control) was intranasally inoculated into the mice under inhalation anesthesia with isoflurane. The body score and body weight of mice were monitored twice daily, one time in the morning and one time in the afternoon. Mice were euthanized 14 days post-infection, spleens, draining mediastinal lymph nodes (mLNs), and lungs were collected for processing and flow cytometric analysis, sera and bronchial alveolar lavages (BAL) were collected for influenza-specific Ig ELISA.

## 2.7 Serum and BAL collection

**Saphenous blood sampling:** Saphenous blood samples were collected following the University of Alberta Health Sciences Laboratory Animal Services saphenous vein blood sampling SOP (SOP reference number: Mouse B-7 Blood Sampling via the Saphenous Vein).

**Serum collection:** Mice were euthanized by CO<sub>2</sub> fixation, and the cardiac blood samples were collected in a microcentrifuge tube. The blood samples were allowed to coagulate at room temperature for 30 minutes and then spun down at 1000g for 10 minutes at 4 °C. The clots were removed, and sera were stored at -20 °C.

**BAL collection:** Mice were euthanized by CO<sub>2</sub> fixation. The catheter was created by inserting a 20-gauge needle into a 2-centimeter piece of transparent plastic polyethylene 21-gauge tubing. The mouse was placed front side up on the Styrofoam panel, and the arms and legs were fixed with 25-gauge needles. An incision was made on the skin from the abdomen to the neck using scissors. The muscle around the neck was gently removed with forceps and scissors to expose the trachea. The prepared catheter was inserted into the trachea, and the catheter and trachea were tied together firmly with the suture line. PBS was slowly injected into the lung through the trachea and aspirated into the syringe 3 times. The syringe was removed from the catheter, and the recovered lavage fluid was transferred into a 5 mL polystyrene round-bottom tube on ice. The fluid was centrifuged at 800g for 5 mins at 4 °C and hemolyzed with Ammonium-Chloride-Potassium (ACK) lysing buffer for 5 minutes to remove red blood cells.

## 2.8 Tissue isolation and Digestion

Mice were euthanized by CO<sub>2</sub> fixation, spleens, ALNs, mLN, and lungs were dissected from mice after euthanasia for processing.

**Spleen:** Spleens were processed into a single cell suspension and filtered through a 40  $\mu\text{m}$  cell strainer prior to hemolysis with ACK lysing buffer for 5 minutes to remove red blood cells.

**ALNs & mLNs:** Lymph nodes were processed by passing through a 40  $\mu\text{m}$  cell strainer with a PBS wash and without hemolysis.

**Lungs:** Lung tissues were minced and subjected to collagenase D digestion (2 mg/mL; Sigma) with DNase I solution (50 U/mL; Sigma) in 800  $\mu\text{L}$  of DMEM media with gentle shaking for 1 hour at 37  $^{\circ}\text{C}$  and were filtered through a 40  $\mu\text{m}$  cell strainer with a PBS wash. Cells were finally hemolyzed with ACK lysing buffer for 5 minutes to remove red blood cells.

## 2.9 Flow cytometry

Immune cells from all mouse tissues were stained with a live/dead exclusion dye (Zombie NIR, Biolegend). Fluorophore-conjugated antibodies were diluted 1/200 unless otherwise recommended by the supplier prior to surface and intracellular staining at 4  $^{\circ}\text{C}$  for 30 minutes. Intracellular staining was done after fixation and permeabilization with a FOXP3 staining buffer set following the manufacturer's instructions (eBioscience). For intracellular cytokine staining, cell suspensions were stimulated with phorbol myristate acetate (PMA) and ionomycin in the presence of Brefeldin A (PMA+, Biolegend) for 5 hours. PMA is a diacylglycerol mimic and activates protein kinase C<sup>196</sup>, while ionomycin is a calcium ionophore which stimulates the release of intracellular free calcium<sup>197</sup>. Therefore, stimulation with PMA and ionomycin bypasses the requirement for TCR complex signaling and leads to the activation of T cells and the production of a variety of cytokines. Brefeldin A inhibits intracellular protein transport by Golgi<sup>198</sup>, therefore allowing intracellular detection of secreted cytokines and proteins by flow cytometry. OVA antigen-specific CD4<sup>+</sup> T cells from tissues were stained with tetramers (NIH) specific for OVA<sub>323-339</sub>/I-A<sup>b</sup> (ISQAVHAAHAEINEAGR). Influenza virus-specific CD4<sup>+</sup> T cells and CD8<sup>+</sup> T cells from tissues were stained with tetramers (NIH) specific for NP<sub>311-325</sub>/I-A<sup>b</sup> (QVYSLIRPNENPAHK) and NP<sub>366-374</sub>/H-2D<sup>b</sup> (ASNENMDTM), respectively. Permeabilized/fixed samples were resuspended in

permeabilization buffer, while unfixed samples were resuspended in FACS buffer for flow cytometric analysis on BD LSR Fortessa-SORP at the Flow Cytometry Facility (University of Alberta).

### **2.10 B cell isolation**

B cells were isolated using EasySep™ Mouse B Cell Isolation Kit following the manufacturer's instructions (Stem Cell). All isolated B cells were cultured in a medium supplemented with B-cell activating factor (BAFF), which is essential for promoting B cell survival. BAFF binds to specific receptors on B cells, triggering signaling pathways that inhibit apoptosis and support cell survival.

### **2.11 Phospho-flow cytometry assay**

B cells were isolated from the spleens of indicated mice and kept in the 37°C incubator with 5% CO<sub>2</sub> for 3 hours. The cells were centrifuged at 400g for 5 minutes and resuspended in lymphocyte culture medium, insulin was added into the culture system to stimulate the cells for 5-, 15-, 30-, 60-, and 90 minutes prior to staining with a live/dead exclusion dye (Zombie NIR, Biolegend). Subsequently, the fixation and permeabilization with a FOXP3 staining buffer set following the manufacturer's instructions (eBioscience) were done before staining with extracellular antibodies. Cells were finally ready for flow cytometric analysis following 30 minutes of staining with phosphor-target antibodies.

### **2.12 OVA/influenza- specific Ig ELISA assay**

The day before the assay, all wells of an ELISA high-binding plate (Corning) were coated with OVA protein or influenza virus at 4°C overnight. The plate was washed with washing buffer for 5 times and blocked with PBST containing 3% FBS for 1 hour at room temperature. Diluted serum samples were added into the wells and incubated for 2 hours at room temperature. Biotinylated Ig

antibodies (Biolegend) were added to incubate for 1 hour at room temperature, followed by 30 minutes of incubation with streptavidin-horseradish peroxidase conjugate (Biolegend) at room temperature. The plate was washed for 5 minutes with washing buffer between steps. The tetramethylbenzidine substrate (Sigma) was finally added into the wells to detect horseradish peroxidase, and the whole reaction was ended by adding H<sub>2</sub>SO<sub>4</sub>. Absorbance at 450 nm was determined with a Cytation 10 plate reader (Agilent).

### 2.13 Seahorse metabolic flux assay

**Glycolysis stress test:** The day before the assay, all wells of an XFe96 cell culture microplate (Agilent) were coated with poly-D-lysine (Gibco) overnight at 4 °C. A sensor cartridge (Agilent) was hydrated in Seahorse XF calibrant medium (Agilent) overnight at 37 °C in a non-CO<sub>2</sub> incubator. On the day of the assay, B cells isolated from interested mice were cultured into the cell culture microplate. Glutamine (Gibco) was added into Seahorse XF DMEM medium (Agilent) to prepare the Seahorse Glycolysis Stress Test medium. The cell culture microplate was gently washed with Seahorse Glycolysis Stress Test medium for 5 times. Cells were kept at 37 °C in a non-CO<sub>2</sub> incubator. The needed drugs were diluted in Seahorse Glycolysis Stress Test medium and loaded into the corresponding ports of the sensor cartridge: port A-Glucose (20 μL, Fisher chemical), port B-Oligomycin (22 μL, Sigma), port C-2-DG (25 μL, Sigma). Finally, the sensor cartridge and XFe96 cell culture microplate were loaded into Seahorse XF Analyzer to run the assay (Agilent). The Seahorse Glycolysis Stress Test assesses cellular glycolytic activity by quantifying the rate at which cells convert glucose into lactate<sup>199</sup>. Lactate production is coupled with the release of protons, which acidify the extracellular environment<sup>199</sup>. The Seahorse Analyzer uses specialized sensors to measure real-time changes in the pH of the medium around the cells, reflecting their glycolytic activity<sup>199</sup>(**Figure 2.1 A-B**). Specifically, the extracellular acidification rate (ECAR) was initially measured to establish the baseline level of glycolysis under normal conditions<sup>199</sup>. The Seahorse Glycolysis Stress Test medium initially did not contain glucose<sup>199</sup>. Glucose was then injected into the wells to promote cells relying on the glycolysis pathway to generate energy and upregulate the

ECAR<sup>199</sup>. Oligomycin, an ATP synthase inhibitor, was then injected into wells to inhibit mitochondrial ATP production, thereby, forcing cells to rely more on glycolysis for ATP production, and further increasing the ECAR<sup>199</sup>. Finally, 2-Deoxy-D-Glucose (2-DG), a glycolysis inhibitor, was injected to block glycolysis, resulting in a decrease in ECAR, confirming the observed changes in acidification are due to glycolysis<sup>199</sup>.

**Mitochondrial stress test:** The day before the assay, all wells of an XFe96 cell culture microplate (Agilent) were coated with poly-D-lysine (Gibco) overnight at 4 °C. A sensor cartridge (Agilent) was hydrated in Seahorse XF calibrant medium (Agilent) overnight at 37 °C in a non-CO<sub>2</sub> incubator. On the day of the assay, B cells isolated from interested mice were cultured into the cell culture microplate. Glutamine (Gibco), sodium pyruvate (Gibco), and glucose (Fisher chemical) were added into Seahorse XF DMEM medium (Agilent) to prepare the Seahorse Mitochondrial Stress Test medium. The cell culture microplate was gently washed with Seahorse Mitochondrial Stress Test medium for 5 times. Cells were kept at 37 °C in a non-CO<sub>2</sub> incubator. The needed drugs were diluted in Seahorse Mitochondrial Stress Test medium and loaded into the corresponding ports of the sensor cartridge: port A-Oligomycin (20 μL, Sigma), port B-FCCP (22 μL, Sigma), port C-Rotenone/Antimycin A (25 μL, Sigma). Finally, the sensor cartridge and XFe96 cell culture microplate were loaded into Seahorse XF Analyzer to run the assay (Agilent). The Seahorse Mitochondrial Stress Test is a dynamic analysis that measures the activity of the OXPHOS pathway by assessing the oxygen consumption rate (OCR) of cells in real time<sup>199</sup> (**Figure 2.1 C-D**). The OCR reflects the rate at which cells consume oxygen, which is primarily driven by mitochondrial respiration<sup>199</sup>. Initially, the OCR was measured to establish the basal respiration rate<sup>199</sup>. Oligomycin was then injected to inhibit ATP synthase and decrease the OCR<sup>199</sup>. Next, carbonyl cyanide-4 (trifluoromethoxy) phenylhydrazone (FCCP), an uncoupling agent, was injected to collapse the proton gradient across the mitochondrial membrane, inducing the maximum electron transport chain activity and upregulating OCR<sup>199</sup>. Lastly, rotenone and antimycin A were injected to inhibit the early components of the electron transport chain and completely inhibit mitochondrial respiration<sup>199</sup>.

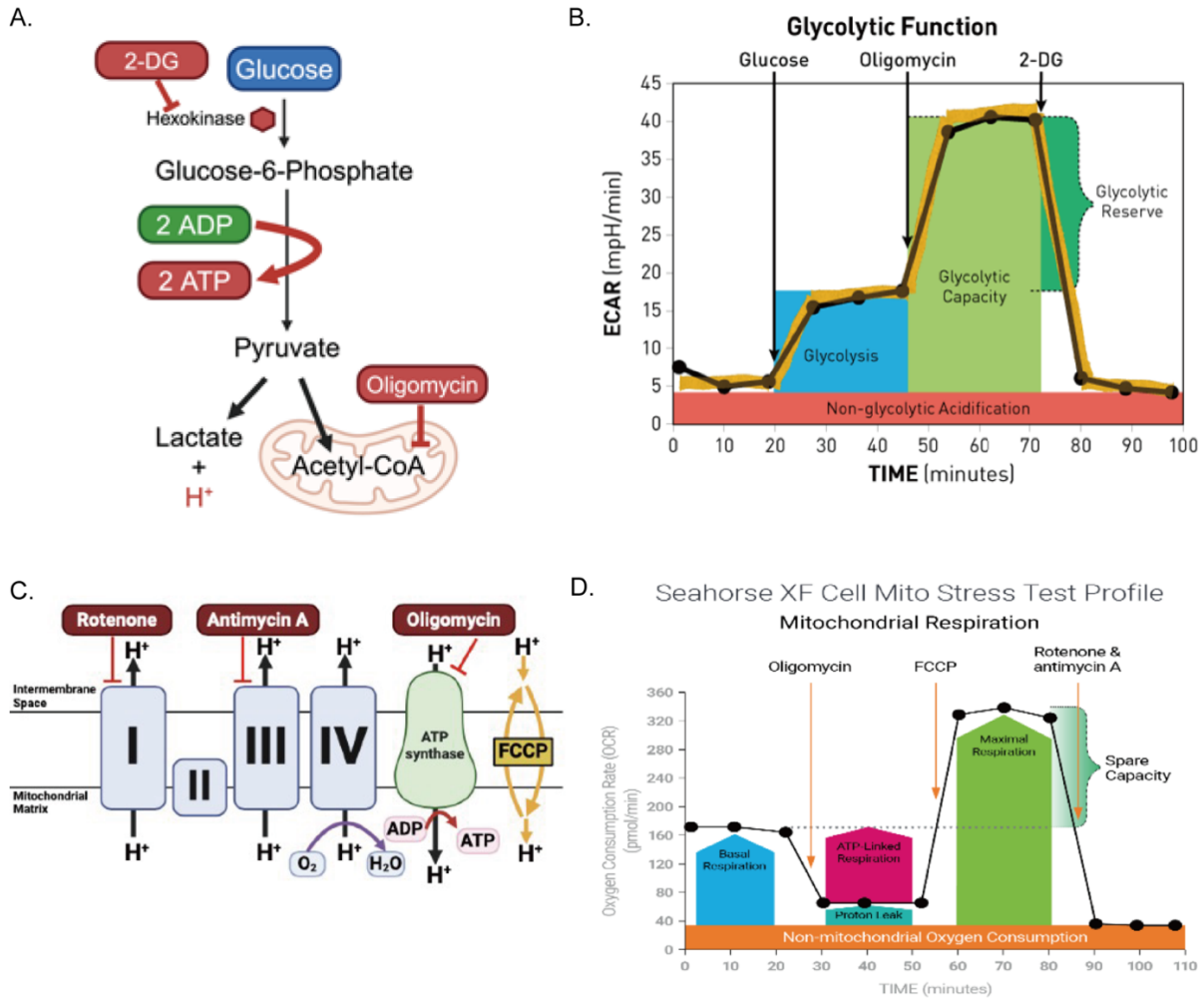


**Figure 2.1 Schematic diagram of the principle of the Seahorse metabolic flux assay. (A)** The principle of the Glycolysis Stress Test by Seahorse Extracellular Flux analysis. **(B)** Seahorse XF Glycolysis Stress Test profile of the key parameters of glycolytic functions. Sequential compound injections measure glycolysis and glycolytic capacity and allow calculation of glycolytic reserve and non-glycolytic acidification. **(C)** The principle of the Mitochondrial Stress Test by Seahorse Extracellular Flux analysis. **(D)** Seahorse XF Cell Mito Stress Test profile, showing the key parameters of mitochondrial function, including basal respiration, ATP-linked respiration, proton leak, maximal respiration, and spare capacity. Figure A-B were drawn in BioRender.com. Figure C-D were cited from the “Agilent Seahorse XF Cell Mito Stress Test Kit User Guide” and the “Agilent Seahorse XF Glycolysis Stress Test Kit User Guide”.

## 2.14 Statistical analysis

All statistical analyses were performed using GraphPad Prism 10 software. The numbers of replicates are listed as the n value in figure legends. Statistical significance was assessed using Mann-Whitney U-test or Two-Way ANOVA set at  $p < 0.05$ .

## 2.15 Table of reagents and software

**Table 2.1** List of antibodies used for flow cytometry. All listed antibodies are available commercially.

Antibodies	Clone	Source	Catalog Number
Phosflow™ PE Mouse Anti-AKT (pS473)	M89-61	BD Biosciences	561671
Phosflow™ Brilliant Violet 421 Mouse Anti-AKT (pT308)	J1-223.371	BD Biosciences	558275
Phosflow™ Alexa Fluor 488 Mouse Anti-S6	N4-41	BD Biosciences	560430
Brilliant Violet 711 anti-mouse CD45 antibody	30-F11	BioLegend	103147
PE/Cyanine7 anti-mouse CD19 antibody	1D3/CD19	BioLegend	152417
APC/Cyanine 7 anti-mouse CD19 antibody	1D3/CD19	BioLegend	152411
Brilliant Violet 421 anti-mouse CD19 antibody	1D3/CD19	BioLegend	152421
Brilliant Violet 421 anti-mouse/human CD45R/B220 antibody	RA3-6B2	BioLegend	103239

Alexa Fluor 700 anti-mouse/human CD45R/B220 antibody	RA3-6B2	BioLegend	103231
PerCP/Cyanine 5.5 anti-mouse/human CD45R/B220 antibody	RA3-6B2	BioLegend	103235
Brilliant Violet 605 anti-mouse CD95/Fas antibody	SA367H8	BioLegend	152612
PE anti-mouse CD95/Fas antibody	SA367H8	BioLegend	152607
PE/Cyanine7 anti-mouse CD95/Fas antibody	SA367H8	BioLegend	152617
Alexa Fluor 488 anti-mouse/human GL-7 antibody	GL7	BioLegend	144611
PE anti-mouse CD38 antibody	S21016F	BioLegend	165609
PE/Cyanine7 anti-mouse CD38 antibody	S21016F	BioLegend	165611
Brilliant Violet 421 anti-mouse CD38 antibody	90	BioLegend	102732
Alexa Fluor 647 anti-mouse CD138 antibody	281-2	BioLegend	142525
PE/Dazzle 594 anti-mouse CD138 antibody	281-2	BioLegend	142527
Brilliant Violet 650 anti-mouse CD138 antibody	281-2	BioLegend	142518
Alexa Fluor 488 anti-mouse CD3 antibody	17A2	BioLegend	100210

PE/Cyanine7 anti-mouse CD3 antibody	17A2	BioLegend	100219
PE/Dazzle 594 anti-mouse CD4 antibody	GK1.5	BioLegend	100456
Alexa Fluor 488 anti-mouse CD4 antibody	GK1.5	BioLegend	100425
Alexa Fluor 700 anti-mouse CD8 $\beta$ antibody	YTS156.7.7	BioLegend	126617
FITC anti-mouse CD8 $\beta$ antibody	YTS156.7.7	BioLegend	126605
Brilliant Violet 711 anti-mouse CD185 (CXCR5) antibody	L138D7	BioLegend	145529
Brilliant Violet 605 anti-mouse PD1 antibody	29F.1A12	BioLegend	135220
PerCP-Cyanine 5.5 anti-mouse PD1 antibody	RMP1-30	BioLegend	109119
Brilliant Violet 421 anti-mouse IFN- $\gamma$ antibody	XMG1.2	BioLegend	505830
PE anti-mouse TNF $\alpha$ antibody	55R-286	BioLegend	113003
PE/Dazzle 594 anti-mouse CD86 antibody	A17199A	BioLegend	159209
Pacific Blue anti-mouse CD40 antibody	3/23	BioLegend	124625
PerCP-Cy 5.5 anti-mouse I-Ab antibody	AF6-120.1	BioLegend	116415
Biotin anti-mouse IgA antibody	RMA-1	BioLegend	407003
Biotin anti-mouse IgM antibody	RMM-1	BioLegend	406503
Biotin anti-mouse IgG1 antibody	RMG1-1	BioLegend	406603

Biotin anti-mouse IgG2b antibody	RMG2b-1	BioLegend	406703
Biotin anti-mouse IgG2c antibody	MRG2c-67	BioLegend	407603
Biotin anti-mouse IgG3 antibody	RMG3-1	BioLegend	406803

**Table 2.2** List of reagents.

<b>Chemicals</b>	<b>Source</b>	<b>Catalog number</b>
Zombie NIR™ Fixable Viability Kit	BioLegend	423105
Murine OVA/I-Ab Tetramer	NIH	N/A
Murine Influenza/I-Ab Tetramer	NIH	N/A
Murine Influenza/H-2Db Tetramer	NIH	N/A
RPMI 1640 Medium	Wisent	350-002-CL
Fetal Bovine Serum	Sigma	F1051
L-glutamine	Gibco	25030081
Penicillin-Streptomycin	Sigma	P4333
2-Mercaptoethanol	Sigma	60-24-2
Sodium Pyruvate	Gibco	11360-070
DMEM Medium	Wisent	219-010-XX
Collagenase	Sigma	C0130
DNase	Sigma	D5025
Bovine Serum Albumin	Sigma	A8806
Insulin Lispro U-100	Humalog	N/A
Isoflurane	Sigma	792632
HRP Streptavidin	Biolegend	405210
Tetramethylbenzidine substrate	Sigma	T0440
Seahorse XF DMEM medium	Agilent	103680-100
Seahorse XF Calibrant solution	Agilent	103059-000
Glucose	Fisher chemical	205936
Oligomycin A	Sigma	75351

GlutaMax™ supplement	Gibco	35050061
Rotenone	Sigma	R8875
FCCP	Sigma	C2920
Antimycin A	Sigma	A8674
2-DG	Sigma	D8375
Poly-D-lysine	Gibco	A38904-01

**Table 2.3** List of commercial assays and kits used.

<b>Commercial Assays/Kits</b>	<b>Source</b>	<b>Catalog Number</b>
EasySep™ Mouse B Cell Isolation Kit	Stem Cell	19854
FOXP3/Transcription Factor Staining Buffer Set	eBioscience	00-5523-00
Anti-Rat and Anti-Hamster Igk Negative Control Compensation Particles Set	BD Biosciences	552845

**Table 2.4** List of software used for data analysis.

<b>Software</b>	<b>Source</b>	<b>Catalog number</b>
FlowJo	FlowJo, LLC	N/A
GraphPad Prism 10	GraphPad Softwares	N/A

## Chapter 3: The impact of insulin signaling and IR on B cell activation and metabolism

### 3.1 Introduction

Obesity is characterized by chronic low-grade inflammation conditions and predisposes to IR, which is related to many diseases that significantly increase mortality<sup>17, 18</sup>. Recent studies have demonstrated that obesity is accompanied by impaired adaptive immunity elicited by vaccination and virus infection<sup>131-133</sup>. B cells contribute significantly to adaptive immunity, and B cells have been reported to show alterations in the recruitment and function under obese conditions<sup>89, 90</sup>. Upon encountering foreign antigens, B cells need to undergo activation and differentiation to ultimately produce high-affinity antibodies essential for maintaining humoral immunity. Many metabolic signaling pathways work together to support the activation and function of B cells. Among them, the glucose uptake and glycolysis pathways are rapidly upregulated in activated B cells to meet the energy and intermediate metabolites requirement of proliferating B cells<sup>170</sup>. Insulin is an essential hormone for maintaining glucose homeostasis in insulin-dependent tissues and cells. Recent studies have reported that immune cells also rely on insulin signaling to modulate glucose uptake and related metabolic signaling pathways<sup>175-180</sup>. Existing studies showed that B cells express *Insr* through development<sup>181</sup>. However, unlike other immune cells that have been well described, the role of insulin signaling in B cells is an ongoing research direction and needs deeper investigation. Therefore, this chapter aims to explore if and how insulin signaling and IR regulate the activation and metabolism of B cells.

### 3.2 Results

#### 3.2.1 *DIO induced IR in B cells*

Serum insulin levels in mammals, including humans, can fluctuate between <1 ng/mL (fasting) and 11 ng/mL (postprandial) in healthy individuals and reach as high as 38 ng/mL in IR individuals<sup>179</sup>. I first isolated splenic B cells from C57BL/6 mice and stimulated them using 10

ng/mL of insulin to see if insulin induces the activation of insulin signaling in B cells. B cells were collected at indicated time points, and Phospho-flow analysis was used to determine the changes in the phosphorylation level of insulin signaling key proteins, including AKT and S6 ribosomal protein (S6RP). As shown in **Figure 3.1**, fresh B cells stimulated with insulin showed phosphorylation of AKT on S473 (**Figure 3.1 A-B**) and T308 (**Figure 3.1 C-D**). The phosphorylation of S6RP was also detected (**Figure 3.1 E-F**).

Next, I tested if 20 weeks of HFD feeding impacts insulin signaling in B cells. 6 weeks old C57BL/6 male mice were fed a 60% kcal HFD for 20 weeks to induce IR. In addition, age-matched C57BL/6 male mice fed a 4% kcal NCD were used as baseline controls. 20 weeks later, to assess responses to exogenous insulin and insulin sensitivity, I conducted an ITT, followed by an IPGTT a week apart to measure the ability to produce and respond to insulin. Compared with NCD-fed mice, the HFD-fed mice exhibited significantly higher body weights (**Figure 3.2 A**). In response to an insulin challenge, the NCD-fed mice showed a significant reduction in their blood glucose levels compared with HFD-fed mice (**Figure 3.2 B-C**), indicating a normal insulin response. Moreover, there was a significant decrease in glucose excursion in HFD-fed mice compared with NCD-fed mice during the IPGTT (**Figure 3.2 D-E**), indicating impairment in insulin production and an abnormal insulin response. Next, I isolated splenic B cells from NCD-fed and HFD-fed mice and stimulated them using 10 ng/mL of insulin for indicated time points. The changes in the phosphorylation level of insulin signaling key proteins were then measured using Phospho-flow analysis. As shown in **Figure 3.3**, B cells from HFD-fed mice showed decreased insulin-stimulating p-AKT<sup>S473</sup> (**Figure 3.3 A-B**), p-AKT<sup>T308</sup> (**Figure 3.3 C-D**), and p-S6RP (**Figure 3.3 E-F**). Taken together, these data suggested that insulin induced the activation of insulin signaling in B cells, whereas 20 weeks of HFD-feeding impaired the insulin signaling in B cells, leading to IR.

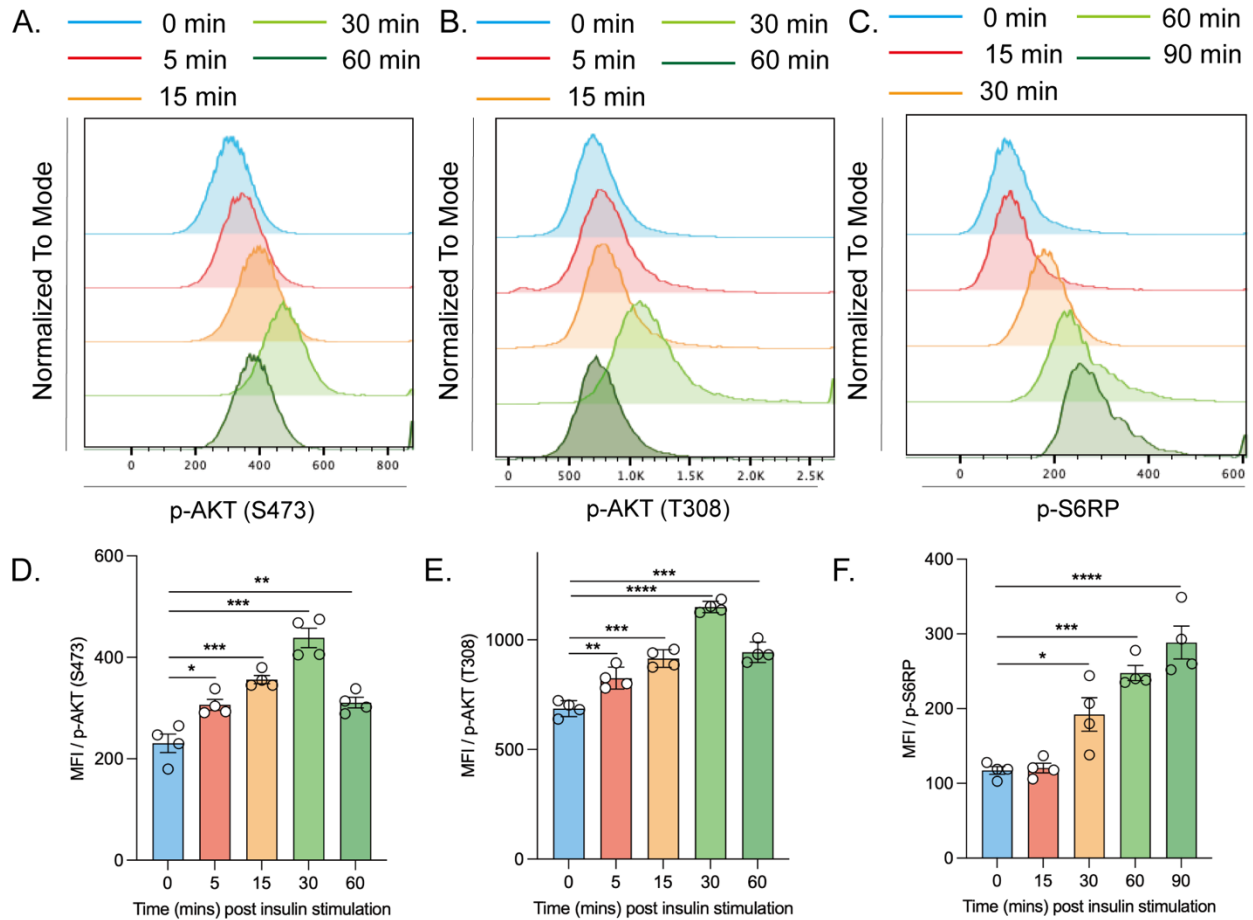


**Figure 3.1 Insulin induced the activation of insulin signaling in B cells.** Splenic B cells were isolated from C57BL/6 mice using EasySep™ Mouse B Cell Isolation Kit (Stem Cell) and stimulated using 10 ng/mL of insulin for 5-, 15-, 30-, 60-, and 90- minutes. (A-C) Histogram showing the distribution of p-AKTS<sup>473</sup> (A), p-AKT<sup>T308</sup> (B), and p-S6RP (C) mean fluorescence intensity (MFI) in B cells stimulated with insulin for different time points. (D-F) The changes in MFI of p-AKTS<sup>473</sup> (D), p-AKT<sup>T308</sup> (E), and p-S6RP (F) in stimulated B cells were measured by flow cytometry (n=4, each dot represents one mouse). \*P<0.05, \*\*P<0.01, \*\*\*P<0.001, \*\*\*\*P<0.0001 with Mann Whitney U-test. Data are represented as mean±SEM.

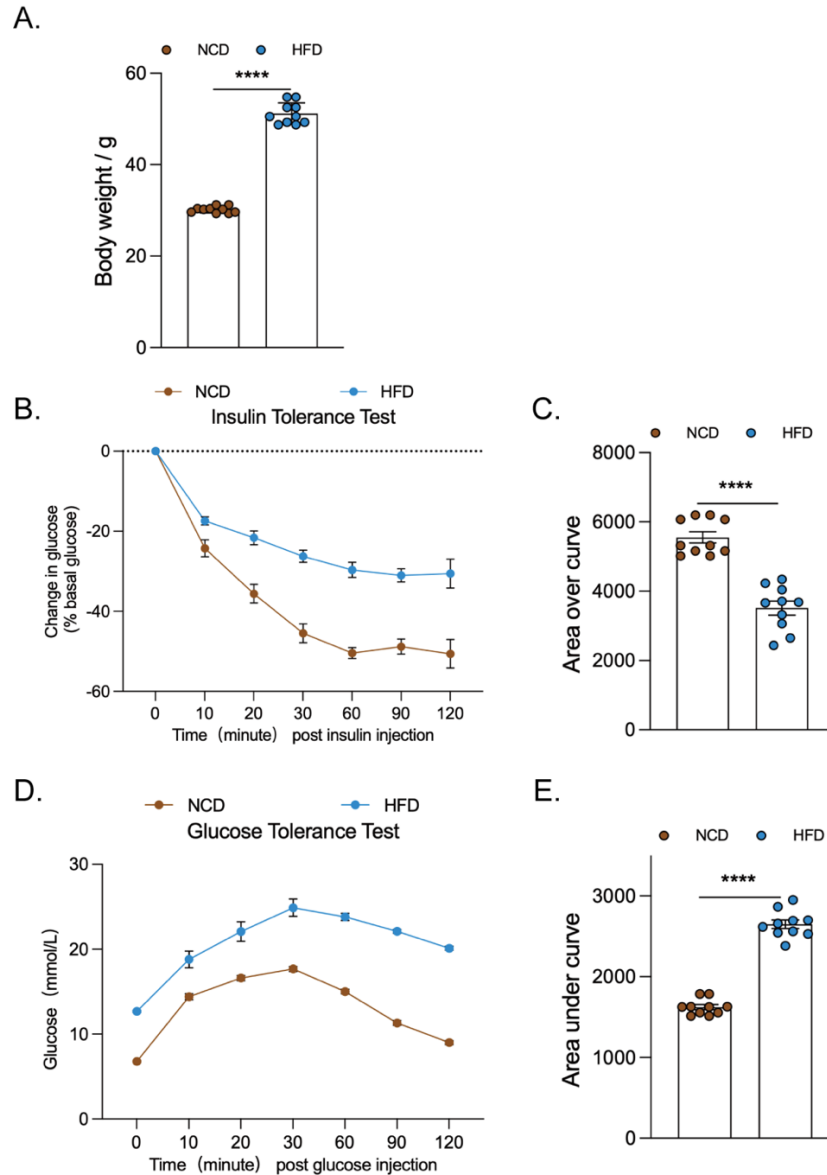


**Figure 3.2 HFD-feeding induced IR.** 6-week-old male C57BL/6 mice were fed a 60% kcal HFD for 20 weeks. Age-matched NCD-fed mice were used as baseline controls. (A) Body weight of NCD-fed or HFD-fed mice (n=10, each dot represents one mouse). (B) Glucose excursion during an ITT. Blood glucose was expressed as a percent change in blood glucose from time point 0. (C) Integrated area above the curve during a 120-min ITT (n=10, each dot represents one mouse). (D) Glucose excursion during an IPGTT. (E) Integrated area under the curve of glucose excursion during a 120-min IPGTT (n=10, each dot represents one mouse). \*\*\*\*P<0.0001 with Mann Whitney U-test. Data are represented as mean±SEM.

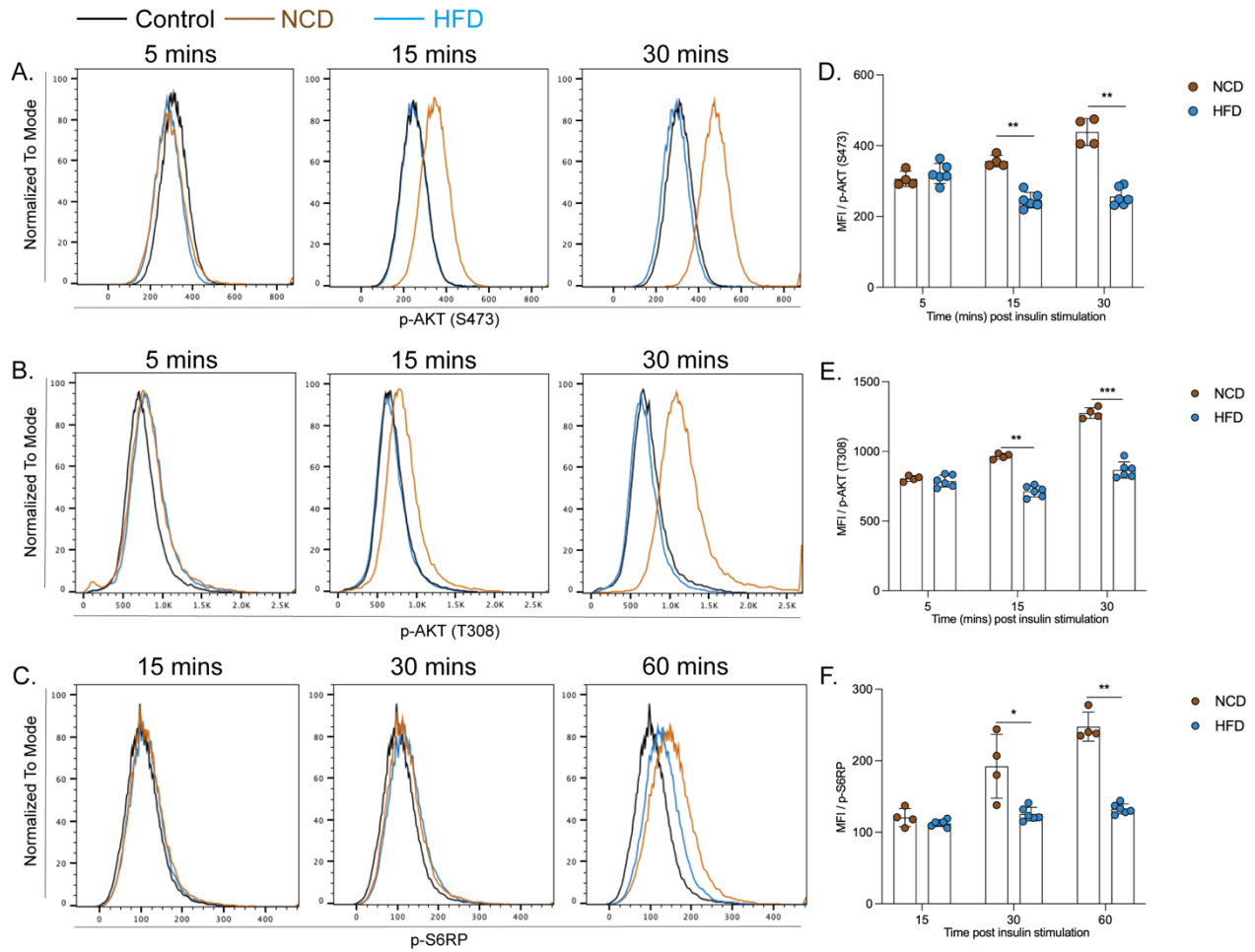


**Figure 3.3 DIO induced IR in B cells.** Splenic B cells were isolated from NCD- or HFD-fed mice using EasySep™ Mouse B Cell Isolation Kit (Stem Cell) and stimulated using 10 ng/mL of insulin for 5-, 15-, 30-, and 60- minutes. (A-C) Histogram showing the distribution of p-AKT<sup>S473</sup> (A), p-AKT<sup>T308</sup> (B), and p-S6RP (C) MFI in B cells stimulated with insulin for different time points. (D-F) The changes in MFI of p-AKT<sup>S473</sup> (D), p-AKT<sup>T308</sup> (E), and p-S6RP (F) in B cells were measured by flow cytometry. B cells isolated from HFD-fed mice showed a decrease in insulin-stimulating p-AKT<sup>S473</sup> (D), p-AKT<sup>T308</sup> (E), and p-S6RP (F) (n=4-6, each dot represents one mouse). \*P<0.05, \*\*P<0.01, \*\*\*P<0.001, \*\*\*\*P<0.0001 with Mann Whitney U-test. Data are represented as mean±SEM.

### ***3.2.2 Insulin stimulation and B cell-intrinsic IR did not affect LPS- and CpG-stimulated B cell activation in vitro***

Next, to test the hypothesis that insulin signaling impacts B cell activation, I stimulated splenic B cells isolated from C57BL/6 mice with activating agents (LPS, CpG) and different concentrations of insulin (0, 10, 100 ng/mL) for 48 hours. The expression levels of costimulatory molecules and MHC class II, which indicate the activation of B cells, were measured via flow cytometry. LPS is a potent stimulant of B cells, which binds to TLR4 and mediates B cell proliferation and activation via the PI3K-dependent signaling pathway<sup>200</sup>. Cytidine monophosphate guanosine oligodeoxynucleotides (CpG) can be divided into five different categories based on their sequence, secondary structure, and effect on human peripheral blood mononuclear cells (PBMCs)<sup>201</sup>. In my experiments, class B CpG, which is specific for B cells, was used to stimulate B cells via binding to TLR9<sup>201</sup> and compared with LPS. As shown in **Figure 3.4**, I observed a significant increase in CD86 (**Figure 3.4 A-C**) and MHC class II (**Figure 3.4 D-F**) expression in LPS-stimulated B cells versus unstimulated controls. However, B cells stimulated with LPS and different concentrations of insulin showed no differences compared with non-insulin treatment controls. CpG-stimulated B cells showed results similar to LPS-stimulated B cells, the expression level of CD86 (**Figure 3.4 G-I**) and MHC class II (**Figure 3.4 J-L**) showed a significant increase in CpG-stimulated B cells, and insulin supplementation did not affect the expression of CD86 and MHC class II.

I next tested the effect of insulin signaling impairment on B cell activation. Splenic B cells isolated from WT (CD19 Cre<sup>+/-</sup> InsR<sup>wt/wt</sup>) and B cell-specific InsR-deficient (CD19 Cre<sup>+/-</sup> InsR<sup>fl/fl</sup>) mice were subjected to the same treatments as B cells isolated from C57BL/6 mice. **Figure 3.5** shows that after LPS stimulation, WT and InsR-deficient B cells all showed a significant increase in the expression of CD86 (**Figure 3.5 A-C**), MHC class II (**Figure 3.5 D-F**), and CD40 (**Figure 3.5 G-I**). Similarly, CpG-stimulated WT and InsR-deficient B cells also showed a significant increase in the expression of CD86 (**Figure 3.6 A-C**), MHC class II (**Figure 3.6 D-F**), and CD40 (**Figure 3.6 G-I**). Moreover, no differences in the expression of costimulatory molecules and MHC

class II were observed after insulin supplementation, and no differences in the expression of costimulatory molecules and MHC class II were observed between WT and InsR-deficient B cells.

Taken together, these data demonstrated that insulin stimulation and B cell-intrinsic IR both did not affect the expression of costimulatory molecules and MHC class II in stimulated B cells, suggesting that the activation and disruption of insulin signaling may have no effect on B cell activation under the above intro conditions.

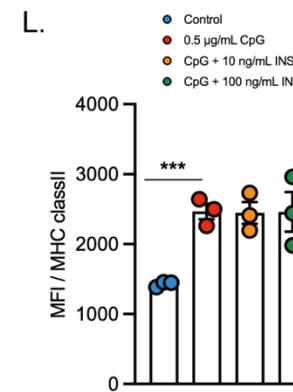
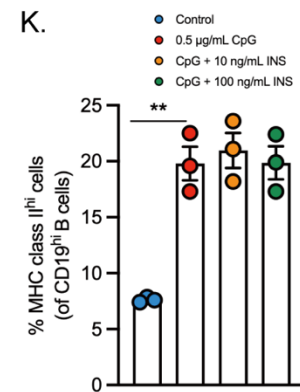
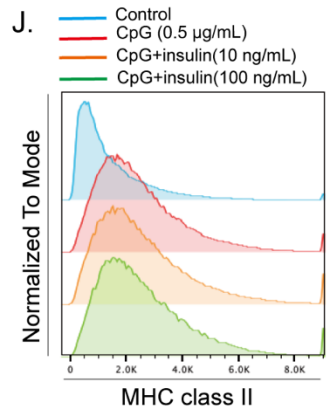
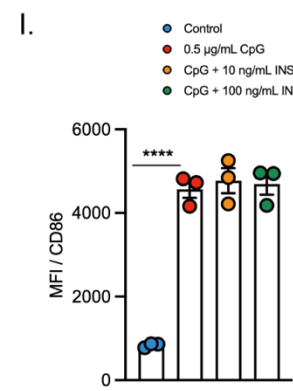
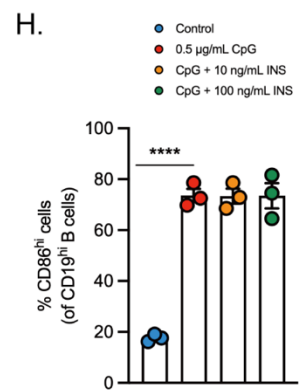
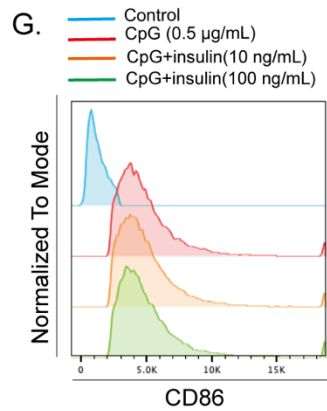
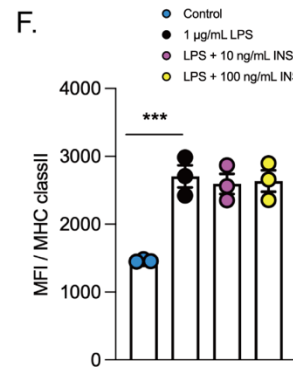
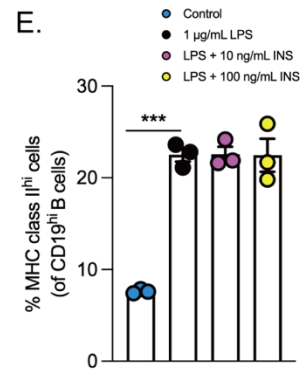
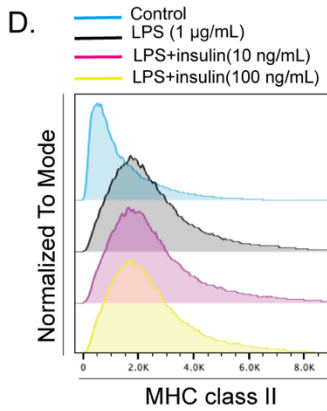
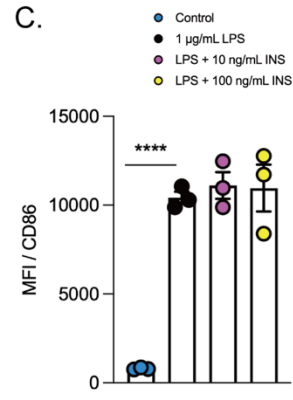
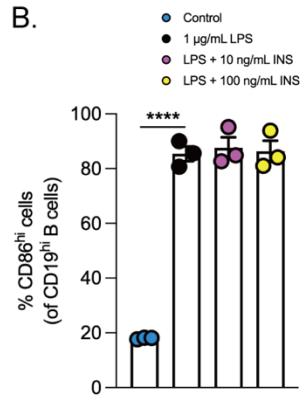
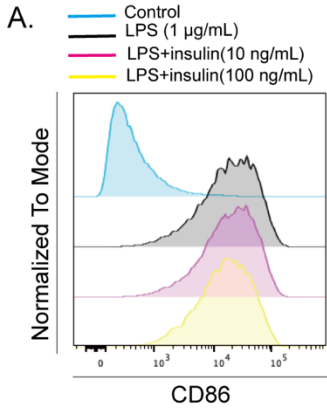


**Figure 3.4 Insulin stimulation did not impact LPS- and CpG-stimulated B cell activation *in vitro*.** (A-F) Splenic B cells were isolated from C57BL/6 mice using EasySep™ Mouse B Cell Isolation Kit (Stem Cell) and stimulated with 1 µg/mL LPS and different concentrations of insulin (10, 100 ng/mL) for 48 hours. (A, D) Histogram showing the distribution of CD86 (A) and MHC class II (D) MFI in B cells stimulated with LPS and insulin for different time points. (B, E) Changes in the percentage of CD86<sup>hi</sup> (B) and MHC class II<sup>hi</sup> (E) cells were measured by flow cytometry (gated out of CD19<sup>hi</sup> cells, n=3, each dot represents one mouse). (C, F) Changes in the MFI of CD86 (C) and MHC class II (F) in stimulated B cells were measured by flow cytometry (n=3, each dot represents one mouse). (G-L) Splenic B cells were isolated from C57BL/6 mice using EasySep™ Mouse B Cell Isolation Kit (Stem Cell) and stimulated with 0.5 µg/mL CpG and different concentrations of insulin (10, 100 ng/mL) for 48 hours. (G, J) Histogram showing the distribution of CD86 (G) and MHC class II (J) MFI in B cells stimulated with CpG and insulin for different time points. (H, K) Changes in the percentage of CD86<sup>hi</sup> (H) and MHC class II<sup>hi</sup> (K) cells were measured by flow cytometry (gated out of CD19<sup>hi</sup> cells, n=3, each dot represents one mouse). (I, L) Changes in the MFI of CD86 (I) and MHC class II (L) in stimulated B cells were measured by flow cytometry (n=3, each dot represents one mouse). \*\*P<0.01, \*\*\*P<0.001, \*\*\*\*P<0.0001 with Mann Whitney U-test. Data are represented as mean±SEM.

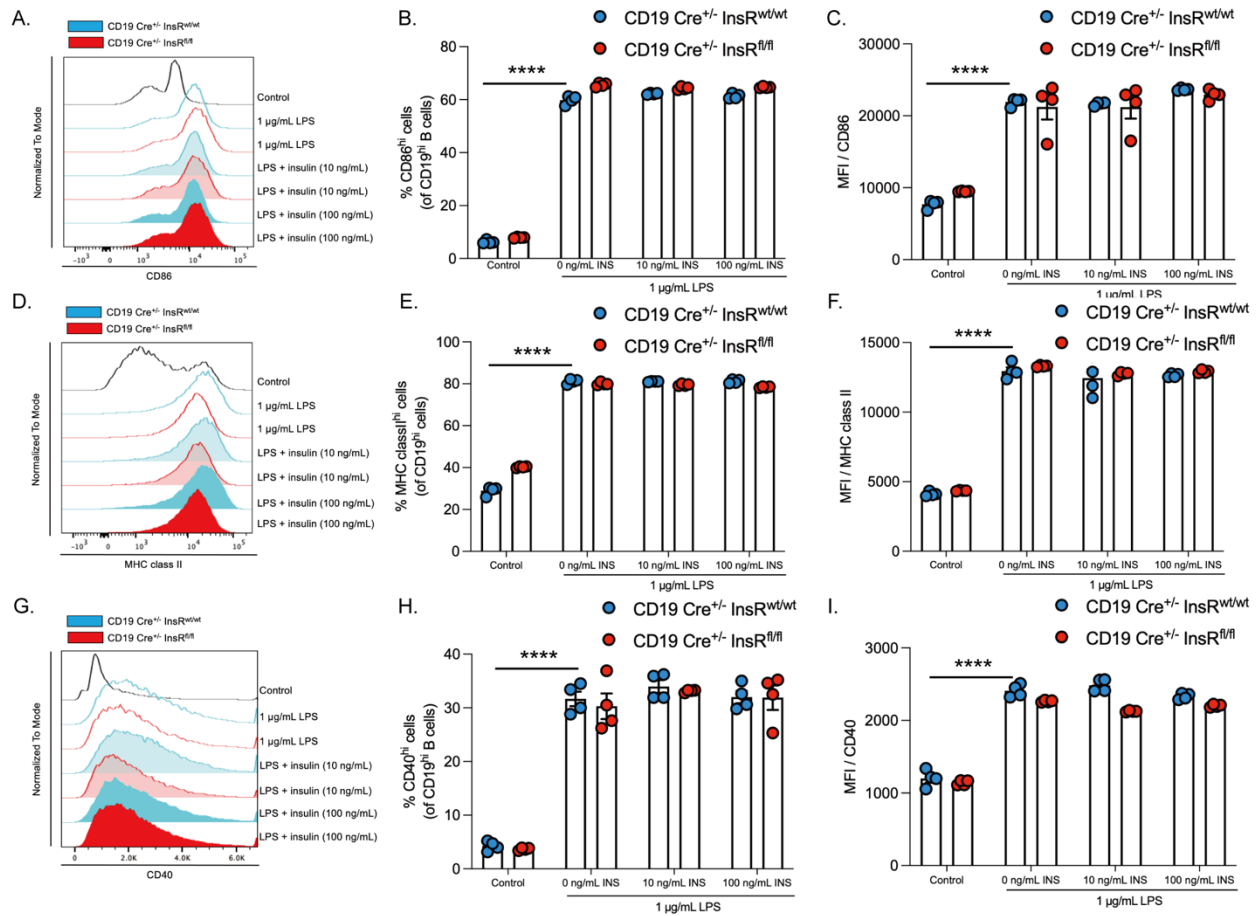


**Figure 3.5 B cell-intrinsic IR did not impact LPS-stimulated B cell activation *in vitro*.** Splenic B cells were isolated from WT (CD19 Cre<sup>+/-</sup> InsR<sup>wt/wt</sup>) and B cell-specific InsR-deficient (CD19 Cre<sup>+/-</sup> InsR<sup>fl/fl</sup>) mice using EasySep™ Mouse B Cell Isolation Kit (Stem Cell) and stimulated with 1 µg/mL LPS and different concentrations of insulin (10, 100 ng/mL) for 48 hours. (A, D, G) Histogram showing the distribution of CD86 (A), MHC class II (D), and CD40 (G) MFI in B cells stimulated with LPS and insulin for different time points. (B, E, H) Changes in the percentage of CD86<sup>hi</sup> (B), MHC class II<sup>hi</sup> (E), and CD40<sup>hi</sup> (H) cells were measured by flow cytometry (gated out of CD19<sup>hi</sup> cells, n=4, each dot represents one mouse). (C, F, I) Changes in the MFI of CD86 (C), MHC class II (F), and CD40 (I) in stimulated B cells were measured by flow cytometry (n=4, each dot represents one mouse). \*\*\*\*P<0.0001 with Mann Whitney U-test. Data are represented as mean±SEM.

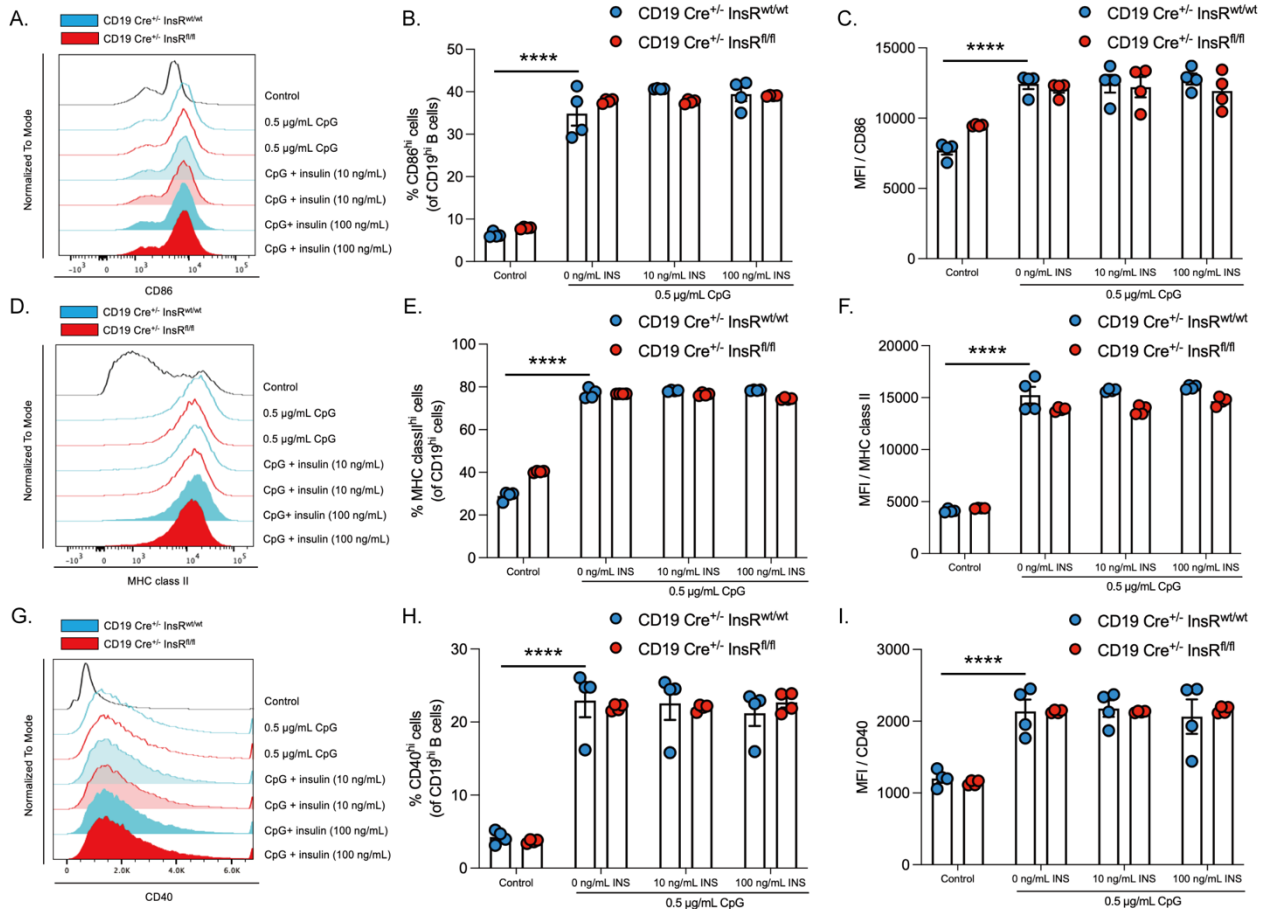


**Figure 3.6 B cell-intrinsic IR did not impact CpG-stimulated B cell activation *in vitro*.** Splenic B cells were isolated from WT (CD19 Cre<sup>+/-</sup> InsR<sup>wt/wt</sup>) and B cell-specific InsR-deficient (CD19 Cre<sup>+/-</sup> InsR<sup>fl/fl</sup>) mice using EasySep™ Mouse B Cell Isolation Kit (Stem Cell) and stimulated with 0.5 µg/mL CpG and different concentrations of insulin (10, 100 ng/mL) for 48 hours. (A, D, G) Histogram showing the distribution of CD86 (A), MHC class II (D), and CD40 (G) MFI in B cells stimulated with CpG and insulin for different time points. (B, E, H) Changes in the percentage of CD86<sup>hi</sup> (B), MHC class II<sup>hi</sup> (E), and CD40<sup>hi</sup> (H) cells were measured by flow cytometry (gated out of CD19<sup>hi</sup> cells, n=4, each dot represents one mouse). (C, F, I) Changes in the MFI of CD86 (C), MHC class II (F), and CD40 (I) in stimulated B cells were measured by flow cytometry (n=4, each dot represents one mouse). \*\*\*\*P<0.0001 with Mann Whitney U-test. Data are represented as mean±SEM.

### 3.2.3 *Insulin stimulation regulated glycolytic and oxidative metabolism in LPS- and CpG-stimulated B cells*

Insulin signaling is known to upregulate nutrient uptake, biosynthetic, and energy metabolism in many cells of the body<sup>202</sup>. Given the strong links between metabolism and immune cell function, even though insulin signaling may have no impact on B cell activation *in vitro*, it still has the potential to regulate B cell differentiation through regulating B cell metabolism. I next measured the changes in the glycolysis and OXPHOS pathways in B cells under indicated culture conditions using Seahorse metabolic flux analysis (Agilent).

I first measured the changes in aerobic glucose metabolism and mitochondrial respiration in B cells stimulated using LPS and different concentrations of insulin (0, 10, 100 ng/mL) for 48 hours. As shown in **Figure 3.7**, LPS stimulation increased aerobic glucose metabolism and mitochondrial respiration in B cells (**Figure 3.7 A, F**). Moreover, insulin demonstrated the ability to regulate both glycolytic and oxidative metabolism in LPS-stimulated B cells (**Figure 3.7 B, G**). The ECAR data collected during the assay is commonly analyzed to determine various parameters of glycolysis, including basal glycolytic rate, glycolytic capacity, and glycolytic reserve<sup>199</sup> (**Figure 2.1 A-B**). Specifically, the basal glycolytic rate was measured as described in section 2.13, and stands for the glycolysis under basal conditions<sup>199</sup>. The glycolytic capacity refers to the maximum rate at which a cell can carry out glycolysis to produce ATP<sup>199</sup>. Moreover, the glycolytic reserve is the difference between the glycolytic capacity and basal glycolytic rate, which indicates the ability of a cell to increase glycolysis under conditions of increased energy demand or metabolic stress<sup>199</sup>. By analyzing collected ECAR data, I observed that LPS stimulation increased the basal glycolysis, glycolytic capacity, and glycolytic reserve in B cells, which were further enhanced by insulin supplementation (**Figure 3.7 C-E**).

Similar to ECAR, the OCR data collected during the assay is commonly analyzed to determine various parameters of mitochondrial respiration, including basal respiration, ATP-linked

respiration, maximal respiration, and spare capacity<sup>199</sup> (**Figure 2.1 C-D**). Basal respiration stands for the mitochondrial respiration under basal conditions<sup>199</sup>. The difference between OCR measured before and after oligomycin injection refers to ATP-linked respiration, reflects the portion of cellular respiration used to produce ATP<sup>199</sup>. The remaining OCR after oligomycin injection represents proton leak respiration, which is the oxygen consumption not coupled to ATP production<sup>199</sup>. Maximal respiration refers to the maximal respiratory capacity of cells, which allows the assessment of the maximum potential for mitochondrial respiration<sup>199</sup>. Moreover, the OCR data can also be used to determine the spare respiratory capacity that indicates the ability of cells to respond to increased energy demands or metabolic stress<sup>199</sup>. By analyzing OCR data, I observed that LPS stimulation increased the maximal respiration and spare capacity in B cells (**Figure 3.7 J-K**). In contrast, no differences were observed in basal respiration and ATP-linked respiration (**Figure 3.7 H-I**). Interestingly, insulin supplementation increased basal respiration and ATP-linked respiration but not maximal respiration and spare capacity in LPS-stimulated B cells (**Figure 3.7 H-K**).

Next, CpG was used to stimulate B cells and the same analysis was performed. Like LPS, CpG stimulation significantly increased the aerobic glucose metabolism and mitochondrial respiration in B cells (**Figure 3.8 A, F**), and insulin demonstrated the ability to regulate both glycolytic and oxidative metabolism in CpG-stimulated B cells (**Figure 3.8 B, G**). Moreover, by analyzing ECAR data, I observed that CpG stimulation had no effect on basal glycolysis but increased glycolytic capacity and glycolytic reserve (**Figure 3.8 C-D**). Additionally, basal glycolysis and glycolytic capacity, but not glycolytic reserve increased after insulin supplementation (**Figure 3.8 C-E**). Regarding the OCR data, CpG stimulation increased the maximal respiration and spare capacity in B cells, which is consistent with LPS stimulation (**Figure 3.8 J-K**). Additionally, supplementation with 10 ng/mL of insulin increased basal respiration and ATP-linked respiration in CpG-stimulated B cells, whereas a 100 ng/mL insulin supplementation resulted in a decrease in these parameters (**Figure 3.8 H-I**). CpG-stimulated B cells with both 10 ng/mL of insulin supplementation and 100

ng/mL of insulin supplementation showed an increase in the maximal respiration (**Figure 3.8 J**). However, both concentrations of insulin had no effect on the spare capacity (**Figure 3.8 K**).

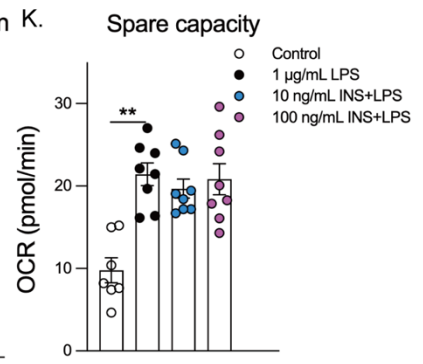
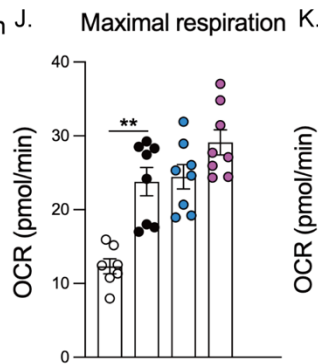
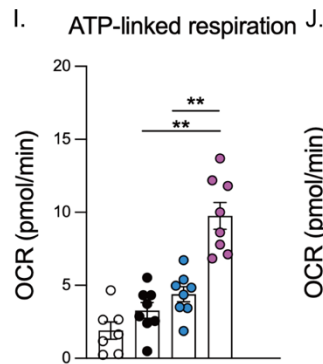
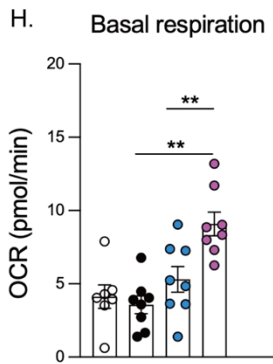
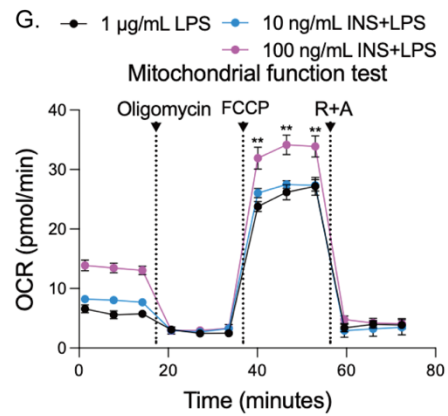
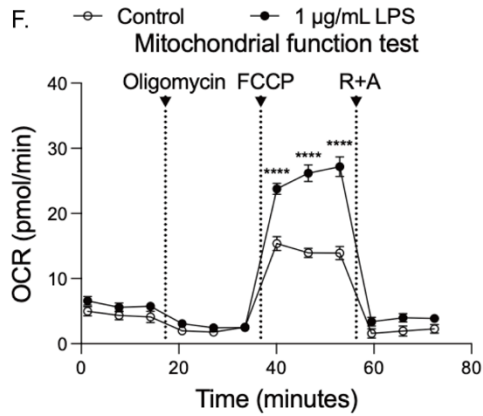
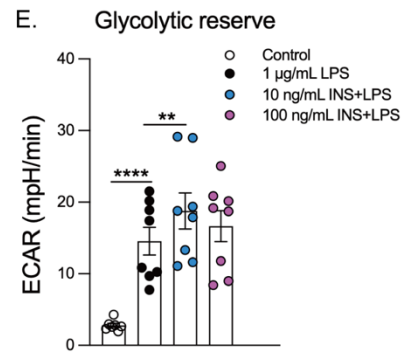
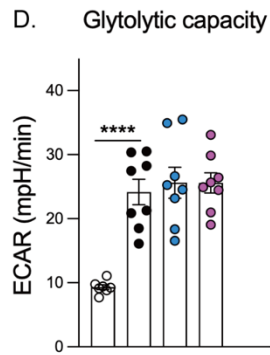
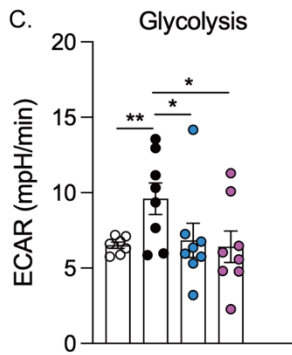
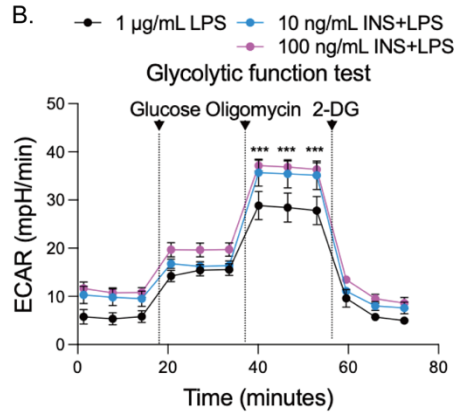
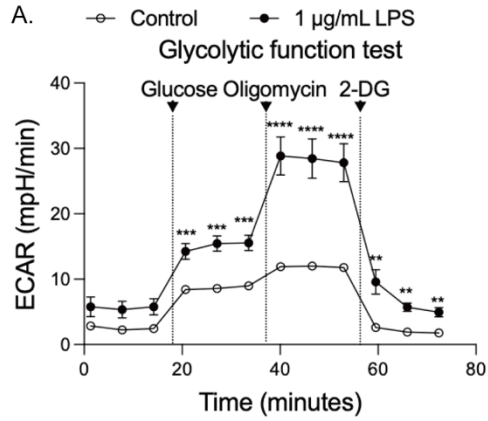


**Figure 3.7 Insulin stimulation regulated glycolytic and oxidative metabolism in LPS-stimulated B cells.** (A-B) B cells were isolated from C57BL/6 mice using EasySep™ Mouse B Cell Isolation Kit (Stem Cell). (A) Real-time changes in ECAR ratios in isolated B cells stimulated with 1 µg/mL LPS for 48 hours were measured using a Seahorse metabolic flux analyzer. (B) Real-time changes in ECAR ratios in isolated B cells stimulated with 1 µg/mL LPS and different concentrations of insulin (10, 100 ng/mL) for 48 hours were measured using a Seahorse metabolic flux analyzer. (C-E) Changes in basal glycolysis (C), glycolytic capacity (D), and glycolytic reserve (E) in stimulated B cells were assessed by analyzing ECAR data (n=7-8, each dot represents one replicate). (F-G) B cells were isolated from C57BL/6 mice using EasySep™ Mouse B Cell Isolation Kit (Stem Cell). (F) Real-time changes in OCR ratios in isolated B cells stimulated with 1 µg/mL LPS for 48 hours were measured using a Seahorse metabolic flux analyzer. (G) Real-time changes in OCR ratios in isolated B cells stimulated with 1 µg/mL LPS and different concentrations of insulin (10, 100 ng/mL) for 48 hours were measured using a Seahorse metabolic flux analyzer. (H-K) Changes in basal respiration (H), ATP-linked respiration (I), maximal respiration (J), and spare capacity (K) in stimulated B cells were assessed by analyzing OCR data (n=7-8, each dot represents one replicate). Each mouse was subjected to two or three replicates, and two independent experiments were performed. \*P<0.05, \*\*P<0.01, \*\*\*P<0.001, \*\*\*\*P<0.0001 with Two-Way ANOVA (A, B, F, G) or Mann Whitney U-test (C-E, H-K). Data are represented as mean±SEM.

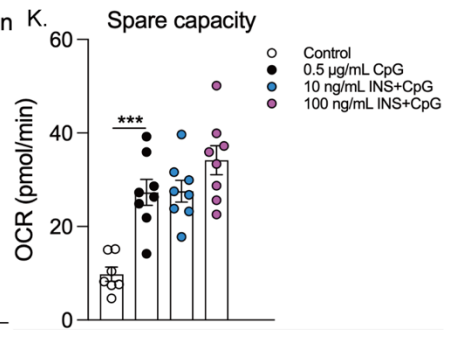
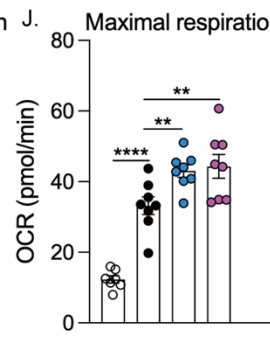
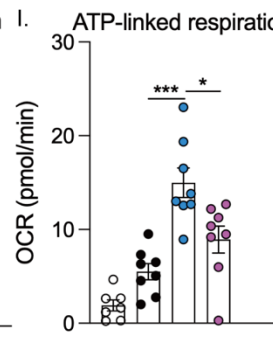
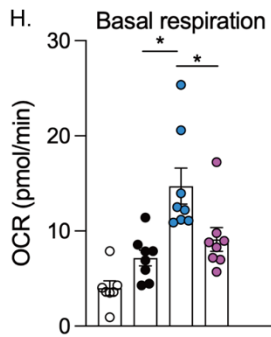
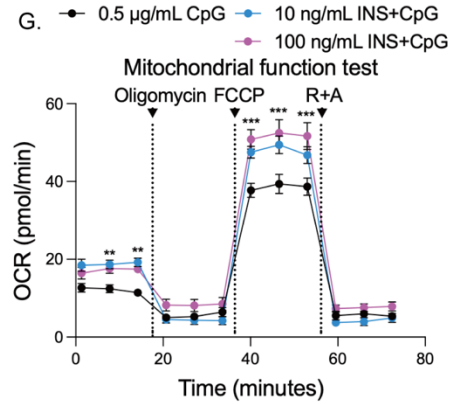
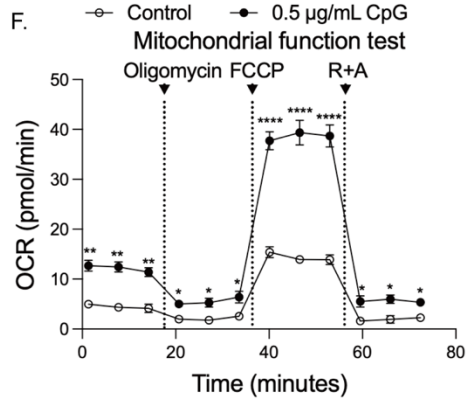
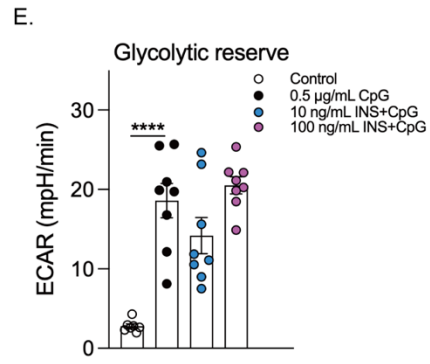
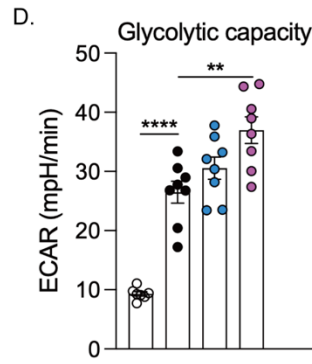
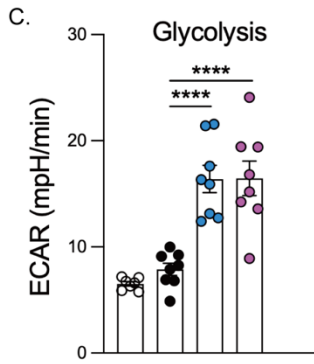
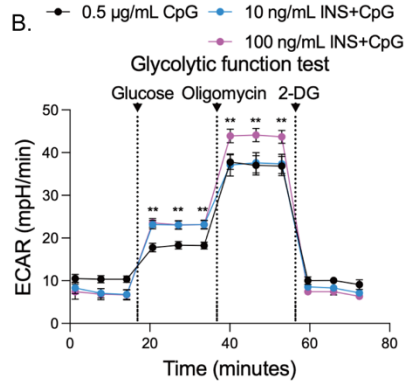
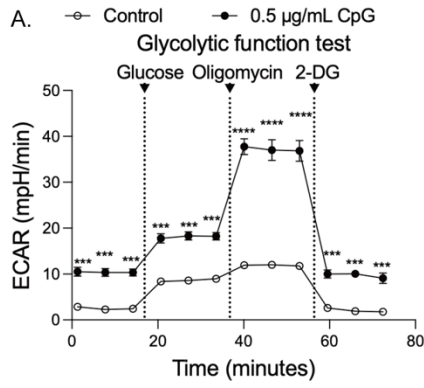


**Figure 3.8 Insulin stimulation regulated glycolytic and oxidative metabolism in CpG-stimulated B cells.** (A-B) B cells were isolated from C57BL/6 mice using EasySep™ Mouse B Cell Isolation Kit (Stem Cell). (A) Real-time changes in ECAR ratios in isolated B cells stimulated with 0.5 µg/mL CpG for 48 hours were measured using a Seahorse metabolic flux analyzer. (B) Real-time changes in ECAR ratios in isolated B cells stimulated with 0.5 µg/mL CpG and different concentrations of insulin (10, 100 ng/mL) for 48 hours were measured using a Seahorse metabolic flux analyzer. (C-E) Changes in basal glycolysis (C), glycolytic capacity (D), and glycolytic reserve (E) in stimulated B cells were assessed by analyzing ECAR data (n=7-8, each dot represents one replicate). (F-G) B cells were isolated from C57BL/6 mice using EasySep™ Mouse B Cell Isolation Kit (Stem Cell). (F) Real-time changes in OCR ratios in isolated B cells stimulated with 0.5 µg/mL CpG for 48 hours were measured using a Seahorse metabolic flux analyzer. (G) Real-time changes in OCR ratios in isolated B cells stimulated with 0.5 µg/mL CpG and different concentrations of insulin (10, 100 ng/mL) for 48 hours were measured using a Seahorse metabolic flux analyzer. (H-K) Changes in basal respiration (H), ATP-linked respiration (I), maximal respiration (J), and spare capacity (K) in stimulated B cells were assessed by analyzing OCR data (n=7-8, each dot represents one replicate). Each mouse was subjected to two or three replicates, and two independent experiments were performed. \*P<0.05, \*\*P<0.01, \*\*\*P<0.001, \*\*\*\*P<0.0001 with Two-Way ANOVA (A, B, F, G) or Mann Whitney U-test (C-E, H-K). Data are represented as mean±SEM.

### ***3.2.4 DIO-induced IR regulated glycolytic and oxidative metabolism in LPS- and CpG-stimulated B cells***

To test whether my findings on insulin-resistant B cells are recapitulated in B cells that are rendered IR in an obesity model, I next measured the changes in aerobic glucose metabolism and mitochondrial respiration in stimulated splenic B cells isolated from NCD-fed and HFD-fed mice. B cells were treated under the conditions described in section 3.2.3, and a Seahorse metabolic flux analyzer was used to measure metabolic flux. As shown in **Figure 3.9**, compared with normal B cells, DIO-induced insulin-resistant B cells showed a decrease in aerobic glucose metabolism but not mitochondrial respiration after LPS stimulation (**Figure 3.9 A, F**). Moreover, insulin supplementation increased both metabolisms and led DIO-induced insulin-resistant B cells to show a reduction in mitochondrial respiration (**Figure 3.9 B, G**). By analyzing ECAR data, I observed that DIO induced IR impaired the glycolytic capacity and glycolytic reserve in LPS-stimulated B cells, and insulin supplementation exacerbated the reduction (**Figure 3.9 D-E**). Moreover, the basal glycolysis showed no difference after LPS stimulation but reduced after insulin supplementation (**Figure 3.9 C**). I also observed that DIO induced IR impaired the basal respiration and ATP-linked respiration in B cells after LPS stimulation, which did not exacerbate after insulin supplementation (**Figure 3.9 H-I**). Moreover, the maximal respiration and spare capacity showed no differences after LPS stimulation but reduced after insulin supplementation (**Figure 3.9 J-K**).

Similar experiments were performed with B cells stimulated with CpG. Similar to LPS-stimulated B cells, DIO-induced insulin-resistant B cells showed a decrease in aerobic glucose metabolism but not mitochondrial respiration after CpG stimulation (**Figure 3.10 A, F**), and insulin supplementation further reduced aerobic glucose metabolism and initiated the reduction in mitochondrial metabolism (**Figure 3.10 B, G**). DIO-induced insulin-resistant B cells showed a decrease in all parameters of aerobic glucose metabolism after CpG stimulation, which were exacerbated after insulin supplementation (**Figure 3.10 C-E**). Moreover, all parameters of mitochondrial respiration, except for spare capacity, showed the same trend as parameters of

aerobic glucose metabolism (**Figure 3.10 H-J**). However, spare capacity showed no difference after CpG with or without insulin stimulation (**Figure 3.10 K**).

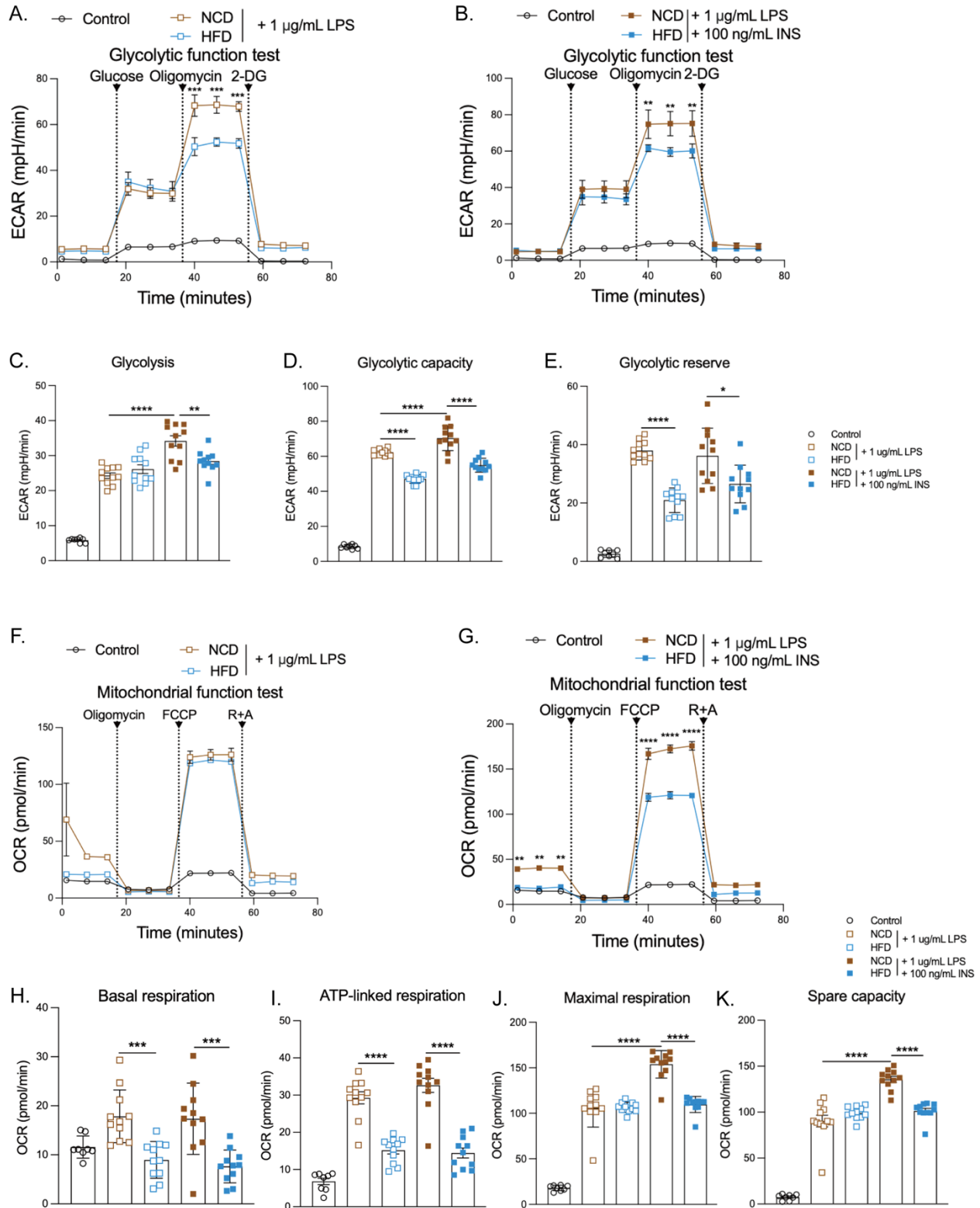


**Figure 3.9 DIO-induced IR regulated glycolytic and oxidative metabolism in LPS-stimulated B cells.** (A-B) B cells were isolated from NCD-fed or HFD-fed mice using EasySep™ Mouse B

Cell Isolation Kit (Stem Cell). (A) Real-time changes in ECAR ratios in isolated B cells stimulated with 1  $\mu\text{g}/\text{mL}$  LPS for 48 hours were measured using a Seahorse metabolic flux analyzer. (B) Real-time changes in ECAR ratios in isolated B cells stimulated with 1  $\mu\text{g}/\text{mL}$  LPS and 100  $\text{ng}/\text{mL}$  of insulin for 48 hours were measured using a Seahorse metabolic flux analyzer. (C-E) Changes in basal glycolysis (C), glycolytic capacity (D), and glycolytic reserve (E) in stimulated B cells were assessed by analyzing ECAR data ( $n=7-11$ , each dot represents one replicate). (F-G) B cells were isolated from C57BL/6 mice using EasySep™ Mouse B Cell Isolation Kit (Stem Cell). (F) Real-time changes in OCR ratios in isolated B cells stimulated with 1  $\mu\text{g}/\text{mL}$  LPS for 48 hours were measured using a Seahorse metabolic flux analyzer. (G) Real-time changes in OCR ratios in isolated B cells stimulated with 1  $\mu\text{g}/\text{mL}$  LPS and 100  $\text{ng}/\text{mL}$  of insulin for 48 hours were measured using a Seahorse metabolic flux analyzer. (H-K) Changes in basal respiration (H), ATP-linked respiration (I), maximal respiration (J), and spare capacity (K) in stimulated B cells were assessed by analyzing OCR data (each dot represents one replicate). Each mouse was subjected to two or three replicates, and two independent experiments were performed. \* $P<0.05$ , \*\* $P<0.01$ , \*\*\* $P<0.001$ , \*\*\*\* $P<0.0001$  with Two-Way ANOVA (A, B, F, G) or Mann Whitney U-test (C-E, H-K). Data are represented as mean $\pm$ SEM.

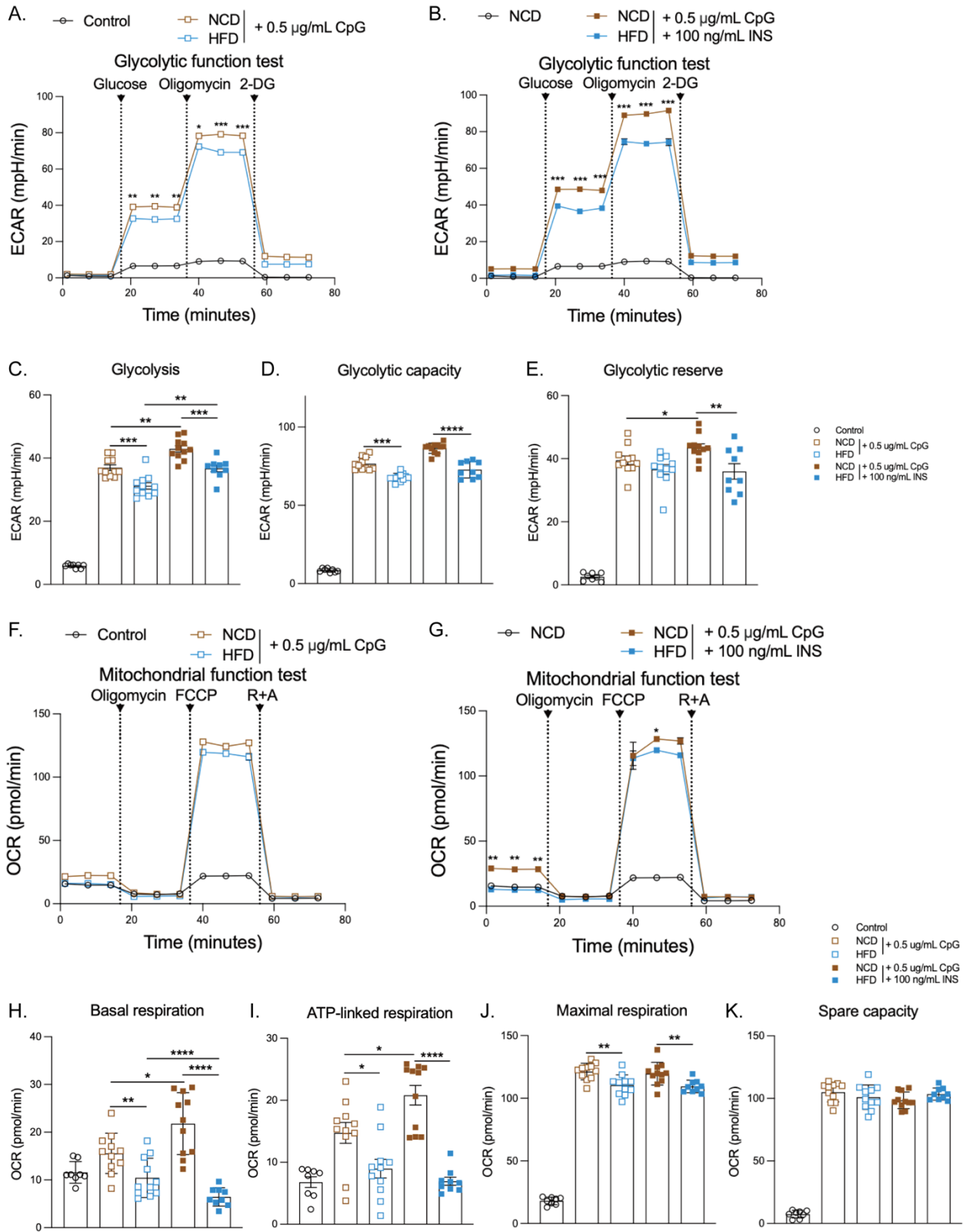


**Figure 3.10 DIO-induced IR regulated glycolytic and oxidative metabolism in CpG-stimulated B cells.** (A-B) B cells were isolated from NCD-fed or HFD-fed mice using EasySep™ Mouse B Cell Isolation Kit (Stem Cell). (A) Real-time changes in ECAR ratios in isolated B cells stimulated with 0.5 µg/mL CpG for 48 hours were measured using a Seahorse metabolic flux analyzer. (B) Real-time changes in ECAR ratios in isolated B cells stimulated with 0.5 µg/mL CpG and 100 ng/mL insulin for 48 hours were measured using a Seahorse metabolic flux analyzer. (C-E) Changes in basal glycolysis (C), glycolytic capacity (D), and glycolytic reserve (E) in stimulated B cells were assessed by analyzing ECAR data (n=7-11, each dot represents one replicate). (F-G) B cells were isolated from NCD-fed or HFD-fed mice using EasySep™ Mouse B Cell Isolation Kit (Stem Cell). (F) Real-time changes in OCR ratios in isolated B cells stimulated with 0.5 µg/mL CpG for 48 hours were measured using a Seahorse metabolic flux analyzer. (G) Real-time changes in OCR ratios in isolated B cells stimulated with 0.5 µg/mL CpG and 100 ng/mL insulin for 48 hours were measured using a Seahorse metabolic flux analyzer. (H-K) Changes in basal respiration (H), ATP-linked respiration (I), maximal respiration (J), and spare capacity (K) in stimulated B cells were assessed by analyzing OCR data (n=7-11, each dot represents one replicate). Each mouse was subjected to two or three replicates, and two independent experiments were performed. \*P<0.05, \*\*P<0.01, \*\*\*P<0.001, \*\*\*\*P<0.0001 with Two-Way ANOVA (A, B, F, G) or Mann Whitney U-test (C-E, H-K). Data are represented as mean±SEM.

### ***3.2.5 B cell-intrinsic IR regulated glycolytic and oxidative metabolism in LPS- and CpG-stimulated B cells***

In addition to DIO induced IR, I also tested the effect of B cell-intrinsic IR on the B cell metabolism. I isolated splenic B cells from WT (CD19 Cre<sup>+/-</sup> InsR<sup>wt/wt</sup>) and B cell-specific InsR-deficient (CD19 Cre<sup>+/-</sup> InsR<sup>fl/fl</sup>) mice. B cells were treated under the same conditions described in section 3.2.3, and a Seahorse metabolic flux analyzer was used to measure metabolic flux. Consistent with hypothesis that the impairment of insulin signaling induces metabolically dysregulation in B cells, I observed that InsR-deficient B cells showed a decrease in aerobic glucose metabolism after LPS stimulation (**Figure 3.11 A**), while no difference was observed in mitochondrial respiration (**Figure 3.11 F**). I also observed that supplementation with a high concentration of insulin increased the aerobic glucose metabolism in LPS-stimulated B cells, and the difference between WT and InsR-deficient B cells was not changed (**Figure 3.11 A-B**). Moreover, no difference in mitochondrial respiration was observed between LPS-stimulated B cells and cells stimulated with LPS and insulin (**Figure 3.11 F-G**). By analyzing ECAR and OCR data, I observed that B cell-intrinsic IR reduced the basal glycolysis and glycolytic reserve in stimulated B cells (**Figure 3.11 C, E**). Interestingly, insulin supplementation increased the basal glycolysis but not glycolytic reserve (**Figure 3.11 C, E**). Additionally, I did not observe any differences in glycolytic capacity and parameters of mitochondrial respiration (**Figure 3.11 D, H-K**).

Similar experiments were performed with B cells activated with CpG. Similar to what was observed for LPS-stimulated B cells, CpG stimulation increased the aerobic glucose metabolism in both WT and InsR-deficient B cells, which was enhanced by insulin supplementation (**Figure 3.12 A-B**). CpG-stimulated InsR-deficient B cells showed a decrease in aerobic glucose metabolism compared with WT B cells, and insulin supplementation had no effects (**Figure 3.12 A-B**). Furthermore, genetic InsR ablation in B cells had no effect on the parameters of aerobic glucose metabolism after CpG stimulation (**Figure 3.12 C-E**). However, a high concentration of

insulin supplementation increased glycolysis in WT B cells but not InsR-deficient B cells (**Figure 3.12 C-E**). Different from LPS-stimulated B cells which showed no difference in the mitochondrial respiration, CpG stimulation increased the mitochondrial respiration in both WT B cells and InsR-deficient B cells, and the difference was enhanced by supplementation with insulin (**Figure 3.12 F-G**). Moreover, InsR-deficient B cells showed a decrease in mitochondrial respiration after CpG stimulation, which was more significant following supplementation with a high concentration of insulin (**Figure 3.12 F-G**). B cell-intrinsic IR impaired the ATP-linked respiration and spare capacity in CpG-stimulated B cells, which were more significant after supplementation with a high concentration of insulin (**Figure 3.12 I, K**). CpG stimulation did not impair the basal respiration and maximal respiration, while B cell-intrinsic IR impaired the basal respiration and maximal respiration in CpG-stimulated B cells following supplementation with a high concentration of insulin (**Figure 3.12 H, J**).

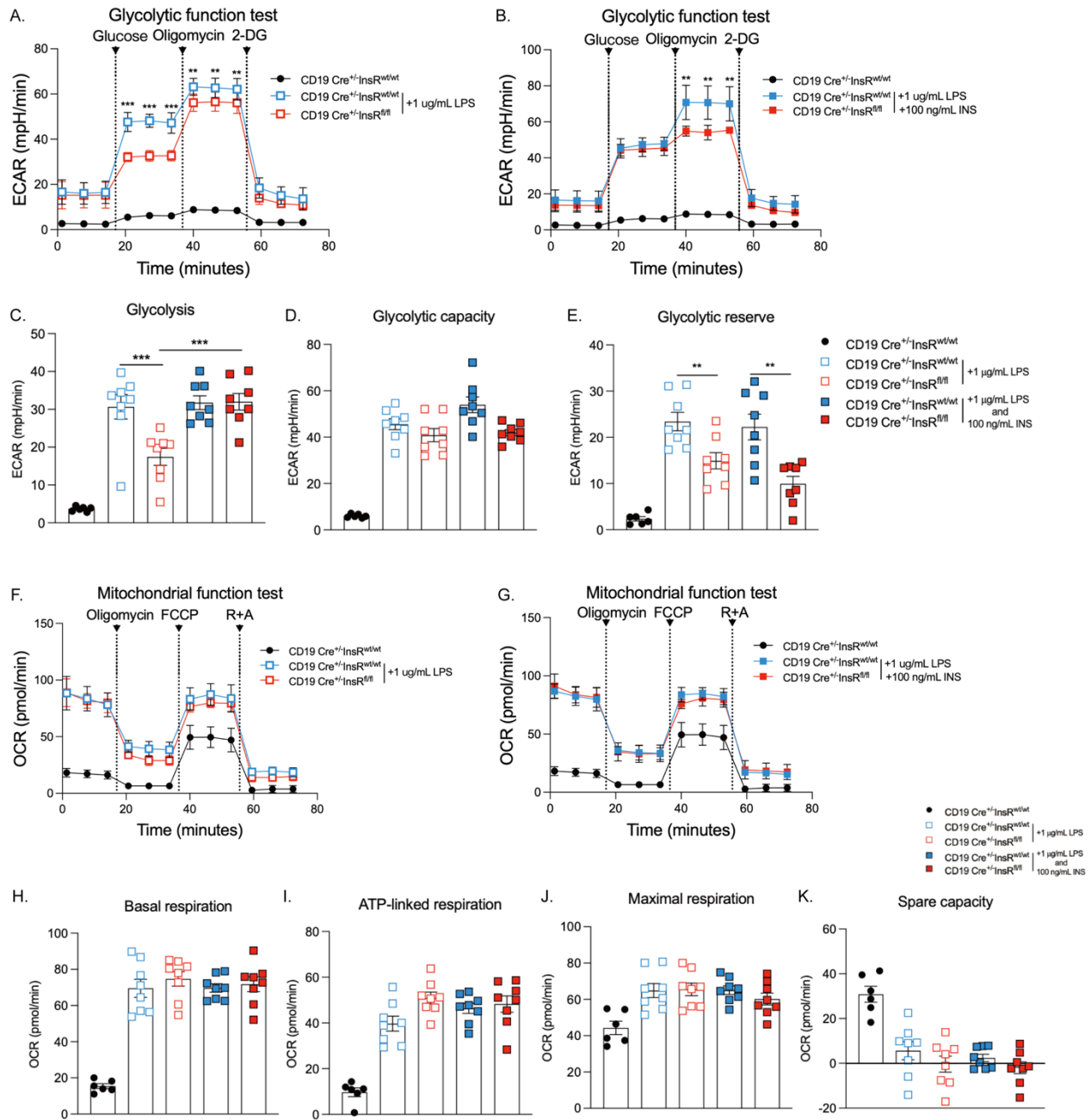


**Figure 3.11 B cell-intrinsic IR regulated glycolytic and oxidative metabolism in LPS-stimulated B cells.** (A-B) B cells were isolated from WT (CD19 Cre<sup>+/-</sup> InsR<sup>wt/wt</sup>) and B cell-specific InsR-deficient (CD19 Cre<sup>+/-</sup> InsR<sup>fl/fl</sup>) mice using EasySep™ Mouse B Cell Isolation Kit (Stem Cell). (A) Real-time changes in ECAR ratios in isolated B cells stimulated with 1 μg/mL LPS for 48 hours were measured using a Seahorse metabolic flux analyzer. (B) Real-time changes in ECAR ratios in isolated B cells stimulated with 1 μg/mL LPS and 100 ng/mL insulin for 48

hours were measured using a Seahorse metabolic flux analyzer. (C-E) Changes in basal glycolysis (C), glycolytic capacity (D), and glycolytic reserve (E) in stimulated B cells were assessed by analyzing ECAR data (n=6-8, each dot represents one replicate). (F-G) B cells were isolated from WT (CD19 Cre<sup>+/-</sup> InsR<sup>wt/wt</sup>) and B cell-specific InsR-deficient (CD19 Cre<sup>+/-</sup> InsR<sup>fl/fl</sup>) mice using EasySep™ Mouse B Cell Isolation Kit (Stem Cell). (F) Real-time changes in OCR ratios in isolated B cells stimulated with 1 µg/mL LPS for 48 hours were measured using a Seahorse metabolic flux analyzer. (G) Real-time changes in OCR ratios in isolated B cells stimulated with 1 µg/mL LPS and 100 ng/mL insulin for 48 hours were measured using a Seahorse metabolic flux analyzer. (H-K) Changes in basal respiration (H), ATP-linked respiration (I), maximal respiration (J), and spare capacity (K) in stimulated B cells were assessed by analyzing OCR data (n=6-8, each dot represents one replicate). Each mouse was subjected to two or three replicates, and two independent experiments were performed. \*\*P<0.01, \*\*\*P<0.001 with Two-Way ANOVA (A, B, F, G) or Mann Whitney U-test (C-E, H-K). Mann Whitney U-test. Data are represented as mean±SEM.

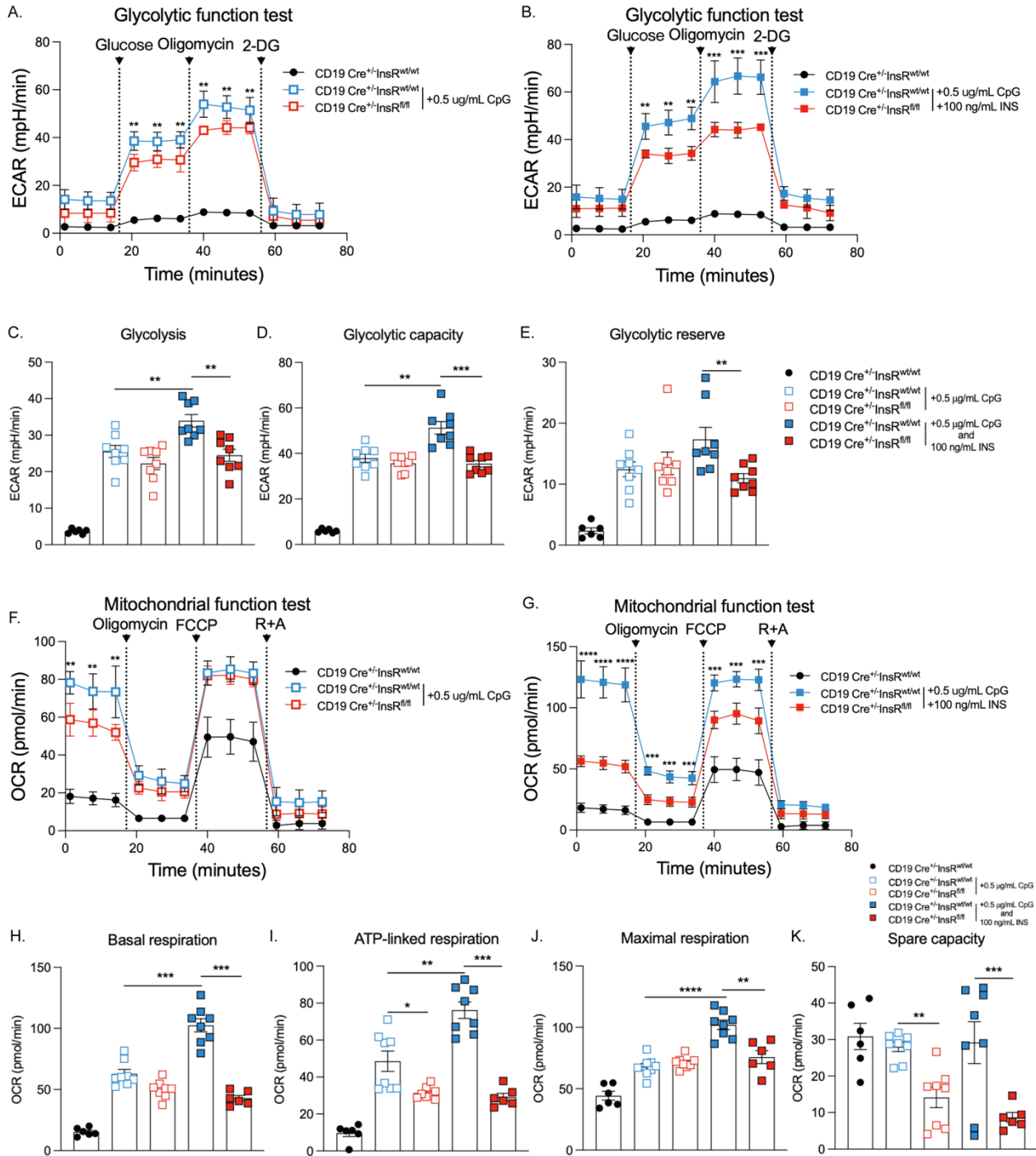


**Figure 3.12 B cell-intrinsic IR regulated glycolytic and oxidative metabolism in CpG-stimulated B cells.** (A-B) B cells were isolated from WT (CD19 Cre<sup>+/-</sup> InsR<sup>wt/wt</sup>) and B cell-specific InsR-deficient (CD19 Cre<sup>+/-</sup> InsR<sup>fl/fl</sup>) mice using EasySep™ Mouse B Cell Isolation Kit (Stem Cell). (A) Real-time changes in ECAR ratios in isolated B cells stimulated with 0.5 μg/mL CpG for 48 hours were measured using a Seahorse metabolic flux analyzer. (B) Real-time changes

in ECAR ratios in isolated B cells stimulated with 0.5  $\mu\text{g}/\text{mL}$  CpG and 100 ng/mL insulin for 48 hours were measured using a Seahorse metabolic flux analyzer. (C-E) Changes in basal glycolysis (C), glycolytic capacity (D), and glycolytic reserve (E) in stimulated B cells were assessed by analyzing ECAR data (n=6-8, each dot represents one replicate). (F-G) B cells were isolated from WT (CD19 Cre<sup>+/-</sup> InsR<sup>wt/wt</sup>) and B cell-specific InsR-deficient (CD19 Cre<sup>+/-</sup> InsR<sup>fl/fl</sup>) mice using EasySep™ Mouse B Cell Isolation Kit (Stem Cell). (F) Real-time changes in OCR ratios in isolated B cells stimulated with 0.5  $\mu\text{g}/\text{mL}$  CpG for 48 hours were measured using a Seahorse metabolic flux analyzer. (G) Real-time changes in OCR ratios in isolated B cells stimulated with 0.5  $\mu\text{g}/\text{mL}$  CpG and 100 ng/mL insulin for 48 hours were measured using a Seahorse metabolic flux analyzer. (H-K) Changes in basal respiration (H), ATP-linked respiration (I), maximal respiration (J), and spare capacity (K) in stimulated B cells were assessed by analyzing OCR data (n=6-8, each dot represents one replicate). Each mouse was subjected to two or three replicates, and two independent experiments were performed. \*\*P<0.01, \*\*\*P<0.001 with Two-Way ANOVA (A, B, F, G) or Mann Whitney U-test (C-E, H-K). Data are represented as mean $\pm$ SEM.

### 3.3 Discussion

In this chapter, I set out to understand if and how obesity impacts B cell activation and metabolism. I first showed that insulin induced downstream signaling in B cells (**Figure 3.1**), and that HFD-feeding impaired insulin signaling cascades in B cells (**Figure 3.3**), suggesting DIO induced IR in B cells. Based on these observations, I started to test the effect of insulin signaling on B cell activation and observed that both LPS and CpG stimulation induced the activation of B cells. However, no differences in the expression levels of co-stimulatory molecules and MHC class II were observed after supplementation with different concentrations of insulin, indicating that the activation of insulin signaling may have no impact on the B cell activation under the experimental conditions I used (**Figure 3.4**). However, one of the possible explanations for no difference in insulin-treated B cells is related to the medium I used for cell culture, which contains fetal bovine serum. Fetal bovine serum can naturally contain small amounts of insulin, as it is a complex mixture of growth factors, hormones, and other proteins present in bovine blood<sup>203</sup>. Although the concentration of insulin in FBS is generally low, around 10 $\mu$ U/mL, it still has the potential to impact my results. Moreover, more experiments are still ongoing to measure the changes in the proliferation and cytokine production of B cells. By combining these data with existing data, we can better address the question if insulin signaling affects B cell activation.

By using a mouse model of B cell-specific InsR ablation, I also tried to answer whether B cell-intrinsic IR impacts B cell activation. My data showed that both LPS and CpG stimulation induced the activation of B cells, and no difference was observed between WT and InsR-deficient B cells (**Figure 3.5-3.6**). Insulin can not only bind to the InsR but also the insulin-like growth factor receptor (IGFR)<sup>204</sup>. Although the affinity is much lower, the binding between insulin and IGFR can still initiate the activation of many downstream signaling pathways that highly overlap with insulin signaling, and further affecting the survival, proliferation, and activation of cells<sup>204</sup>. Thus, insulin supplementation was used to see if the activation of insulin downstream signaling can make any changes in InsR-deficient B cells compared with WT B cells. However, insulin

supplementation showed no impact on the expression of co-stimulatory molecules and MHC class II (**Figure 3.5-3.6**). Same as mentioned before, more experiments still need to be done to confirm that there are no changes in the proliferation and cytokine production of B cells.

Given the strong link between cell activation, differentiation, and metabolism, I next tried to address if insulin stimulation regulates the metabolism in LPS- and CpG-stimulated B cells. By stimulating B cells isolated from C57BL/6 mice with LPS or CpG together with insulin and running the Seahorse metabolic flux assay, I reported that insulin increased the aerobic glucose metabolism and mitochondrial respiration in LPS- and CpG-stimulated B cells (**Figure 3.7-3.8**). Interestingly, in terms of mitochondrial respiration, insulin supplementation increased the basal respiration and ATP-linked respiration in LPS-stimulated B cells, which is totally different from LPS stimulation that increased the maximal respiration and spare capacity in B cells (**Figure 3.7 H-K**). The changes in basal respiration and ATP-linked respiration are related to many factors, including the mitochondrial content and mitochondrial integrity, cells with a higher number of functional mitochondria generally have higher basal respiration rates<sup>205, 206</sup>. Thus, the data suggested that insulin has the potential to increase mitochondrial content and maintain the function of mitochondria to produce enough ATP in B cells. Different from LPS-stimulated B cells, 10 ng/mL of insulin supplementation increased the basal respiration and ATP-linked respiration in CpG-stimulated B cells, while 100ng/mL of insulin supplementation reduced them (**Figure 3.8 H-I**). Serum insulin levels reach as high as 38 ng/mL in IR individuals<sup>179</sup>, indicating that 100 ng/mL insulin supplementation has the potential to induce IR in B cells, thereby resulting in the decrease. The differences between LPS- and CpG-stimulated B cells may be related to the difference in downstream signalling pathways. LPS binds to TLR4, and CpG binds to TLR9, even though they both activate NF- $\kappa$ B and MAPK through MyD88-dependent pathway and induce the production of pro-inflammatory cytokines, their specificity for different IRF activation reflects their distinct roles in immune response modulation<sup>200, 201</sup>. The binding between LPS and TLR4 leads to the activation of IRF3, which primarily induces the early production of type I IFNs<sup>200</sup>. However, the binding between CpG and TLR9 results in the activation of IRF7, which is crucial for the amplification and

sustained production of type I IFNs<sup>201</sup>. Type I IFNs can impair insulin signaling by inducing inflammatory responses, activating SOCS proteins, and altering the expression of genes involved in glucose metabolism, ultimately contributing to IR<sup>207-209</sup>. Thus, CpG stimulation can amplify the production of type I IFNs, making B cells more susceptible to insulin resistance when exposed to high concentrations of insulin.

I next tested if DIO-induced IR and B cell-intrinsic IR regulate the metabolism in LPS- and CpG-stimulated B cells. I stimulated NCD B cells, HFD B cells, WT B cells, and InsR-deficient B cells with LPS or CpG together with 100 ng/mL insulin and measured the changes in aerobic glucose metabolism and mitochondrial respiration. In LPS-stimulated B cells, I observed that DIO-induced IR impaired the aerobic glucose metabolism but not the mitochondrial respiration, which was exacerbated or initiated by the insulin supplementation (**Figure 3.9**). The CpG-stimulated B cells showed the same trends (**Figure 3.10**). However, B cell-intrinsic IR showed a different impact compared with DIO-induced IR. In LPS-stimulated B cells, B cell-intrinsic IR impaired the aerobic glucose metabolism but not the mitochondrial respiration, which was not changed by high concentration of insulin supplementation (**Figure 3.11**). In CpG-stimulated B cells, B cell-intrinsic IR impaired both aerobic glucose metabolism and mitochondrial respiration, which was exacerbated by a high concentration of insulin supplementation (**Figure 3.12**). The difference between DIO-induced IR B cells and genetic InsR-deficient B cells can be explained by the difference between systemic IR and B cell-intrinsic IR. Systemic IR affects multiple tissues, organs, and immune cells, leading to broad metabolic disturbances. Systemic IR can disrupt B cell metabolism through altered insulin signaling, increased inflammation, and changes in interactions with other immune cells. However, B cell-intrinsic IR is confined to B cells, which primarily affects B cell metabolism and immune function without disturbing systemic homeostasis.

In summary, this chapter demonstrated that insulin induced the activation of insulin signaling in B cells, and 20 weeks of HFD-feeding resulted in IR in B cells. In terms of activation, the activation and disruption of insulin signaling both had no effect on the expression level of co-

stimulatory molecules and MHC class II in LPS- and CpG-stimulated B cells. However, insulin stimulation, DIO induced IR, and B cell-intrinsic IR all showed the capacity to regulate the glycolysis and OXPHOS pathways in LPS- and CpG-stimulated B cells, suggesting that insulin signaling modulates metabolic adaptation in B cells, likely serving the purpose to support their differentiation and function.

### **3.4 Contributions**

The PCR and gel electrophoresis used for confirming the genotypes of mice were all completed by Dr. Masoud Akbari. The protocols of the Phospho-flow assay and Seahorse metabolic flux assay were kindly organized and provided by Dr. Paulo José Basso. All other experiments mentioned in this chapter were completed by me.

## **Chapter 4: The role of IR on B cell-mediated adaptive immunity elicited by vaccination and influenza virus infection**

### **4.1 Introduction**

B cells play an important role in vaccine-induced protection<sup>210-212</sup>. Upon encountering antigens in vaccines, B cells are activated, rapidly proliferate and enter the GC reaction with the help of T<sub>FH</sub> cells. These cells can differentiate into plasma cells that produce antibodies specific to the antigens presented in the vaccines or MBCs that facilitate a faster and more robust immune response upon encountering the same antigen. Plasma cells and MBCs function together to provide durable protection against infections even years after vaccination. Obesity decreased the efficacy of vaccination and increased the mortality rates in mice and humans upon infection<sup>131-133</sup>. Moreover, emerging studies have demonstrated that obesity altered the recruitment, cytokine production, and antibody production of B cells, which may be associated with obesity-associated IR<sup>89,90</sup>. However, the exact role of insulin signaling and IR on B cell differentiation and function after vaccination remains unknown.

In addition to vaccination, abundant studies indicated that individuals with IR exhibited poorer anti-viral immunity. Recent studies have demonstrated that patients with IR were more susceptible to COVID virus infection or influenza virus infection<sup>213-218</sup>. Moreover, hepatitis C virus has been reported to induce IR irrespective of the severity of liver disease, and IR reversely contributed to the fibrotic progression in chronic hepatitis C virus infection<sup>219</sup>. IR and related metabolic disturbances also contributed to the complications in human immunodeficiency virus (HIV)-infected individuals and cytomegalovirus (CMV)-infected individuals<sup>220-224</sup>. B cells are integral to the adaptive immune responses against viral infections through antibody production, generation of memory cells, antigen presentation, cytokine secretion, and immune regulation. However, whether and how IR regulates B cell-mediated anti-viral immunity is unknown.

Overall, in this chapter, I used mice with InsR ablation in B cells to understand the role of B cell-intrinsic IR on B cell-mediated adaptive immunity within the context of OVA/CFA/IFA immunization and H1N1/PR8 influenza virus infection.

## 4.2 Results

### *4.2.1 DIO induced IR impaired OVA/CFA-induced GC reaction during OVA/CFA-induced primary immune responses*

As mentioned in Chapter 3, I have confirmed that 20 weeks of HFD-feeding induced IR in B cells. To test if DIO-induced IR affects OVA/CFA-induced primary immune response, I immunized NCD-fed and HFD-fed mice with the same dose of OVA/CFA emulsion and euthanized the mice 14 days post-immunization for further analysis. The OVA-specific Ig ELISA results showed a decrease in the OVA-specific IgM level in the sera (**Figure 4.1 A**). However, the expression levels of all other isotypes of antibodies, including IgA, IgE, IgG<sub>1</sub>, IgG<sub>2b</sub>, IgG<sub>2c</sub>, and IgG<sub>3</sub>, showed no differences in the sera (**Figure 4.1 B-G**). GC reaction is essential for effective T cell-dependent B cell responses, through facilitating affinity maturation. HFD-fed mice showed no differences in the frequency and number of OVA-bound B cells on day 14 post-immunization (**Figure 4.2 A-C**), but a decrease in the frequency and number of total GC B cells (CD19<sup>+</sup>B220<sup>+</sup>CD95<sup>+</sup>GL-7<sup>+</sup>, **Figure 4.2 D-F**) in draining ALNs on day 14 post-immunization. CFA is a water-in-oil emulsion containing heat-killed mycobacterium tuberculosis<sup>225</sup>, and is commonly used as an adjuvant to induce autoimmune disease in animal models<sup>226</sup>. Additionally, CFA has ligands for TLR2, TLR4, and TLR9, suggesting it can induce the generation of GC B cells. Thus, I measured the GC B cells that recognize OVA by staining with fluorescent OVA conjugates and observed that HFD-fed mice showed a decrease in the frequency and number of OVA-specific GC B cells (CD19<sup>+</sup>B220<sup>+</sup>OVA<sup>+</sup>CD95<sup>+</sup>GL-7<sup>+</sup>, **Figure 4.2 G-I**) in draining ALNs on day 14 post immunization.

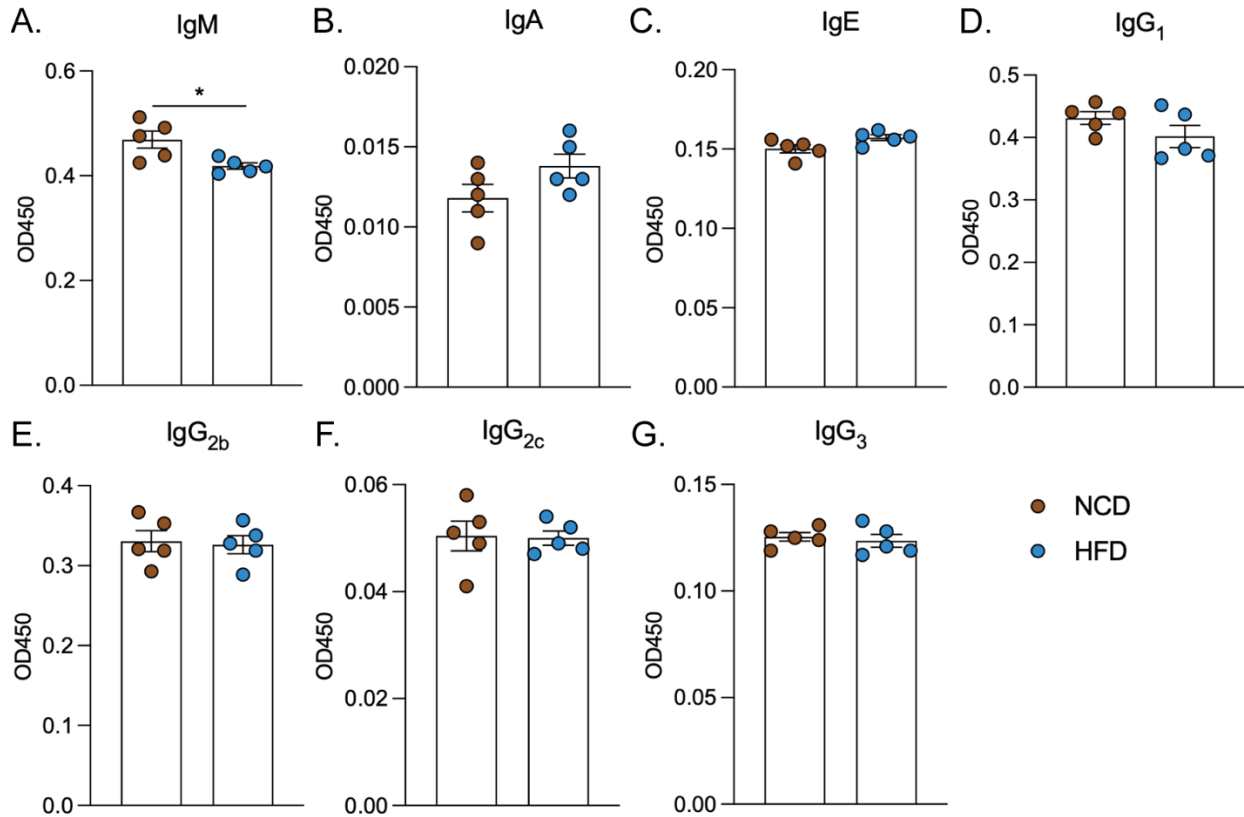


**Figure 4.1 DIO-induced IR altered antibody production by B cells during OVA/CFA-induced primary immune response.** OVA-specific antibody responses on 14 days post-immunization, as determined by OVA-specific Ig ELISA (n=5, each dot represents one mouse). Dilution ratios are as follows: IgM/IgG<sub>2b</sub>/IgG<sub>2c</sub>/IgG<sub>3</sub>: 1:400; IgA/IgE: 1:200; IgG<sub>1</sub>: 1:1000. \*P<0.05 with Mann Whitney U-test. Data are represented as mean±SEM.

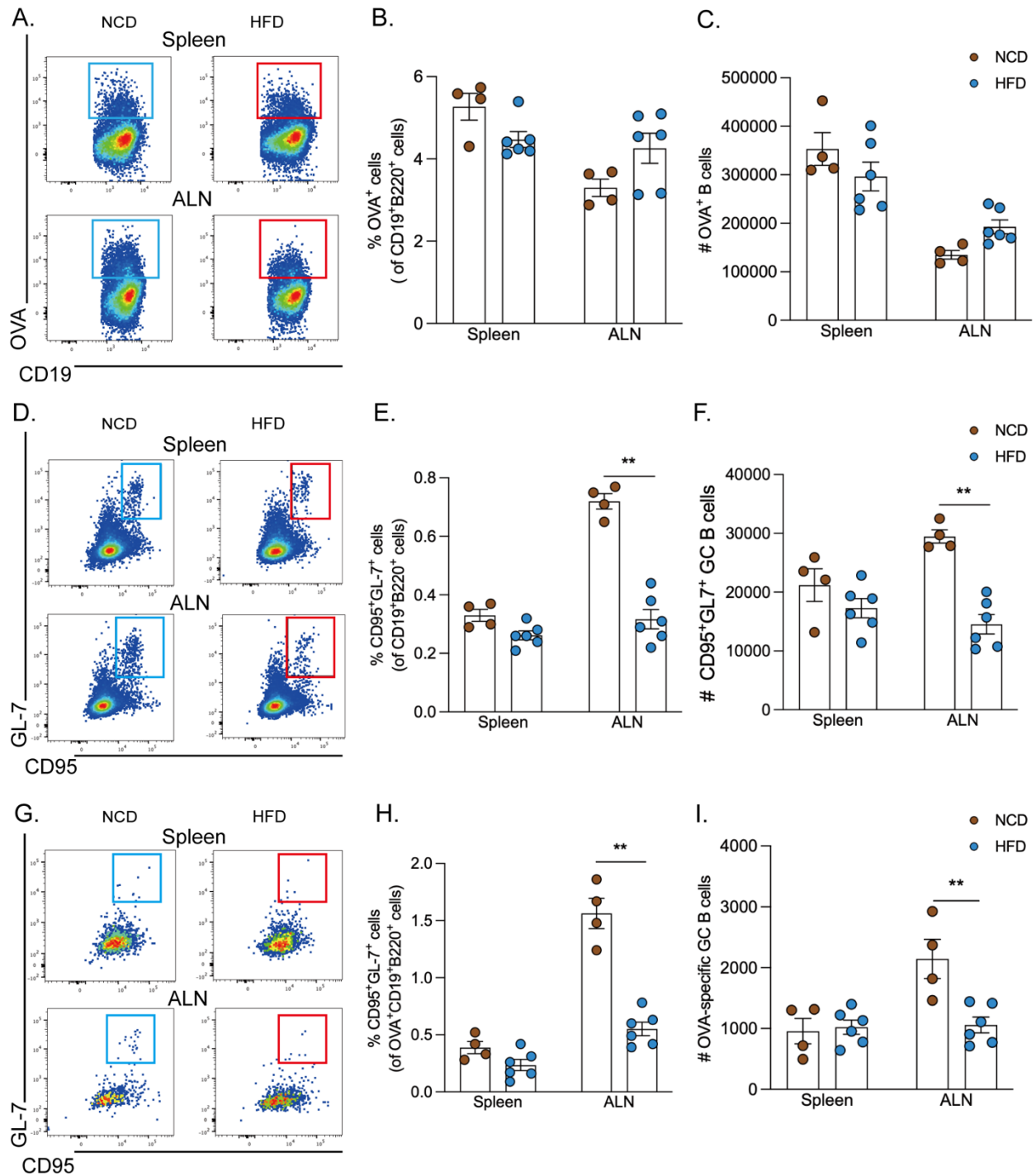


**Figure 4.2 DIO-induced IR impaired OVA/CFA-induced GC reaction during primary immune response.** (A) Flow plots of OVA-specific B cells in immunized NCD-fed and HFD-fed mice by staining using Alexa647-conjugated OVA. (B-C) HFD-fed mice showed no differences in the frequency and number of OVA-bound B cells (splens & ALNs, day 14), as determined by

flow cytometry (gated out of CD19<sup>+</sup>B220<sup>+</sup> cells, n=4-6, each dot represents one mouse). (D) Flow plots of total GC B cells in immunized NCD-fed and HFD-fed mice. (E-F) HFD-fed mice showed reduced frequency and number of total GC B cells (ALNs, day 14), as determined by flow cytometry (gated out of CD19<sup>+</sup>B220<sup>+</sup> cells, n=4-6, each dot represents one mouse). (G) Flow plots of OVA-specific GC B cells in immunized NCD-fed and HFD-fed mice. (H-I) HFD-fed mice showed reduced frequency and number of OVA-specific GC B cells (ALNs, day 14), as determined by flow cytometry (gated out of Alexa647-OVA<sup>+</sup>CD19<sup>+</sup>B220<sup>+</sup> cells, n=4-6, each dot represents one mouse). \*\*P<0.01 with Mann Whitney U-test. Data are represented as mean±SEM.

#### ***4.2.2 B cell-intrinsic IR altered the B cell antibody production and GC reaction during OVA/CFA-induced primary immune response***

DIO not only induces IR in B cells, but also in other immune cells such as macrophages, DCs, adipocytes, and T cells. The phenotype and function of all these mentioned cells can be affected by the chronic inflammation conditions in obese mice, further contributing to the dysregulation of B cell-mediated immune responses. To exclude the influence from other immune cells, WT (MB1 Cre<sup>+/-</sup> InsR<sup>wt/wt</sup>) and B cell-specific InsR-deficient (MB1Cre<sup>+/-</sup> InsR<sup>fl/fl</sup>) mice were immunized subcutaneously with OVA/CFA, one set of mice were euthanized on day 14 after immunization and continued following the serum antibody responses weekly in another cohort. By conducting an OVA-specific Ig ELISA assay on collected sera, I first did a full titration test to confirm the appropriate diluted concentrations of serum samples for different isotypes, and data showed that the appropriate diluted concentrations are 1:200 for IgA and IgE, 1:400 for IgM, IgG<sub>2b</sub>, IgG<sub>2c</sub>, and IgG<sub>3</sub>, and 1:1000 for IgG<sub>1</sub> (data not shown). Under such determined diluted concentrations, I observed a decrease in OVA-specific IgM, IgA, and IgG<sub>3</sub> (**Figure 4.3 A-C**). The reduced IgM could reflect a defect in B cell activation, while reduced IgA and IgG<sub>3</sub> could suggest B cell-intrinsic IR to play a role in the antibody class-switching to specific isotypes. Interestingly, B cell-specific InsR-deficient mice produced more IgE (**Figure 4.3 D**), an antibody related to allergy, and the reasons remain unclear. It will be our next step to investigate the function of IgE antibody in this setting. Moreover, no differences in IgG<sub>1</sub>, IgG<sub>2b</sub>, and IgG<sub>2c</sub> were observed in B cell-specific InsR-deficient mice compared with WT mice (**Figure 4.3 E-G**). Altogether, B cell-intrinsic IR altered the antibody production by B cells during OVA/CFA-induced primary immune response.

Next, to test the hypothesis that the impairment of insulin signaling affects B cell GC reaction during primary immune responses, I tested the effect of B cell-intrinsic IR on the antigen-binding ability of B cells via measuring the frequency, number and OVA staining intensity of OVA-bound B cells (OVA<sup>+</sup>CD19<sup>+</sup>B220<sup>+</sup>) on day 14 post-immunization. As shown in **Figure 4.4**, no differences were observed when comparing immunized WT mice and immunized B cell-specific InsR-

deficient mice (**Figure 4.4 A-D**). I next tested the effect of B cell-intrinsic IR on OVA/CFA-induced GC reaction via measuring the total GC B cells (CD19<sup>+</sup>B220<sup>+</sup>CD95<sup>+</sup>GL-7<sup>+</sup>) in immunized WT and B cell-specific InsR-deficient mice and observed a significant decrease in the frequency and number of total GC B cells in draining ALNs on day 14 post-immunization (**Figure 4.4 E-G**). Similar to DIO mice, I also observed that B cell-specific InsR-deficient mice showed a significant decrease in the frequency and number of OVA-specific GC B cells (CD19<sup>+</sup>B220<sup>+</sup>OVA<sup>+</sup> CD95<sup>+</sup>GL-7<sup>+</sup>) in draining ALNs on day 14 post-immunization (**Figure 4.4 H-J**), suggesting that B cell-intrinsic IR impaired OVA-induced GC reaction.

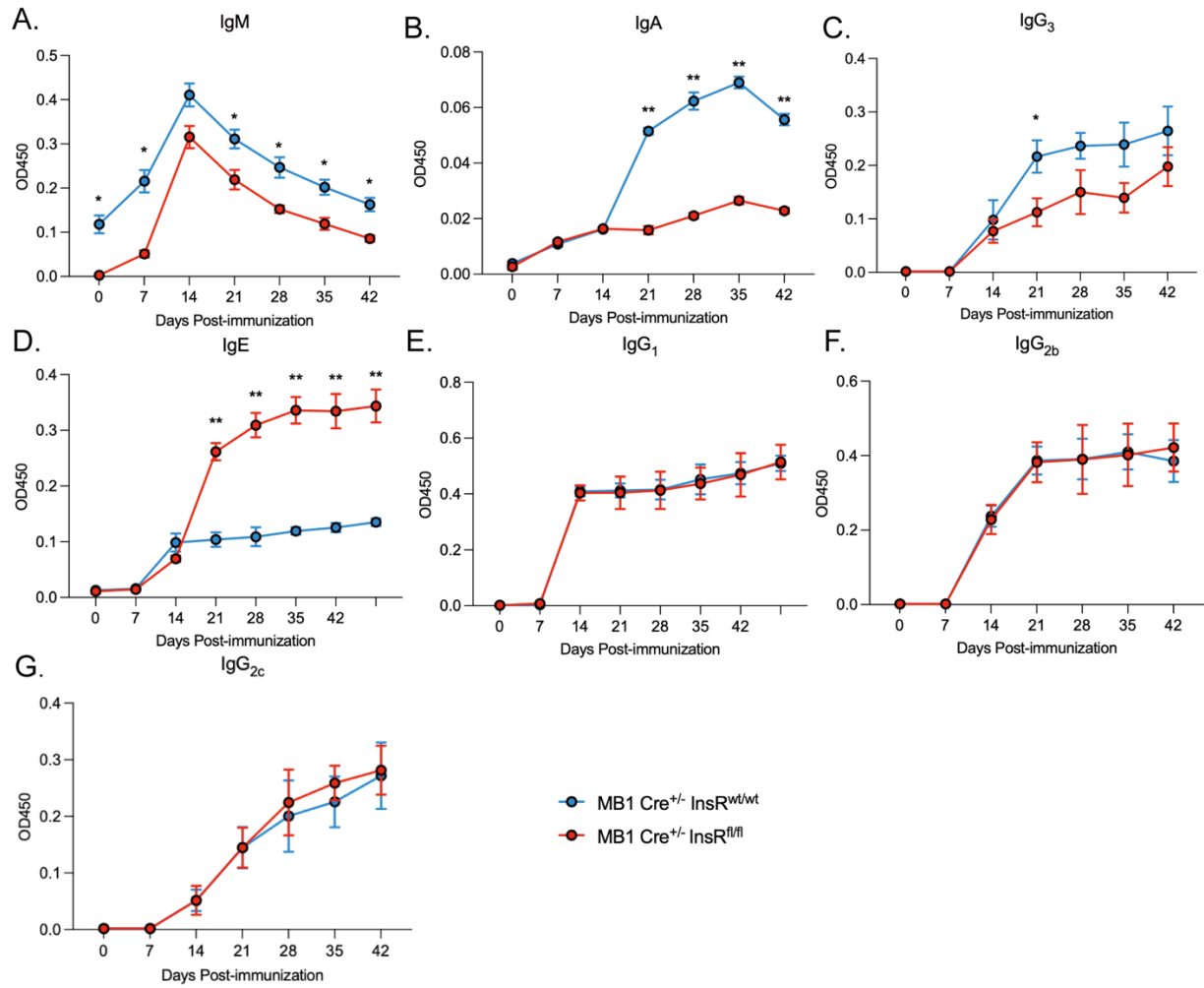


**Figure 4.3 B cell-intrinsic IR altered antibody production by B cells during OVA/CFA-induced primary immune response.** OVA-specific antibody responses on indicated days post-immunization, as determined by OVA-specific Ig ELISA (n=6). Dilution ratios are as follows: IgM/IgG<sub>2b</sub>/IgG<sub>2c</sub>/IgG<sub>3</sub>: 1:400; IgA/IgE: 1:200; IgG<sub>1</sub>: 1:1000. \*P<0.05, \*\*P<0.01 with Two-way ANOVA test. Data are represented as mean±SEM.

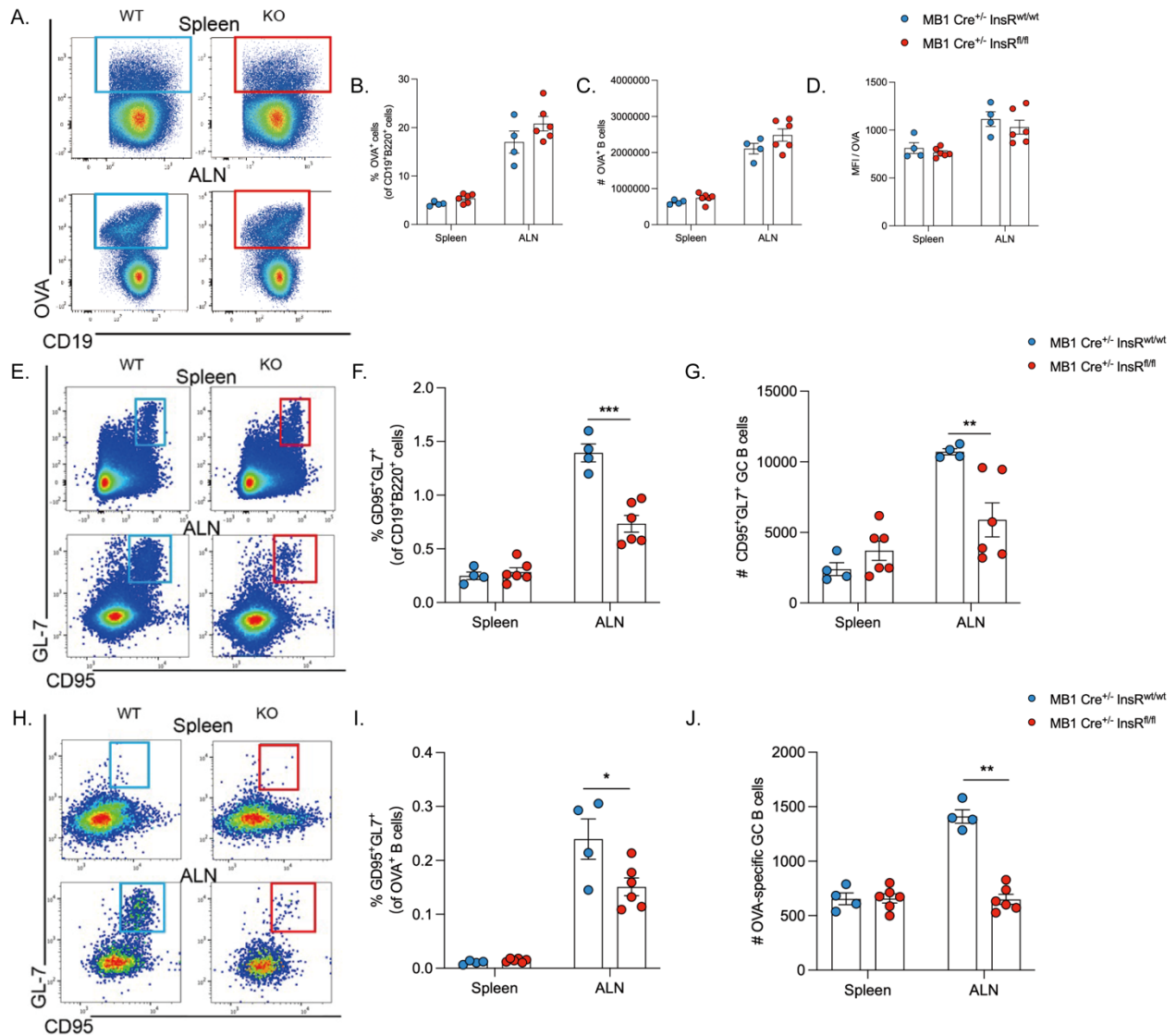


**Figure 4.4 B cell-intrinsic IR impaired OVA/CFA-induced primary GC reaction.** (A) Flow plots of OVA-specific B cells in immunized WT (MB1 Cre<sup>+/-</sup> InsR<sup>wt/wt</sup>) and B cell-specific InsR-deficient (MB1 Cre<sup>+/-</sup> InsR<sup>fl/fl</sup>) mice by staining using Alexa647-conjugated OVA. (B-D) B cell-specific InsR-deficient (MB1 Cre<sup>+/-</sup> InsR<sup>fl/fl</sup>) mice showed no differences in the frequency (B), number (C), and OVA staining intensity(D) of OVA-bound B cells (spleens & ALNs, day 14), as determined by flow cytometry (gated out of CD19<sup>+</sup>B220<sup>+</sup> cells, n=4-6, each dot represents one mouse). (E) Flow plots of total GC B cells in immunized WT (MB1 Cre<sup>+/-</sup> InsR<sup>wt/wt</sup>) and B cell-specific InsR-deficient (MB1 Cre<sup>+/-</sup> InsR<sup>fl/fl</sup>) mice. (F-G) B cell-specific InsR-deficient (MB1 Cre<sup>+/-</sup> InsR<sup>fl/fl</sup>) mice showed reduced frequency and number of total GC B cells (ALNs, day 14), as

determined by flow cytometry (gated out of CD19<sup>+</sup>B220<sup>+</sup> cells, n=4-6, each dot represents one mouse). (H) Flow plots of OVA-specific GC B cells in immunized WT (MB1 Cre<sup>+/-</sup> InsR<sup>wt/wt</sup>) and B cell-specific InsR-deficient (MB1 Cre<sup>+/-</sup> InsR<sup>fl/fl</sup>) mice. (I-J) B cell-specific InsR-deficient (MB1 Cre<sup>+/-</sup> InsR<sup>fl/fl</sup>) mice showed reduced frequency and number of OVA-specific GC B cells (ALNs, day 14), as determined by flow cytometry (gated out of Alexa647-OVA<sup>+</sup>CD19<sup>+</sup>B220<sup>+</sup> cells, n=4-6, each dot represents one mouse). ns p>0.05, \*P<0.05, \*\*P<0.01, \*\*\*P<0.001 with Mann Whitney U-test. Data are represented as mean±SEM.

### ***4.2.3 The negative impact of B cell-intrinsic IR on GC reaction may result from the deficiency in help from CD4<sup>+</sup> T cells and T<sub>FH</sub> cells***

The proliferation of antigen-activated B cells needs to receive costimulatory signals from antigen-activated CD4<sup>+</sup> T cells, while the subsequent entry of activated B cells into GC needs to receive costimulatory signals from T<sub>FH</sub> cells, which suggest that the impairment in GC reaction in immunized B cell-specific InsR-deficient mice has the potential to be related to the loss of help from antigen-specific CD4<sup>+</sup> T cells and T<sub>FH</sub> cells. Thus, I measured the OVA-specific CD4<sup>+</sup> T cells in immunized WT and B cell-specific InsR-deficient mice by staining using fluorescent OVA<sub>323-339</sub>/I-A<sup>b</sup> tetramer and observed a decrease in the frequency and number of OVA-specific CD4<sup>+</sup> T cells (CD3<sup>+</sup>CD4<sup>+</sup>OVA<sub>323-339</sub>/I-A<sup>b</sup> tetramer<sup>+</sup>) in the spleens on day 14 post-immunization (**Figure 4.5 A-C**). T follicular helper (T<sub>FH</sub>) cells are specialized providers of T cell help to B cells, and are essential for GC formation, affinity maturation, and the development of high-affinity antibody-secreting plasma cells and long-term lasting memory B cells. To examine if the impairment in GC reaction is resulting from the loss of help from T<sub>FH</sub> cells, I measured the proportions of total T<sub>FH</sub> cells in immunized WT and B cell-specific InsR-deficient mice, and observed that compared with immunized WT mice, immunized B cell-specific InsR-deficient mice showed no differences in the frequency and number of total T<sub>FH</sub> cells (CD3<sup>+</sup>CD4<sup>+</sup>CXCR5<sup>+</sup>PD-1<sup>+</sup>) in the spleens and draining ALNs on day 14 post immunization (**Figure 4.5 D-F**). I next measured the OVA-specific T<sub>FH</sub> cells by staining with OVA<sub>323-339</sub>/I-A<sup>b</sup> tetramer. Consistent with my hypothesis, the immunized B cell-specific InsR-deficient mice showed a significant decrease in the frequency and number of OVA-specific T<sub>FH</sub> cells (CD3<sup>+</sup>CD4<sup>+</sup>OVA<sub>323-339</sub>/I-A<sup>b</sup> tetramer<sup>+</sup>CXCR5<sup>+</sup>PD-1<sup>+</sup>) in the spleens on day 14 post-immunization (**Figure 4.5 G-I**).

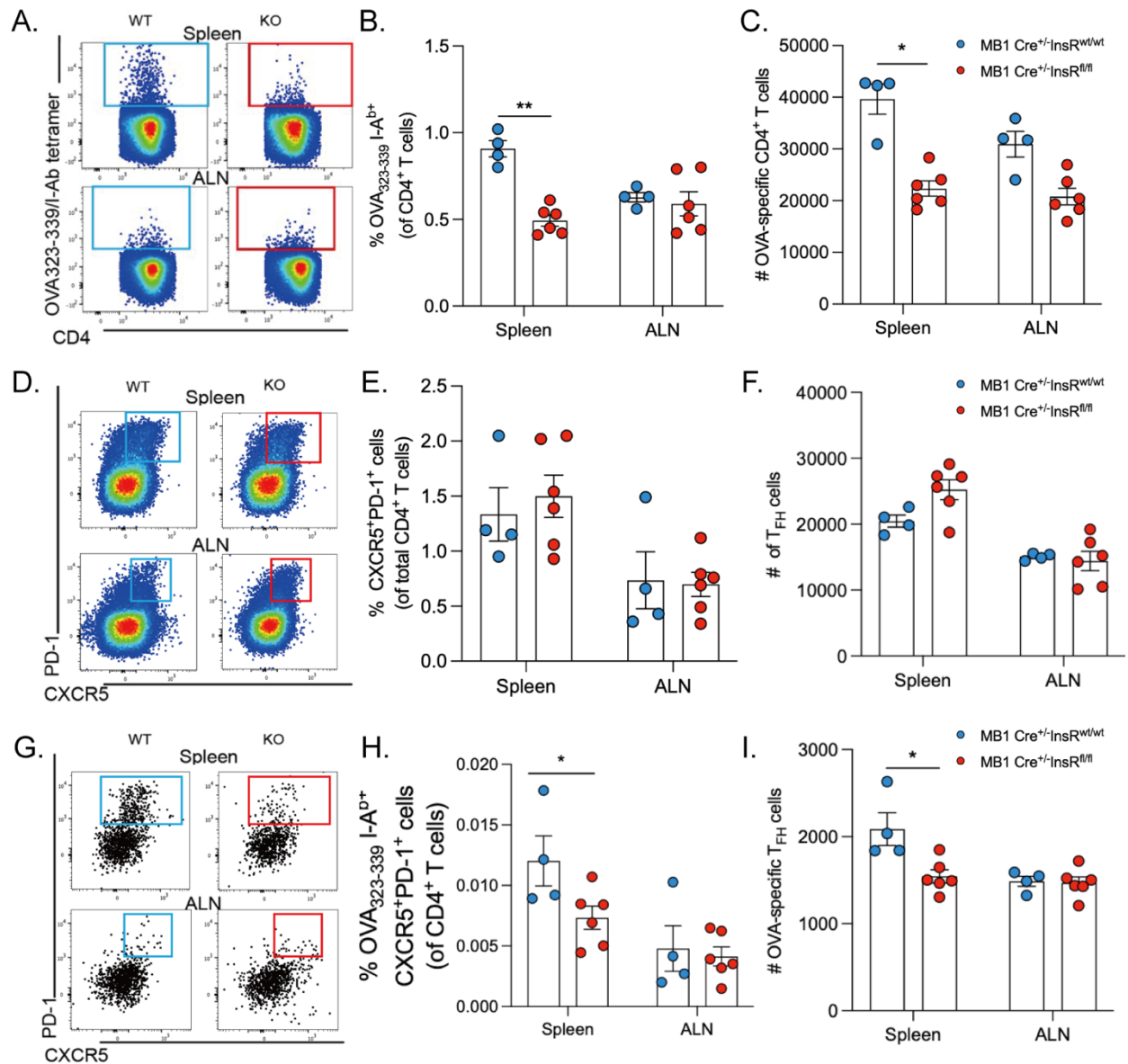


**Figure 4.5** The negative impact of B cell-intrinsic IR on OVA/CFA-induced primary GC reaction may result from the deficiency in help from CD4<sup>+</sup> T cells and T<sub>FH</sub> cells. (A) Flow plots of OVA-specific CD4<sup>+</sup> T cells in immunized WT (MB1 Cre<sup>+/-</sup> InsR<sup>wt/wt</sup>) and B cell-specific InsR-deficient (MB1 Cre<sup>+/-</sup> InsR<sup>fl/fl</sup>) mice. (B-C) B cell-specific InsR-deficient (MB1 Cre<sup>+/-</sup> InsR<sup>fl/fl</sup>) mice showed reduced frequency and number of OVA-specific CD4<sup>+</sup> T cells (splens, day 14), as determined by flow cytometry (gated out of CD3<sup>+</sup>CD4<sup>+</sup> cells, n=4-6, each dot represents one mouse). (D) Flow plots of total T<sub>FH</sub> cells in immunized WT (MB1 Cre<sup>+/-</sup> InsR<sup>wt/wt</sup>) and B cell-specific InsR-deficient (MB1 Cre<sup>+/-</sup> InsR<sup>fl/fl</sup>) mice. (E-F) B cell-specific InsR-deficient (MB1 Cre<sup>+/-</sup> InsR<sup>fl/fl</sup>) mice showed reduced frequency and number of OVA-specific CD4<sup>+</sup> T cells (splens, day 14), as determined by flow cytometry (gated out of CD3<sup>+</sup>CD4<sup>+</sup> cells, n=4-6, each dot represents one mouse). (G-H) B cell-specific InsR-deficient (MB1 Cre<sup>+/-</sup> InsR<sup>fl/fl</sup>) mice showed reduced frequency and number of OVA-specific T<sub>FH</sub> cells (splens, day 14), as determined by flow cytometry (gated out of CD3<sup>+</sup>CD4<sup>+</sup> cells, n=4-6, each dot represents one mouse). (I) B cell-specific InsR-deficient (MB1 Cre<sup>+/-</sup> InsR<sup>fl/fl</sup>) mice showed reduced number of OVA-specific T<sub>FH</sub> cells (splens, day 14), as determined by flow cytometry (gated out of CD3<sup>+</sup>CD4<sup>+</sup> cells, n=4-6, each dot represents one mouse).

InsR<sup>fl/fl</sup>) mice showed no differences in the frequency and number of total T<sub>FH</sub> cells (spleens & ALNs, day 14), as determined by flow cytometry (gated out of CD3<sup>+</sup>CD4<sup>+</sup> cells, n=4-6, each dot represents one mouse). (G) Flow plots of OVA-specific T<sub>FH</sub> cells in immunized WT (MB1 Cre<sup>+/-</sup> InsR<sup>wt/wt</sup>) and B cell-specific InsR-deficient (MB1 Cre<sup>+/-</sup> InsR<sup>fl/fl</sup>) mice. (H-I) B cell-specific InsR-deficient (MB1 Cre<sup>+/-</sup> InsR<sup>fl/fl</sup>) mice showed reduced frequency and number of OVA-specific T<sub>FH</sub> cells (spleens, day 14), as determined by flow cytometry (gated out of CD3<sup>+</sup>CD4<sup>+</sup> OVA<sub>323-339</sub>/I-A<sup>b</sup> tetramer<sup>+</sup> cells, n=4-6, each dot represents one mouse). \*P<0.05, \*\*P<0.01 with Mann Whitney U-test. Data are represented as mean±SEM.

#### **4.2.4 B cell-intrinsic IR regulated glycolytic and oxidative metabolism in B cells during OVA/CFA-induced primary immune response**

The differentiation and function of B cells rely on several metabolic pathways, especially the glycolysis and OXPHOS pathways. To test if there are metabolic changes in InsR-deficient B cells when activated *in vivo* by OVA/CFA, I isolated splenic B cells from non-immunized WT (MB1 Cre<sup>+/-</sup> InsR<sup>wt/wt</sup>) mice as well as immunized WT (MB1 Cre<sup>+/-</sup> InsR<sup>wt/wt</sup>) and B cell-specific InsR-deficient (MB1 Cre<sup>+/-</sup> InsR<sup>fl/fl</sup>) mice 14 days post-immunization, and ran Seahorse metabolic flux assay to measure the changes in glycolysis and OXPHOS pathways. As shown, OVA/CFA immunization increased the aerobic glucose metabolism and mitochondrial respiration in B cells isolated from immunized WT and B cell-specific InsR-deficient mice compared with B cells isolated from non-immunized WT mice (**Figure 4.6 A, E**). Moreover, by comparing B cells isolated from immunized WT mice with B cells isolated from B cell-specific InsR-deficient mice, I observed that B cell-intrinsic IR reduced aerobic glucose metabolism and mitochondrial respiration in B cells (**Figure 4.6 A, E**). By analyzing ECAR and OCR data, I observed that OVA/CFA immunization increased the basal glycolysis, glycolytic capacity, and glycolytic reserve in B cells, while the lack of InsR brought them back down to the pre-immunized levels (**Figure 4.6 B-D**). Moreover, OVA/CFA immunization also significantly increased ATP-linked respiration, maximal respiration, and spare capacity in B cells, along with a slight increase in basal respiration (**Figure 4.6 F-I**). Consistent with my hypothesis, the lack of InsR brought them back down to the pre-immunized levels. Specifically, B cell-intrinsic IR significantly reduced the maximal respiration in B cells, and also slightly decreased basal respiration, ATP-linked respiration, and spare capacity (**Figure 4.6 F-I**). Overall, my data suggested that the negative impact of B cell-intrinsic IR on OVA/CFA-induced primary GC reaction may result from impaired metabolic adaption.

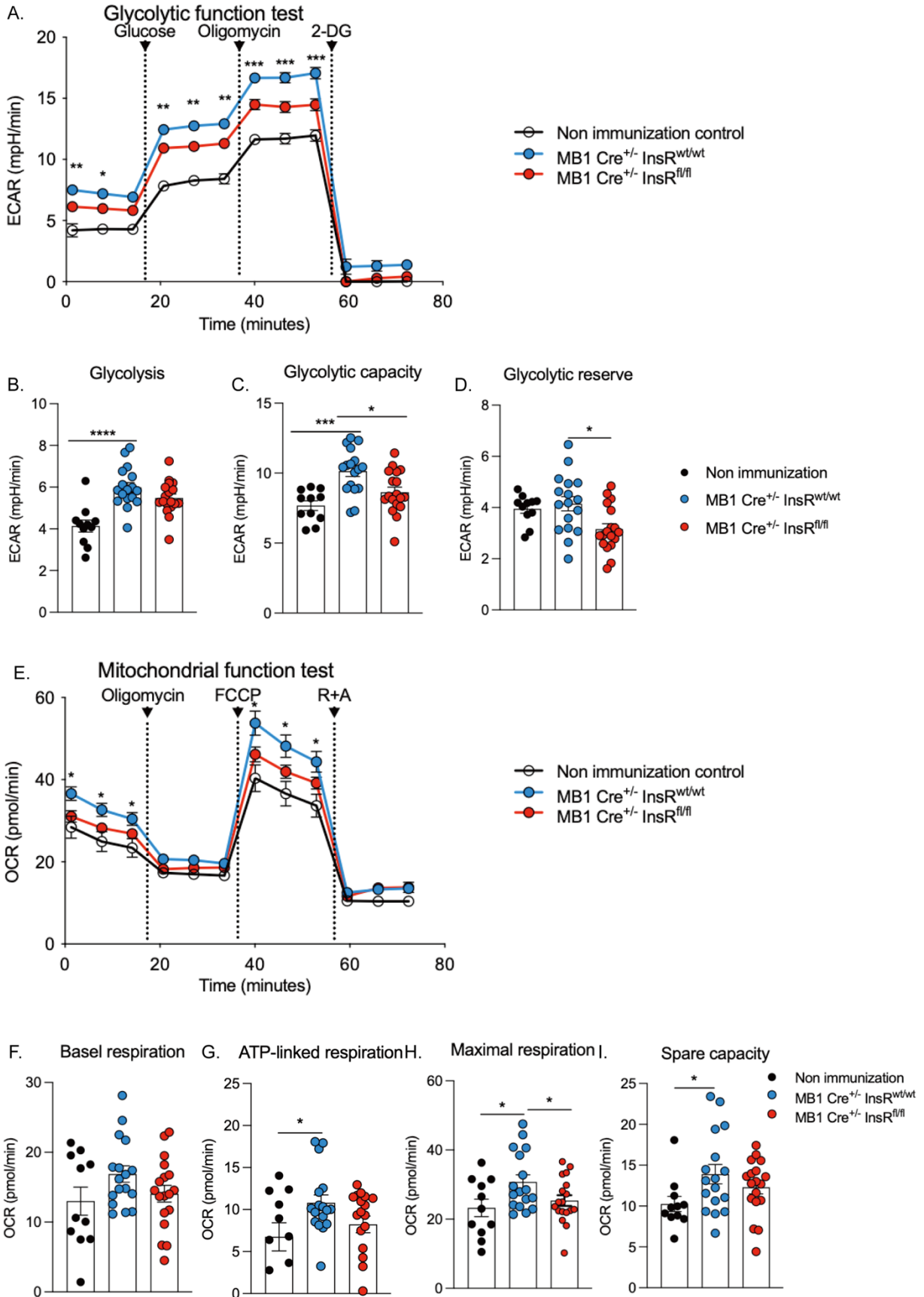


**Figure 4.6 B cell-intrinsic IR regulated B cell glycolytic and oxidative metabolism during OVA/CFA-induced primary immune response.** (A, E) B cells were isolated from non-immunized WT (MB1 Cre<sup>+/-</sup> InsR<sup>wt/wt</sup>) mice and immunized WT (MB1 Cre<sup>+/-</sup> InsR<sup>wt/wt</sup>) and immunized B cell-specific InsR-deficient (MB1 Cre<sup>+/-</sup> InsR<sup>fl/fl</sup>) mice using EasySep™ Mouse B Cell Isolation Kit (Stem Cell). (A) Real-time changes in ECAR ratios in isolated B cells were measured using a Seahorse metabolic flux analyzer. (B-D) Changes in basal glycolysis (B), glycolytic capacity (C), and glycolytic reserve (D) in isolated B cells were assessed by analyzing ECAR data (n=11-17, each dot represents one replicate). (E) Real-time changes in OCR ratios in isolated B cells were measured using a Seahorse metabolic flux analyzer. (F-I) Changes in basal respiration (F), ATP-linked respiration (G), maximal respiration (H), and spare capacity (I) in isolated B cells were assessed by analyzing OCR data (n=11-17, each dot represents one replicate). Each mouse was subjected to two or three replicates, and two independent experiments were performed. \*P<0.05, \*\*P<0.01, \*\*\*P<0.001, \*\*\*\*P<0.0001 with Two-Way ANOVA (A, E) or Mann Whitney U-test (B-D, F-I). Data are represented as mean±SEM.

#### **4.2.5 B cell-intrinsic IR impaired B cell-mediated memory responses to OVA/IFA secondary immunization**

Immunization with OVA/CFA promotes the generation of humoral memory response, which is mediated by long-lived plasma cells and MBCs. I assessed the impact of B cell-intrinsic IR on B cell-mediated memory responses using a prime/boost protocol, where mice were immunized with OVA/CFA on day 0 and boosted at day 42 with OVA/IFA. Mice were euthanized 6 days after the secondary challenge for flow cytometric analysis. I collected the sera on day 48, and observed a decrease in OVA-specific IgA, IgM, and IgG<sub>3</sub> (**Figure 4.7 A-C**). Similar to my data of the primary responses, I also observed an increase in OVA-specific IgE, and the reasons remain unclear (**Figure 4.7 D**), while for IgG<sub>1</sub>, IgG<sub>2b</sub>, and IgG<sub>2c</sub>, no differences were observed (**Figure 4.7 E-G**).

I next tested the effect of B cell-intrinsic IR on the GC reaction during the secondary challenge. Consistent with the literature, the GC B cells (CD19<sup>+</sup>B220<sup>+</sup>CD95<sup>+</sup>GL-7<sup>+</sup>) were not present at day 42 following a primary immunization (**Figure 4.8 A, C, D**). GC B cells measured 6 days after the secondary challenge contain mostly MBCs re-entering into the GC reaction. As shown in **Figure 4.8**, I observed a decrease in the frequency and number of GC B cells in draining ALNs of B cell-specific InsR-deficient mice on day 48 (**Figure 4.8 B, C, D**), suggesting B cell-intrinsic IR impaired the re-entry of MBCs into GC reaction during secondary immunization.

Moreover, I measured the proportions of plasma cells, which are mainly differentiated from MBCs at this time point. Similarly, I compared the number of plasma cells (CD19<sup>lo</sup>B220<sup>lo</sup>CD38<sup>+</sup>CD138<sup>+</sup>) on day 42 (before secondary immunization) and day 48 (6 days post-secondary immunization). Both WT and B cell-specific InsR-deficient mice showed an increase in the frequency and number of plasma cells comparing day 42 with day 48, and B cell-specific InsR-deficient mice showed a decrease in the frequency and number of plasma cells in draining ALNs on day 48 (**Figure 4.8 E-H**). The aforementioned data indicated that B cell-intrinsic IR impaired the rapid differentiation of plasma cells from MBCs during memory response.

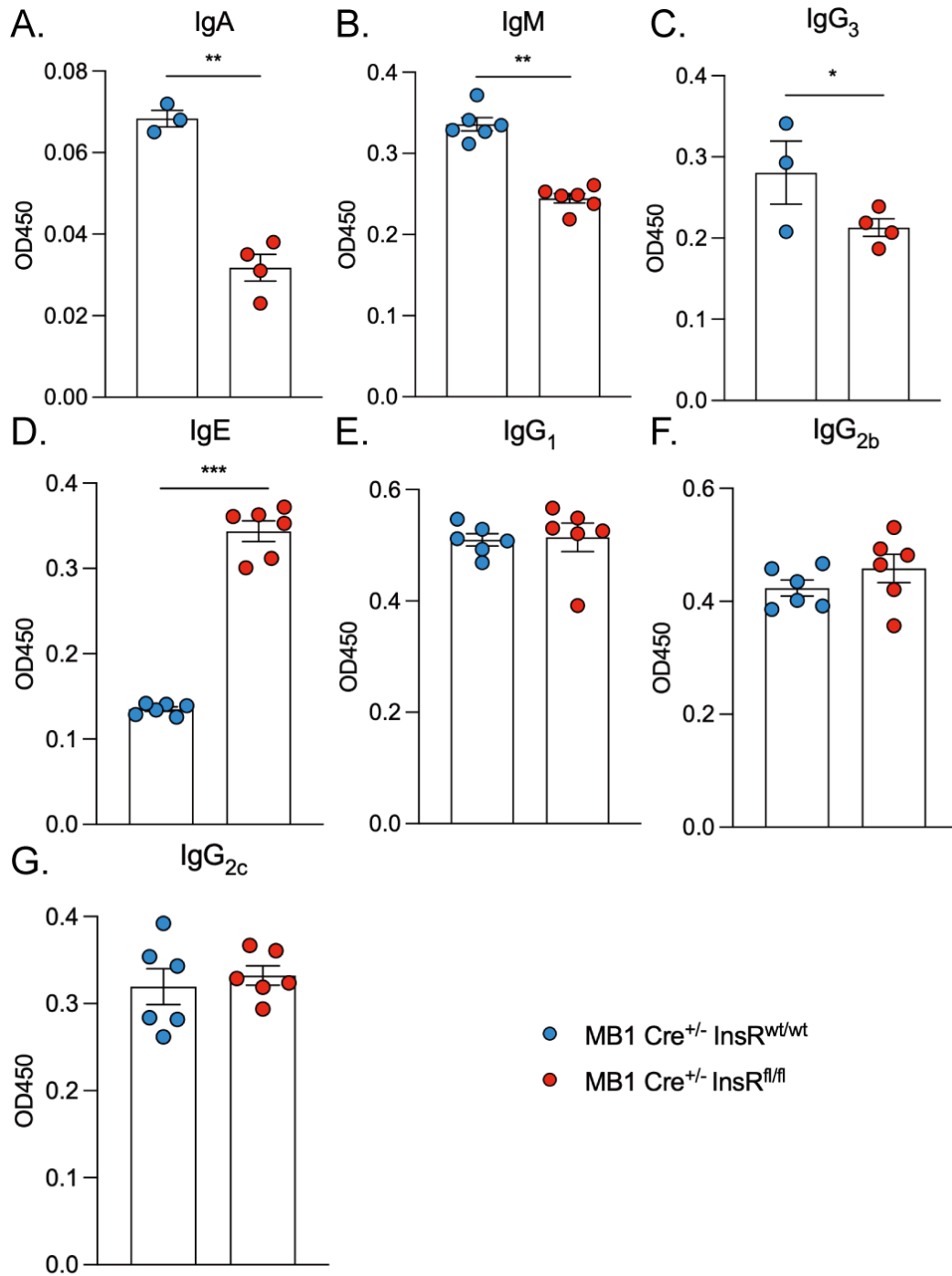


**Figure 4.7 B cell-intrinsic IR altered antibody production by B cells during the OVA/IFA secondary challenge.** OVA-specific antibody responses on 14 days post-immunization, as determined by OVA-specific Ig ELISA (n=6, each dot represents one mouse). Dilution ratios are as follows: IgM/IgG<sub>2b</sub>/IgG<sub>2c</sub>/IgG<sub>3</sub>: 1:400; IgA/IgE: 1:200; IgG<sub>1</sub>: 1:1000. \*P<0.05, \*\*P<0.01, \*\*\*P<0.001 with Mann Whitney U-test. Data are represented as mean±SEM.

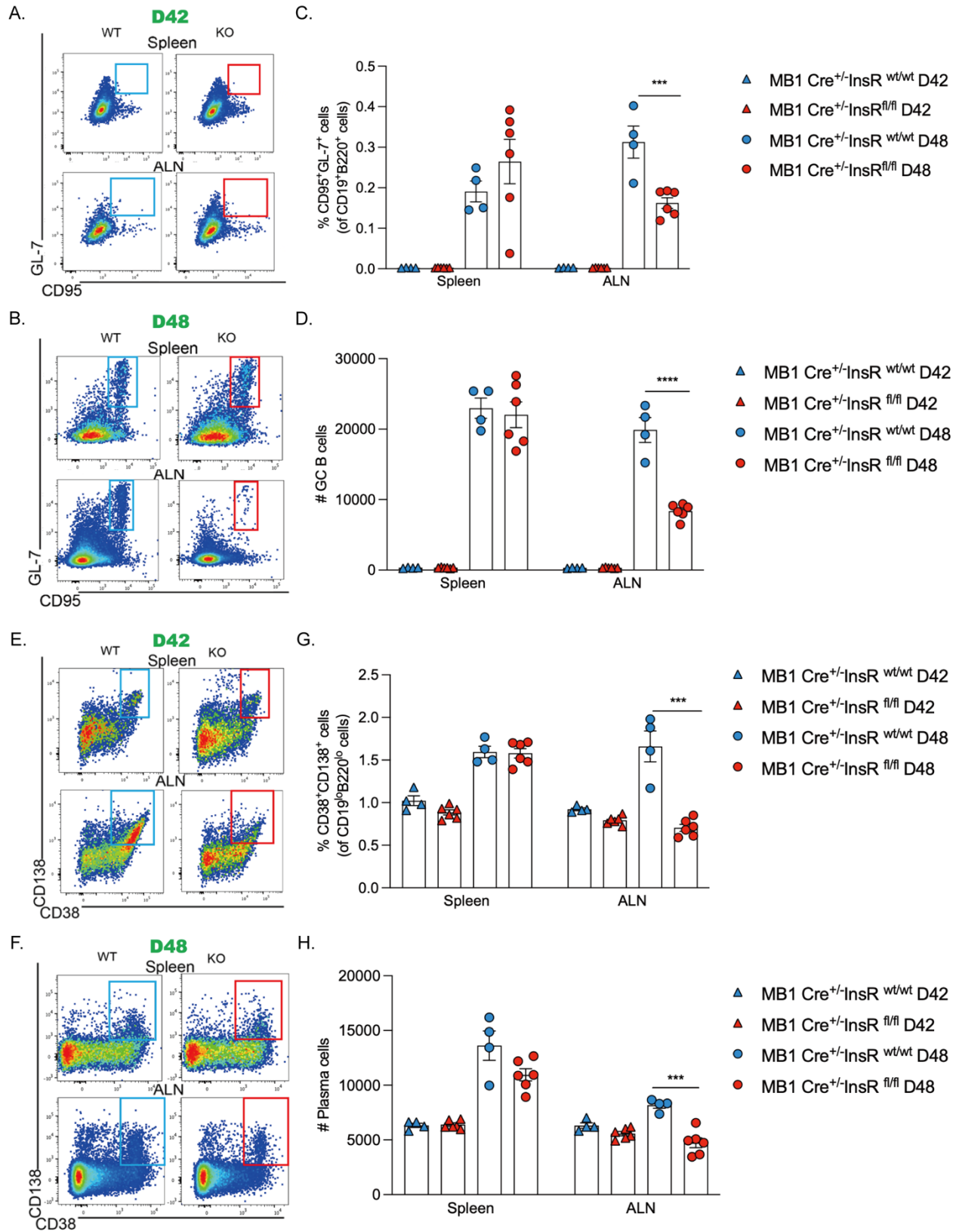


**Figure 4.8 B cell-intrinsic IR impaired B cell-mediated memory responses during the OVA/IFA secondary challenge.** (A) Flow plots of total GC cells in WT (MB1 Cre<sup>+/-</sup> InsR<sup>wt/wt</sup>) and B cell-specific InsR-deficient (MB1 Cre<sup>+/-</sup> InsR<sup>fl/fl</sup>) mice on day 42 post-primary OVA/CFA immunization. (B) Flow plots of total GC cells in WT (MB1 Cre<sup>+/-</sup> InsR<sup>wt/wt</sup>) and B cell-specific InsR-deficient (MB1 Cre<sup>+/-</sup> InsR<sup>fl/fl</sup>) mice on day 6 post-secondary OVA/IFA immunization. (C-D) B cell-specific InsR-deficient (MB1 Cre<sup>+/-</sup> InsR<sup>fl/fl</sup>) mice showed reduced frequency and number of total GC B cells on day 6 post-secondary OVA/IFA immunization (ALNs), as determined by flow cytometry (gated out of CD19<sup>+</sup>B220<sup>+</sup> cells, n=4-6, each dot represents one mouse). (E) Flow plots of plasma cells in WT (MB1 Cre<sup>+/-</sup> InsR<sup>wt/wt</sup>) and B cell-specific InsR-deficient (MB1 Cre<sup>+/-</sup> InsR<sup>fl/fl</sup>) mice on day 42 post primary OVA/CFA immunization. (F) Flow plots of plasma cells in WT (MB1 Cre<sup>+/-</sup> InsR<sup>wt/wt</sup>) and B cell-specific InsR-deficient (MB1 Cre<sup>+/-</sup> InsR<sup>fl/fl</sup>) mice on day 6 post-secondary OVA/IFA immunization. (G-H) B cell-specific InsR-deficient (MB1 Cre<sup>+/-</sup> InsR<sup>fl/fl</sup>) mice showed reduced frequency and number of plasma cells on day 6 post-secondary OVA/IFA immunization (ALNs), as determined by flow cytometry (gated out of CD19<sup>lo</sup>B220<sup>lo</sup> cells, n=4-6, each dot represents one mouse). \*\*\*P<0.001, \*\*\*\*P<0.0001 with Mann Whitney U-test. Data are represented as mean±SEM.

#### ***4.2.6 B cell-intrinsic IR impaired B cell-mediated anti-viral immunity by altering antibody production and impairing the GC reaction***

To test whether and how B cell-intrinsic IR affects B cell-mediated anti-viral immune responses, I performed an infection with a sublethal dose of the H1N1/Puerto Rico/8/34 (PR8) influenza virus in WT (CD19 Cre<sup>+/-</sup> InsR<sup>wt/wt</sup>) and B cell-specific InsR-deficient (CD19 Cre<sup>+/-</sup> InsR<sup>fl/fl</sup>) mice. The body weights of mice were monitored twice daily for 14 days, and the blood samples, spleens, draining mLNs, lungs, and BALs were collected 14 days post-infection. I first compared the changes in disease severity between infected WT and B cell-specific InsR-deficient mice. As shown in **Figure 4.9**, infected B cell-specific InsR-deficient mice showed increased body weight loss at the peak of the disease, but survival was not impacted (determined by the number of mice reaching the humane endpoint).

Next, to test if B cell-intrinsic IR affects the antibody production by B cells upon influenza infection, the sera collected on day 14 post-infection were subjected to influenza-specific Ig ELISA analysis. I did a full-titration test to confirm the appropriate diluted concentrations of serum samples for different isotypes and determined that the best diluted concentration for all samples is 1:100 (data not shown). By using this diluted concentration, I observed a decrease in IgA, IgM, and most interestingly, IgE, which is different from the OVA/CFA immunization model (**Figure 4.10 A-C**). Regarding IgG<sub>1</sub>, IgG<sub>2b</sub>, IgG<sub>2c</sub>, and IgG<sub>3</sub>, I did not observe any difference between infected WT and B cell-specific InsR-deficient mice (**Figure 4.10 D-G**). To assess antibody production in the airway, I collected the BALs from infected mice and measured the influenza-specific antibody production in the BALs. As shown in **Figure 4.10**, IgA and IgM levels showed a significant increase in the BALs (**Figure 4.10 H-I**), and IgG<sub>2c</sub> and IgG<sub>3</sub> levels were decreased (**Figure 4.10 J-K**). No differences were observed in the levels of IgE, IgG<sub>1</sub>, and IgG<sub>2b</sub> (**Figure 4.10 L-N**).

To further understand how B cell-intrinsic IR affects B cell-mediated anti-viral immunity, I next tested the effect of B cell-intrinsic IR on the GC reaction in response to H1N1/PR8 virus infection. I observed a decrease in the frequency of total GC B cells (CD19<sup>+</sup>B220<sup>+</sup>CD95<sup>+</sup>GL-7<sup>+</sup>) in the spleens and draining mLNs on day 14 (**Figure 4.11 A-B**). The absolute number of total GC B cells only showed a decrease in the spleens, not the draining mLNs, which may result from the differences in the mLN cell numbers between mice (**Figure 4.11 C**).

Overall, B cell-intrinsic IR altered the influenza-specific antibody production by B cells and impaired the GC reaction against the H1N1/PR8 influenza virus, which further contributed to the disease severity.

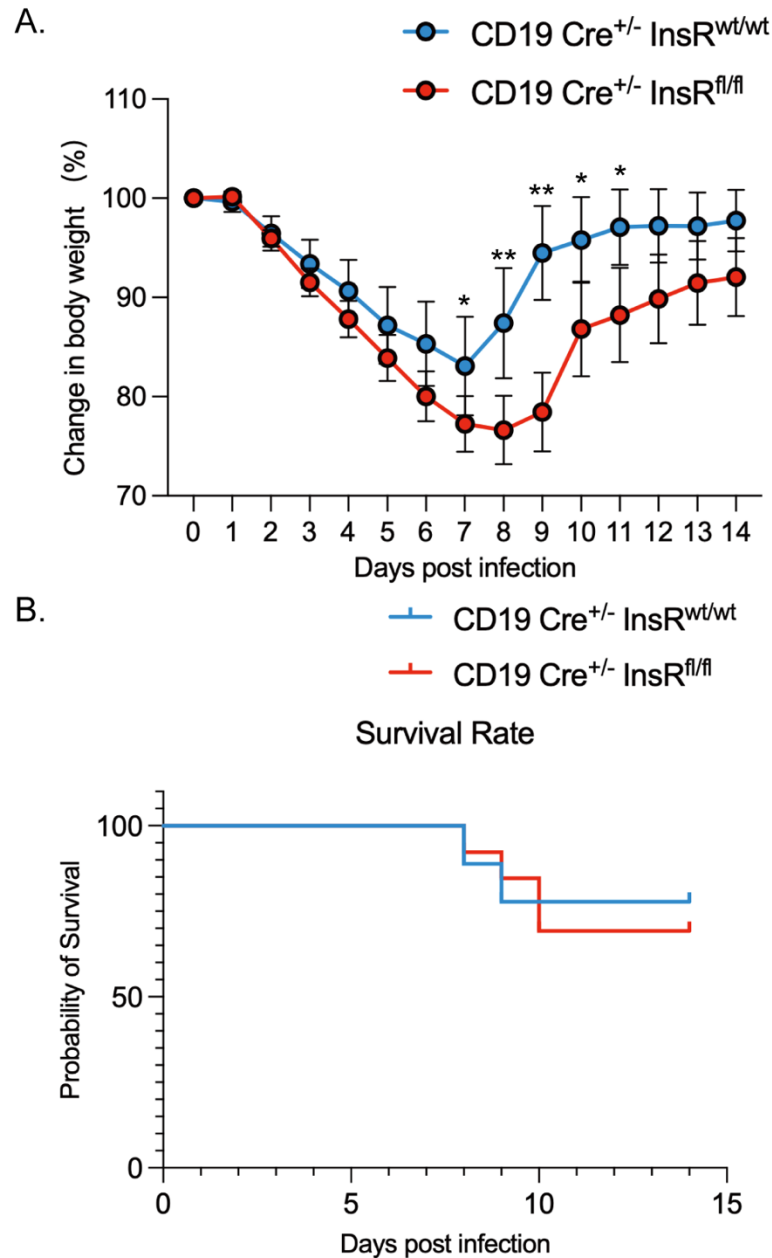


**Figure 4.9 B cell-intrinsic IR increased H1N1/PR8 influenza virus-induced disease severity.**

(A) WT (CD19 Cre<sup>+/-</sup> InsR<sup>wt/wt</sup>) and B cell-specific InsR-deficient (CD19 Cre<sup>+/-</sup> InsR<sup>fl/fl</sup>) mice were infected with H1N1/PR8 influenza virus and monitored for 14 days, B cell-specific InsR-deficient (CD19 Cre<sup>+/-</sup> InsR<sup>fl/fl</sup>) mice showed increased body weight loss (A, n=7-9), while no difference was observed in survival rate (B, n=7-9). \*P<0.05, \*\*P<0.01 with Two-way ANOVA test. Data are represented as mean±SEM.

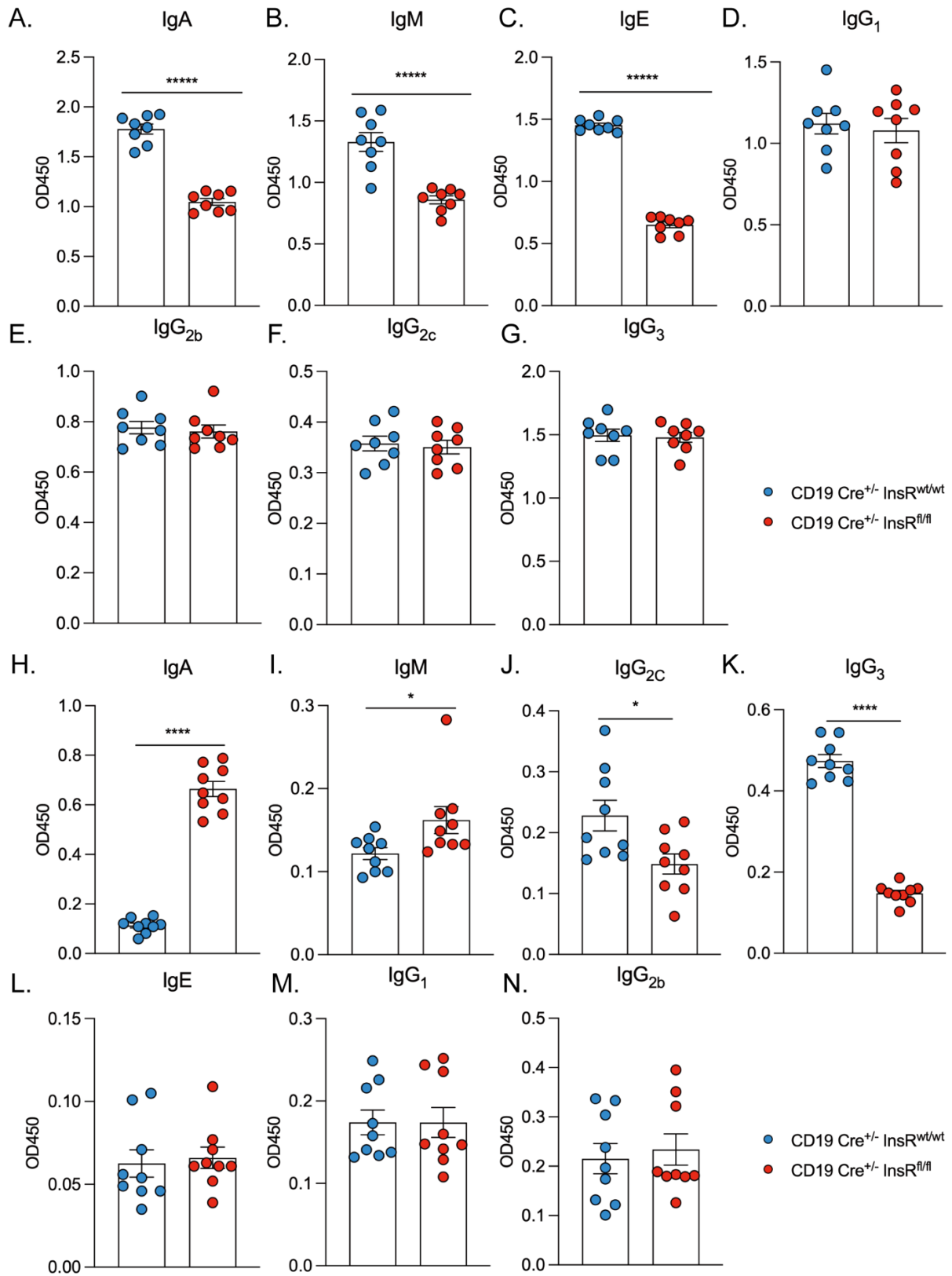


**Figure 4.10 B cell-intrinsic IR altered antibody production by B cells upon H1N1/PR8 influenza virus infection.** (A-G) Influenza-specific antibody responses on day 14 post-infection in sera, as determined by influenza-specific Ig ELISA (n=8, each dot represents one mouse). (H-N) Influenza-specific antibody responses on day 14 post-infection in BALs, as determined by influenza-specific Ig ELISA (n=9, each dot represents one mouse). Dilution ratios are as follows: IgA/IgM/IgE/IgG<sub>1</sub>/IgG<sub>2b</sub>/IgG<sub>2c</sub>/IgG<sub>3</sub>:1:100. ns P>0.05, \*P<0.05, \*\*\*\*P<0.0001 with Mann Whitney U-test. Data are represented as mean±SEM.

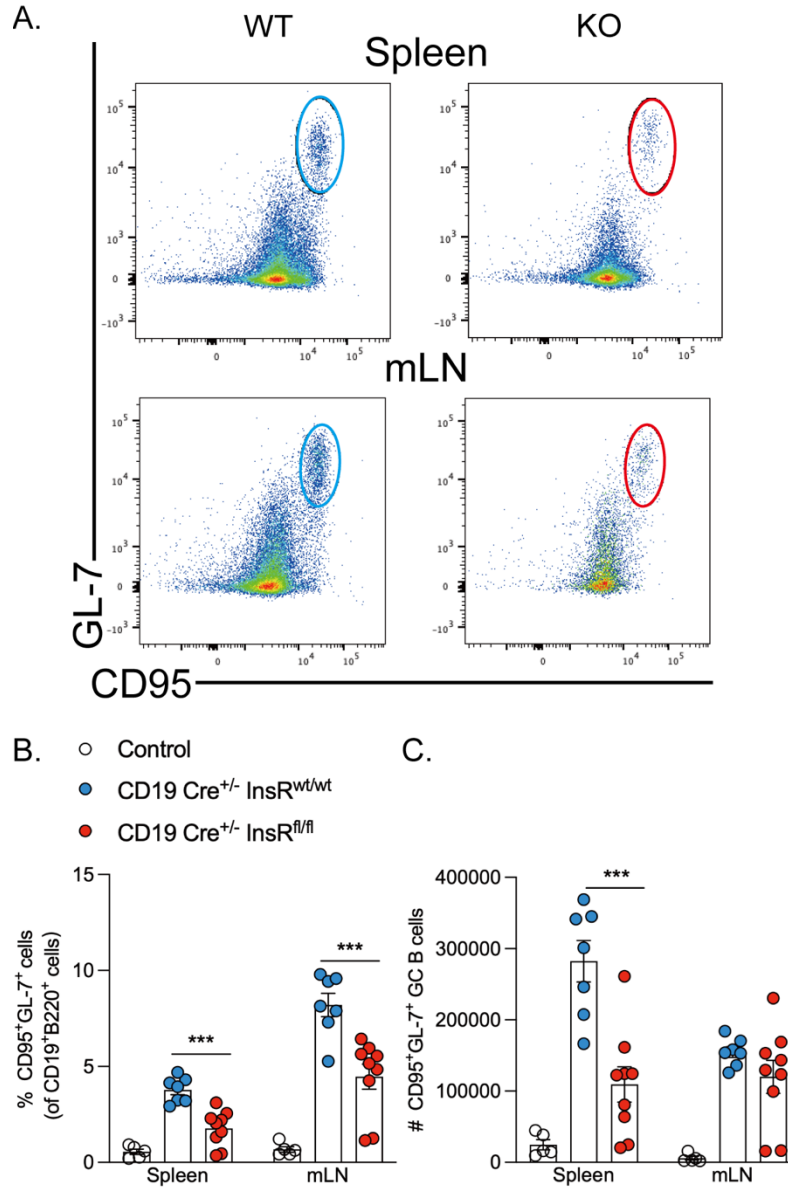


**Figure 4.11 B cell-intrinsic IR impaired GC reaction upon H1N1/PR8 influenza virus infection.** (A) Flow plots of total GC cells in infected WT (CD19 Cre<sup>+/-</sup> InsR<sup>wt/wt</sup>) and B cell-specific InsR-deficient (CD19 Cre<sup>+/-</sup> InsR<sup>fl/fl</sup>) mice on day 14 post-infection with H1N1/PR8 influenza virus. (B-C) B cell-specific InsR-deficient (CD19 Cre<sup>+/-</sup> InsR<sup>fl/fl</sup>) mice showed reduced frequency of total GC B cells in the spleens and mLN (day 14), reduced number of total GC B cells in the spleens (day 14), as determined by flow cytometry (gated from CD19<sup>+</sup>B220<sup>+</sup> cells, n=5-9, each dot represents one mouse). ns P>0.05, \*\*\*P<0.001 with Mann Whitney U-test. Data are represented as mean±SEM.

#### ***4.2.7 The impairment in GC reaction upon H1N1/PR8 influenza infection may result from the loss of help from CD4<sup>+</sup> T cells and T<sub>FH</sub> cells***

As mentioned in Chapter 1, the proliferation of antigen-activated B cells needs to receive help from antigen-activated CD4<sup>+</sup> T cells, while the entry of activated B cells into GC needs to receive help from T<sub>FH</sub> cells. Thus, I measured the influenza-specific CD4<sup>+</sup> T cells by staining with NP<sub>311-325</sub>/I-A<sup>b</sup> influenza tetramer in infected WT and B cell-specific InsR-deficient mice. I observed a decrease in the frequency and number of influenza-specific CD4<sup>+</sup> T cells (CD3<sup>+</sup>CD4<sup>+</sup>NP<sub>311-325</sub>/I-A<sup>b</sup> tetramer<sup>+</sup>) in the spleens of B cell-specific InsR-deficient mice on day 14 post-infection (**Figure 4.12 A-C**). However, no differences were observed in the draining mLNs and lungs on day 14 post-infection. I next euthanized another set of mice on day 8 post-infection, which is the peak time of H1N1/PR8 influenza virus infection according to my data. I observed a significant decrease in the frequency of influenza specific-CD4<sup>+</sup> T cells in the draining mLNs on day 8 post-infection (**Figure 4.12 D-E**). Moreover, I measured the changes in the total T<sub>FH</sub> cells and observed no differences between infected WT and B cell-specific InsR-deficient mice (**Figure 4.13 A-C**). I also observed that the frequency and number of influenza-specific T<sub>FH</sub> cells (CD3<sup>+</sup>CD4<sup>+</sup>NP<sub>311-325</sub>/I-A<sup>b</sup> tetramer<sup>+</sup>CXCR5<sup>+</sup>PD-1<sup>+</sup>) were decreased in the spleens and draining mLNs of B cell-specific InsR-deficient mice on day 14 post-infection (**Figure 4.13 D-F**). Overall, these data suggested that the impairment in GC reaction upon PR8/H1N1 virus infection may result from the deficiency in the help from antigen-specific CD4<sup>+</sup> T cells and T<sub>FH</sub> cells.

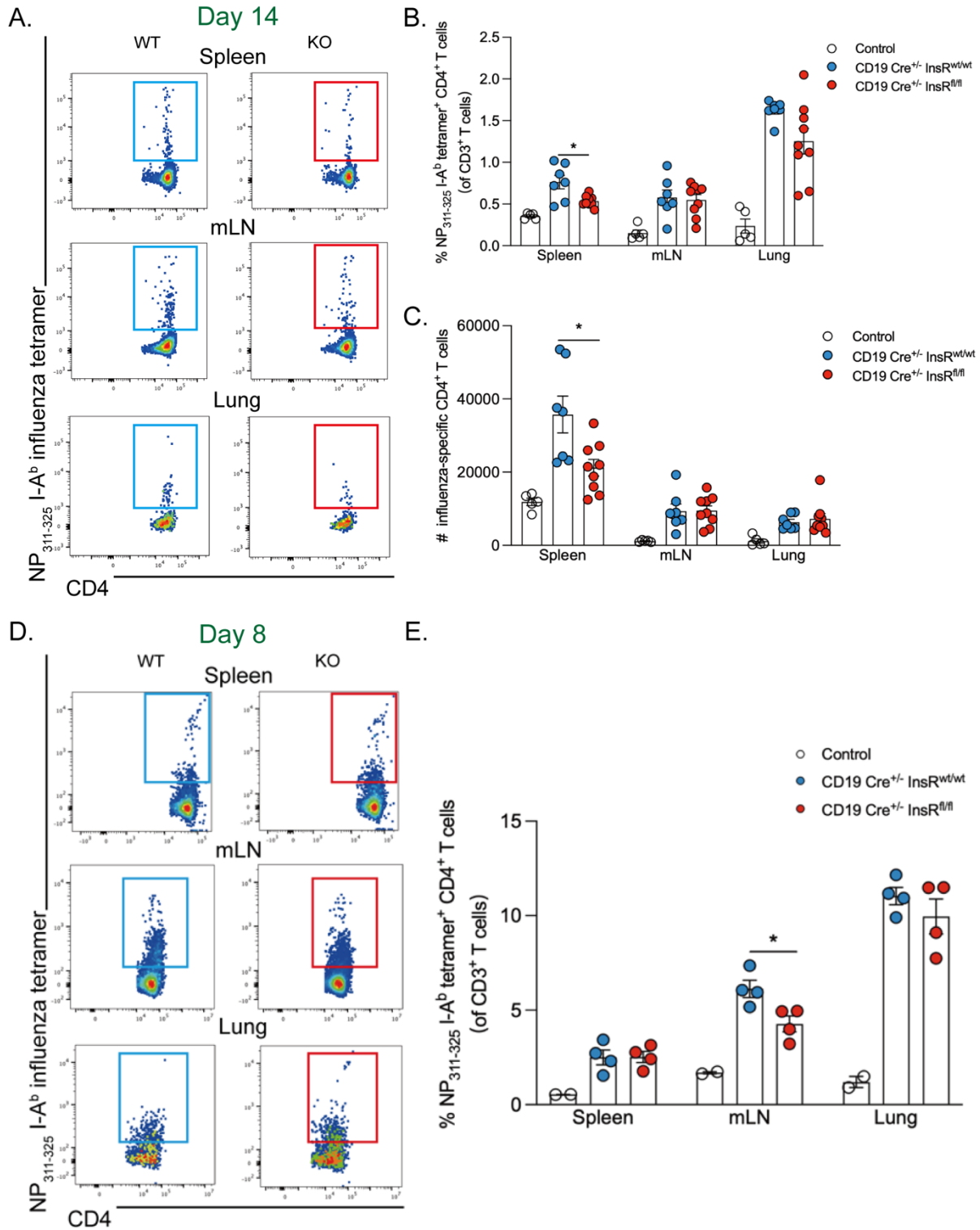


**Figure 4.12 B cell-specific InsR-deficient mice showed reduced influenza-specific CD4<sup>+</sup> T cells upon influenza virus infection.** (A) Flow plots of influenza-specific CD4<sup>+</sup> T cells in infected WT (CD19 Cre<sup>+/-</sup> InsR<sup>wt/wt</sup>) and B cell-specific InsR-deficient (CD19 Cre<sup>+/-</sup> InsR<sup>fl/fl</sup>) mice on day

14 post-infection. (B-C) B cell-specific InsR-deficient (CD19 Cre<sup>+/-</sup> InsR<sup>fl/fl</sup>) mice showed reduced frequency and number of influenza-specific CD4<sup>+</sup> T cells on day 14 post-H1N1/PR8 influenza virus infection (spleens), as determined by flow cytometry (gated from CD3<sup>+</sup>CD4<sup>+</sup> cells, n=5-9, each dot represents one mouse). (D) Flow plots of influenza-specific CD4<sup>+</sup> T cells in infected WT (CD19 Cre<sup>+/-</sup> InsR<sup>wt/wt</sup>) and B cell-specific InsR-deficient (CD19 Cre<sup>+/-</sup> InsR<sup>fl/fl</sup>) mice on day 8 post-infection. (E) B cell-specific InsR-deficient (CD19 Cre<sup>+/-</sup> InsR<sup>fl/fl</sup>) mice showed a decrease in the frequency of influenza-specific CD4<sup>+</sup> T cells on day 8 post-H1N1/PR8 influenza virus infection (mLNs), as determined by flow cytometry (gated from CD3<sup>+</sup>CD4<sup>+</sup> cells, n=2-4, each dot represents one mouse). ns P>0.05, \*P<0.05 with Mann Whitney U-test. Data are represented as mean±SEM.

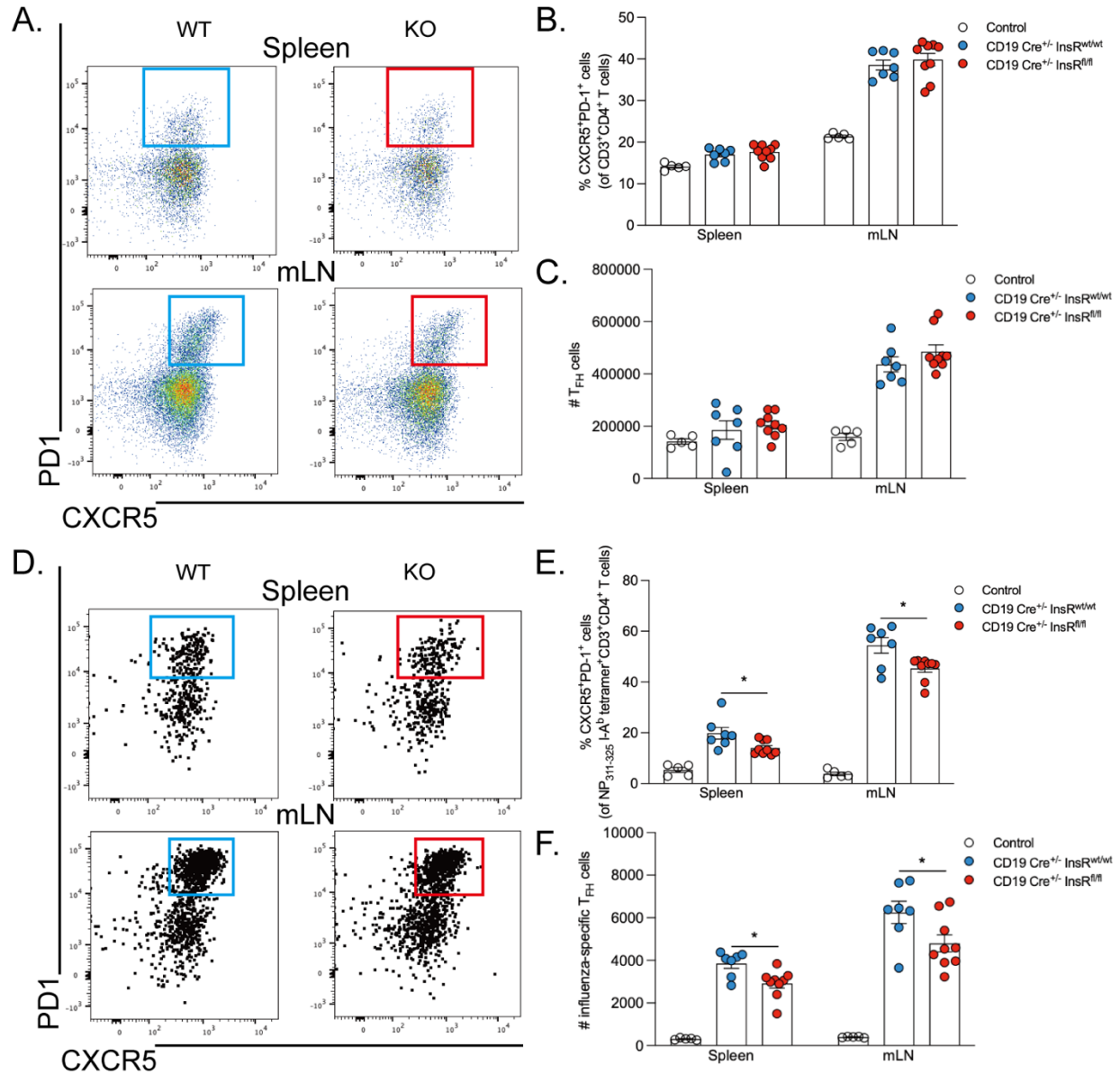


**Figure 4.13 B cell-specific InsR-deficient mice showed reduced influenza-specific  $T_{FH}$  cells upon influenza virus infection.** (A) Flow plots of total  $T_{FH}$  cells in infected WT (CD19 Cre<sup>+/-</sup> InsR<sup>wt/wt</sup>) and B cell-specific InsR-deficient (CD19 Cre<sup>+/-</sup> InsR<sup>fl/fl</sup>) mice on day 14 post-infection. (B-C) B cell-specific InsR-deficient (CD19 Cre<sup>+/-</sup> InsR<sup>fl/fl</sup>) mice showed no differences in the frequency and number of total  $T_{FH}$  cells on day 14 post-H1N1/PR8 influenza virus infection (splens & mLNs), as determined by flow cytometry (gated from CD3<sup>+</sup>CD4<sup>+</sup> cells, n=5-9, each dot represents one mouse). (D) Flow plots of influenza-specific  $T_{FH}$  cells in infected WT (CD19 Cre<sup>+/-</sup> InsR<sup>wt/wt</sup>) and B cell-specific InsR-deficient (CD19 Cre<sup>+/-</sup> InsR<sup>fl/fl</sup>) mice on day 14 post-infection.

(E-F) B cell-specific InsR-deficient (CD19 Cre<sup>+/-</sup> InsR<sup>fl/fl</sup>) mice showed reduced frequency and number of influenza-specific T<sub>FH</sub> cells on day 14 post-H1N1/PR8 influenza virus infection (spleens & mLN), as determined by flow cytometry (gated from CD3<sup>+</sup>CD4<sup>+</sup>NP<sub>311-325</sub>/I-A<sup>b</sup> tetramer<sup>+</sup> cells, n=5-9, each dot represents one mouse). ns P>0.05, \*P<0.05 with Mann Whitney U-test. Data are represented as mean±SEM.

#### ***4.2.8 B cell-intrinsic IR impaired immune dominant T cell responses upon H1N1/PR8 influenza virus infection***

Upon exposure to the virus, B cells can also modulate the activation and function of other immune cells such as T cells through functioning as APCs or secreting cytokines. I next tested whether the genetic InsR ablation in B cells affects their function of modulating T cell-mediated immune responses. I first measured the influenza-specific CD8<sup>+</sup> T cells by staining with NP<sub>366-374</sub>/H-2D<sup>b</sup> influenza tetramer in infected WT (CD19 Cre<sup>+/-</sup> InsR<sup>wt/wt</sup>) and B cell-specific InsR-deficient (CD19 Cre<sup>+/-</sup> InsR<sup>fl/fl</sup>) mice. As shown in **Figure 4.14**, there were no differences in the frequency and number of influenza-specific CD8<sup>+</sup> T cells (CD3<sup>+</sup>CD8<sup>+</sup>NP<sub>366-374</sub>/H-2D<sup>b</sup> tetramer<sup>+</sup>) between WT and B cell-specific InsR-deficient mice on day 14 post-infection (**Figure 4.14 A-C**). I also measured the influenza-specific CD8<sup>+</sup> T cells in all tissues on day 8 post-infection and observed a significant decrease in the frequency of influenza-specific CD8<sup>+</sup> T cells in the draining mLNs and lungs (**Figure 4.14 D-E**).

I next measured the changes in the cytokine production in CD4<sup>+</sup> and CD8<sup>+</sup> T cells. As shown in **Figure 4.15**, I did not observe any difference in the number of TNF $\alpha$ -producing CD4<sup>+</sup> T cells (CD3<sup>+</sup>CD4<sup>+</sup>TNF $\alpha$ <sup>+</sup>) in all tissues between WT and B cell-specific InsR-deficient mice on day 14 post-infection (**Figure 4.15 C**), while B cell-specific InsR-deficient mice showed a decrease in the frequency of TNF $\alpha$ -producing CD4<sup>+</sup> T cells (CD3<sup>+</sup>CD4<sup>+</sup>TNF $\alpha$ <sup>+</sup>) in the lungs on day 14 post-infection, and no differences in the frequency of TNF $\alpha$ -producing CD4<sup>+</sup> T cells (CD3<sup>+</sup>CD4<sup>+</sup>TNF $\alpha$ <sup>+</sup>) were observed in the spleens and draining mLNs (**Figure 4.15 A-B**). I also measured the IFN $\gamma$ -producing CD4<sup>+</sup> T cells in WT and B cell-specific InsR-deficient mice. However, the frequency and number of IFN $\gamma$ -producing CD4<sup>+</sup> T cells showed no differences between WT and B cell-specific InsR-deficient mice (**Figure 4.16 D-F**). I next measured the changes in the cytokine production in CD8<sup>+</sup> T cells. Similar to CD4<sup>+</sup> T cells, I did not observe any difference in the frequency and number of IFN $\gamma$ -producing CD8<sup>+</sup> T cells in all tissues examined (**Figure 4.16 D-F**), but a decrease in the frequency of TNF $\alpha$ -producing CD8<sup>+</sup> T cells in the lungs on day 14 post-

infection (**Figure 4.16 A-C**). In summary, B cell-specific InsR-deficient mice showed impairment in PMA-stimulated cytokine production in lung CD4<sup>+</sup> and CD8<sup>+</sup> T cells.

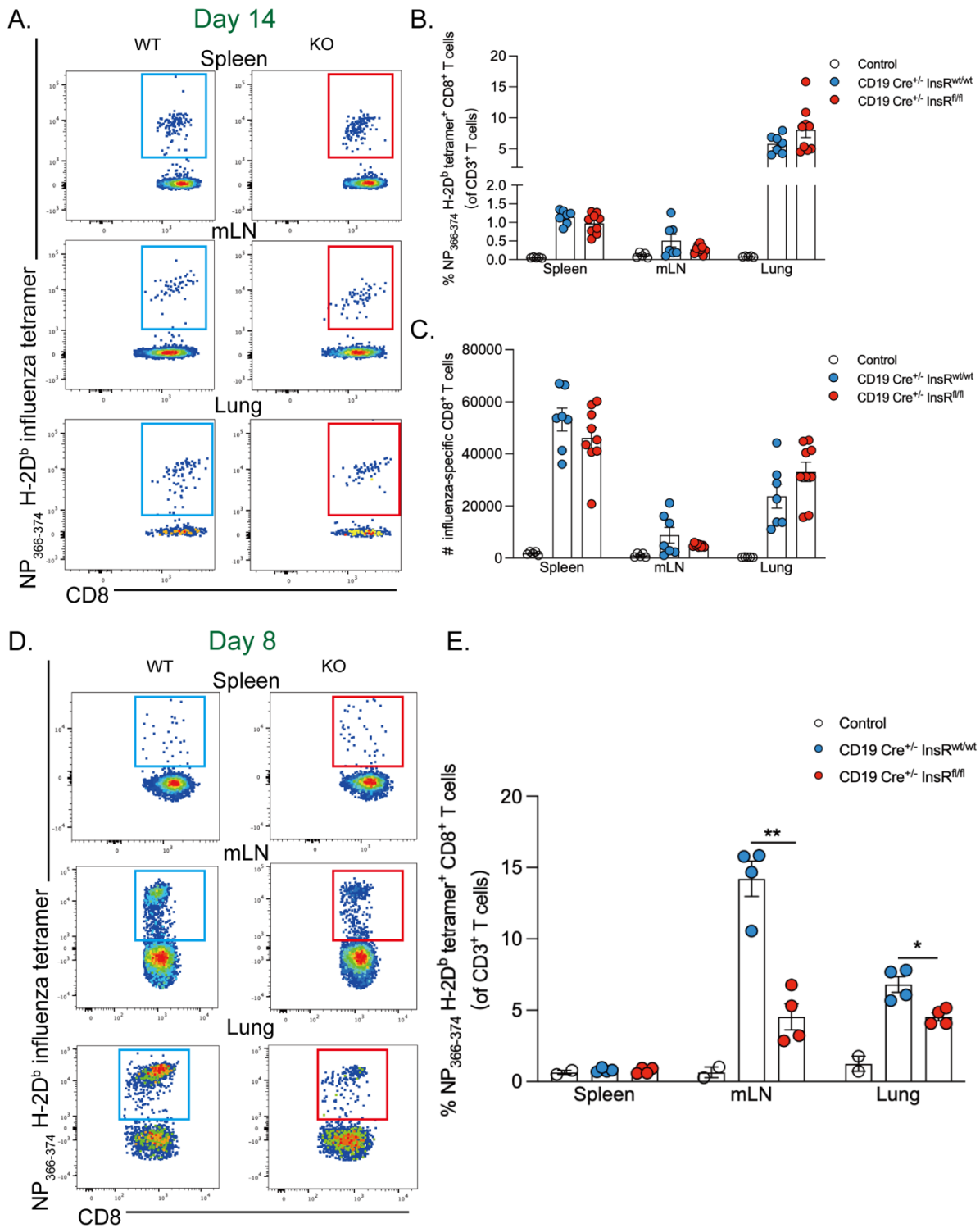


**Figure 4.14 B cell-specific InsR-deficient mice showed reduced influenza-specific CD8<sup>+</sup> T cells upon influenza virus infection.** (A) Flow plots of influenza-specific CD8<sup>+</sup> T cells in infected WT (CD19 Cre<sup>+/-</sup> InsR<sup>wt/wt</sup>) and B cell-specific InsR-deficient (CD19 Cre<sup>+/-</sup> InsR<sup>fl/fl</sup>) mice on day

14 post-infection. (B-C) B cell-specific InsR-deficient (CD19 Cre<sup>+/-</sup> InsR<sup>fl/fl</sup>) mice showed no difference in the frequency and number of influenza-specific CD8<sup>+</sup> T cells on day 14 post-H1N1/PR8 influenza virus infection (spleens & mLNs & lungs), as determined by flow cytometry (gated from CD3<sup>+</sup>CD8<sup>+</sup> cells, n=5-9, each dot represents one mouse). (D) Flow plots of influenza-specific CD8<sup>+</sup> T cells in infected WT (CD19 Cre<sup>+/-</sup> InsR<sup>wt/wt</sup>) and B cell-specific InsR-deficient (CD19 Cre<sup>+/-</sup> InsR<sup>fl/fl</sup>) mice on day 8 post-infection. (B) B cell-specific InsR-deficient (CD19 Cre<sup>+/-</sup> InsR<sup>fl/fl</sup>) mice showed a decrease in the frequency of influenza-specific CD8<sup>+</sup> T cells on day 8 post-H1N1/PR8 influenza virus infection (mLNs & lungs), as determined by flow cytometry (gated from CD3<sup>+</sup>CD8<sup>+</sup> cells, n=2-4, each dot represents one mouse). ns P>0.05, \*P<0.05, \*\*P<0.01 with Mann Whitney U-test. Data are represented as mean±SEM.

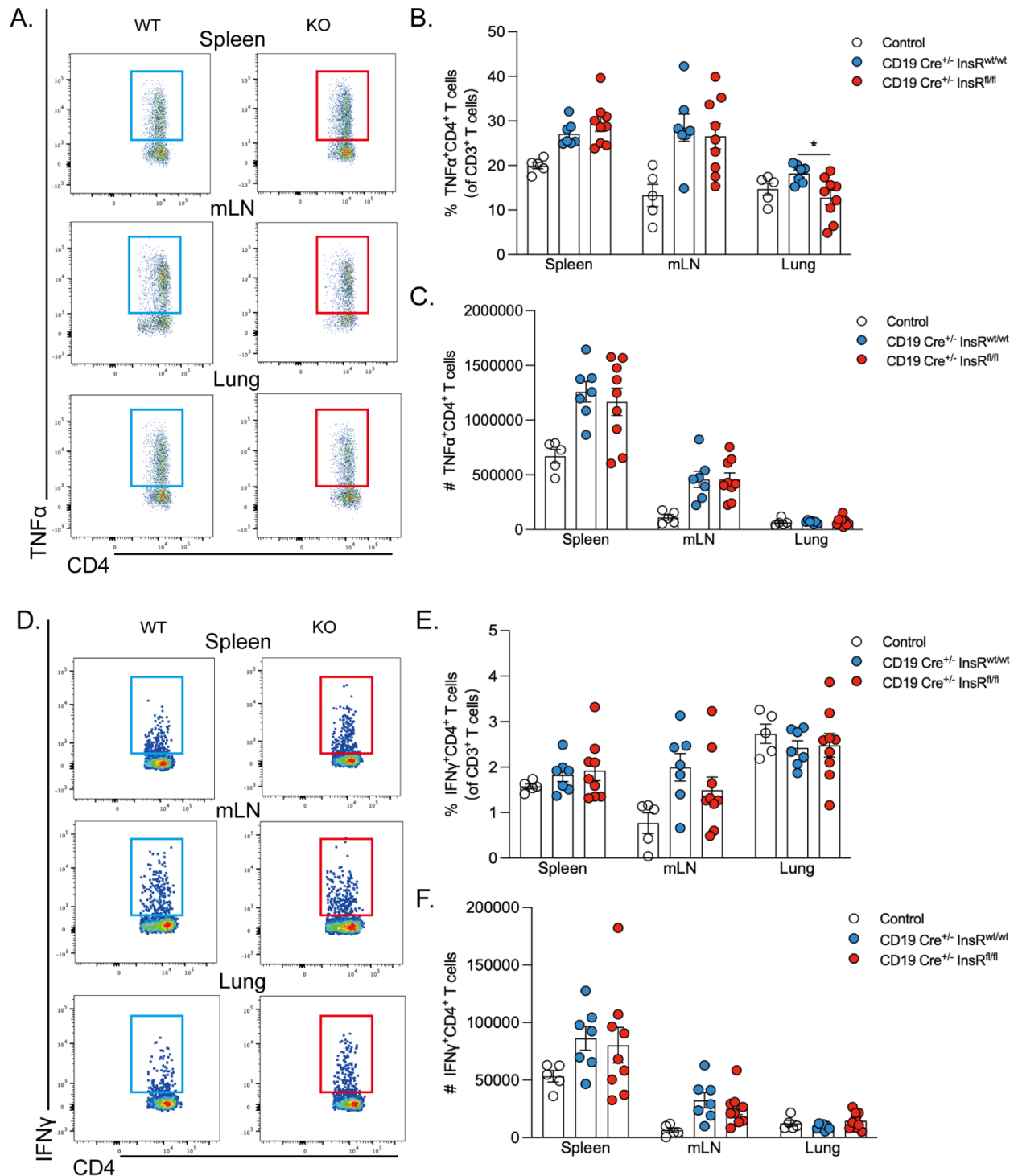


**Figure 4.15** TNF $\alpha$ - and IFN $\gamma$ -producing CD4<sup>+</sup> T cells in H1N1/PR8 influenza-infected mice. (A) Flow plots of TNF $\alpha$ -producing CD4<sup>+</sup> T cells in infected WT (CD19 Cre<sup>+/-</sup> InsR<sup>wt/wt</sup>) and B cell-specific InsR-deficient (CD19 Cre<sup>+/-</sup> InsR<sup>fl/fl</sup>) mice on day 14 post-infection. (B-C) B cell-specific

InsR-deficient (CD19 Cre<sup>+/-</sup> InsR<sup>fl/fl</sup>) mice showed a decrease in the frequency of TNF $\alpha$ -producing CD4<sup>+</sup> T cells on day 14 post-H1N1/PR8 influenza virus infection (lungs), as determined by flow cytometry (gated from CD3<sup>+</sup>CD4<sup>+</sup> cells, n=5-9, each dot represents one mouse). (D) Flow plots of IFN $\gamma$ -producing CD4<sup>+</sup> T cells in infected WT (CD19 Cre<sup>+/-</sup> InsR<sup>wt/wt</sup>) and B cell-specific InsR-deficient (CD19 Cre<sup>+/-</sup> InsR<sup>fl/fl</sup>) mice on day 14 post-infection. (E-F) B cell-specific InsR-deficient (CD19 Cre<sup>+/-</sup> InsR<sup>fl/fl</sup>) mice showed no difference in the frequency and number of IFN $\gamma$ -producing CD4<sup>+</sup> T cells on day 14 post-H1N1/PR8 influenza virus infection (spleens & mLNs & lungs), as determined by flow cytometry (gated from CD3<sup>+</sup>CD4<sup>+</sup> cells, n=5-9, each dot represents one mouse). ns P>0.05, \*P<0.05 with Mann Whitney U-test. Data are represented as mean $\pm$ SEM.

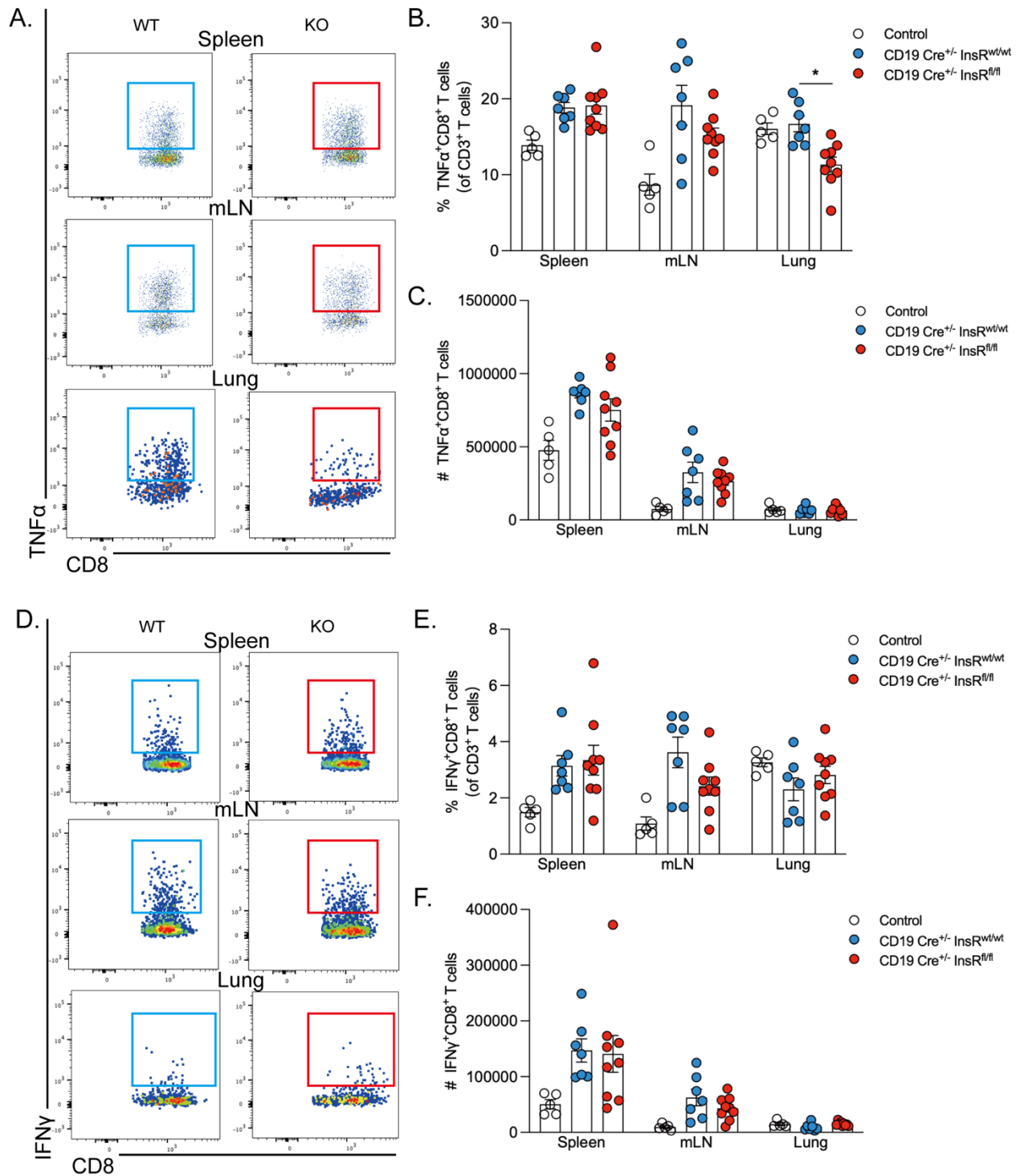


**Figure 4.16** TNF $\alpha$ - and IFN $\gamma$ -producing CD8<sup>+</sup> T cells in H1N1/PR8 influenza-infected mice. (A) Flow plots of TNF $\alpha$ -producing CD8<sup>+</sup> T cells in infected WT (CD19 Cre<sup>+/-</sup> InsR<sup>wt/wt</sup>) and B cell-specific InsR-deficient (CD19 Cre<sup>+/-</sup> InsR<sup>fl/fl</sup>) mice on day 14 post-infection. (B-C) B cell-specific

InsR-deficient (CD19 Cre<sup>+/-</sup> InsR<sup>fl/fl</sup>) mice showed a decrease in the frequency of TNF $\alpha$ -producing CD8<sup>+</sup> T cells on day 14 post-H1N1/PR8 influenza virus infection (lungs), as determined by flow cytometry (gated from CD3<sup>+</sup>CD4<sup>+</sup> cells, n=5-9, each dot represents one mouse). (D) Flow plots of IFN $\gamma$ -producing CD8<sup>+</sup> T cells in infected WT (CD19 Cre<sup>+/-</sup> InsR<sup>wt/wt</sup>) and B cell-specific InsR-deficient (CD19 Cre<sup>+/-</sup> InsR<sup>fl/fl</sup>) mice on day 14 post-infection. (E-F) B cell-specific InsR-deficient (CD19 Cre<sup>+/-</sup> InsR<sup>fl/fl</sup>) mice showed no difference in the frequency and number of IFN $\gamma$ -producing CD8<sup>+</sup> T cells on day 14 post-H1N1/PR8 influenza virus infection (spleens & mLNs & lungs), as determined by flow cytometry (gated from CD3<sup>+</sup>CD4<sup>+</sup> cells, n=5-9, each dot represents one mouse). ns P>0.05, \*P<0.05 with Mann Whitney U-test. Data are represented as mean $\pm$ SEM.

### 4.3 Discussion

B cells contribute significantly to the effectiveness of vaccines by recognizing antigens, producing antibodies, and forming memory cells that provide long-lasting immunity. Insulin signaling is important for maintaining glucose homeostasis which is essential for the activation and function of B cells<sup>171</sup>. In this chapter, by using an OVA/ CFA immunized DIO mouse model, I observed that DIO induced IR reduced the OVA-specific IgM levels in the serum, which reflects a defect in B cell activation (**Figure 4.1**). Moreover, HFD-fed mice showed impaired GC reaction during OVA/CFA-induced primary immune response (**Figure 4.2**), suggesting that B cell-intrinsic defects in insulin signaling have the potential to contribute to the low efficiency of vaccinations in obese individuals.

DIO induces IR in almost all insulin-dependent cells. Thus, to isolate the effect of IR specifically on B cells, I immunized WT and B cell-specific InsR-deficient mice and observed several alterations in antibody production in the sera on day 14 post-immunization (**Figure 4.3**). The decrease in the OVA-specific IgM antibody indicated a defect in B cell activation, as IgM antibody is mainly secreted by the short-lived plasma cells that were differentiated from activated B cells which have BCRs with low affinity with T<sub>FH</sub> cells. These cells cannot receive enough co-stimulatory signals from T<sub>FH</sub> cells and lose the ability to enter GC. Moreover, the decrease in the OVA-specific IgA and IgG<sub>3</sub> and no changes in the OVA-specific IgG<sub>1</sub> and IgG<sub>2b</sub>, and IgG<sub>2c</sub> suggested that insulin signaling may play an important role in antibody class-switching to specific isotypes.

The increase in the OVA-specific IgE in the serum samples post-immunization is surprising. IgE is an antibody involved in allergic reactions<sup>227</sup>. It binds to allergens and triggers the release of histamine and other chemicals from mast cells and basophils, leading to symptoms of allergy and asthma<sup>227</sup>. Recent studies have shown varying results regarding the positive correlation between IgE levels and IR, while the mechanisms are still under investigation<sup>228-234</sup>. The possible

mechanisms involve that insulin signaling regulates the class switching of IgE. Interestingly, our lab previously found that, CD23, also known as the low-affinity IgE receptor (FcεRII), showed a down-regulation in FO B cells of B cell-specific InsR-deficient mice (Unpublished data). CD23 binds to the Fc region of IgE with low affinity. This interaction helps regulate the levels of IgE in the blood by facilitating the removal and degradation of IgE<sup>235</sup>. Thereby, the accumulation of IgE in the serum of immunized B cell-specific InsR-deficient mice may result from the downregulation of CD23, while the precise mechanisms still need further investigation.

Regarding the GC reaction, I observed an impairment in GC reaction in immunized B cell-specific InsR-deficient mice (**Figure 4.4**). However, the precise mechanisms by which B cell-intrinsic IR impairs OVA/CFA-induced primary GC reaction is still a mystery. One of the possible reasons is related to helper T cells as activated B cells need to receive co-stimulatory signals from CD4<sup>+</sup> T cells and T<sub>FH</sub> cells before proliferating and entering the GC. Moreover, the cytokines produced by T<sub>FH</sub> cells are essential for the class-switching of B cells<sup>236, 237</sup>. For example, the class-switching of IgA isotype needs the presence of IL-5 and TGF-β, while IL-4 is essential for IgE and IgG<sub>1</sub> isotypes<sup>236, 237</sup>. Additionally, the generation of IgG<sub>2b</sub> and IgG<sub>2c</sub> isotypes needs the presence of IFN-γ, and IL-6 is important for the IgG<sub>3</sub> isotype<sup>236, 237</sup>. Thus, I next measured the frequency and number of OVA-specific CD4<sup>+</sup> T cells and OVA-specific T<sub>FH</sub> cells in immunized WT and B cell-specific InsR-deficient mice. As shown in **Figure 4.5**, B cell-specific InsR-deficient mice showed a reduction in the frequency and number of OVA-specific CD4<sup>+</sup> T cells and OVA-specific T<sub>FH</sub> cells, suggesting that the defect in T cell help may contribute to the impairment in GC reaction and the alterations in antibody production. Future experiments are needed to examine changes in cytokine production in T<sub>FH</sub> cells under such settings to fully understand how B cell-intrinsic IR alters the class-switching of B cells during the OVA/CFA-induced primary immune response. Moreover, the immunofluorescent staining of B cells, CD4<sup>+</sup> T cells, and T<sub>FH</sub> cells can be used to answer whether the impairment in GC reaction is resulting from unstable or defective B cell: T cell interactions.

In addition to the loss of helper signals from helper T cells, the alterations in metabolic pathways in B cells also have the potential to impact B cell differentiation and function. As mentioned in Chapter 3, B cell-intrinsic IR regulated glycolytic and oxidative metabolisms in LPS- and CpG-stimulated B cells, which can further impact differentiation and function. I next measured the changes in aerobic glucose metabolism and mitochondria respiration in B cells isolated from immunized WT and B cell-specific InsR-deficient mice, and observed reduced basal glycolysis, glycolytic capacity, glycolytic reserve, basal respiration, ATP-linked respiration, maximal respiration, and spare capacity in immunized InsR-deficient B cells compared with immunized WT B cells (**Figure 4.6**). These data indicated impaired glucose metabolism and mitochondrial function in B cells due to the absence of insulin signaling, which may contribute to the dysregulation in differentiation, class-switching, and function of B cells.

The memory response is a cornerstone of long-term immunity and effective vaccination. I next utilized an OVA/CFA/IFA-induced prime/boost protocol to test if B cell-intrinsic IR regulates B cell-mediated memory responses, thereby impacting vaccine efficiency. As shown, B cell-intrinsic IR impaired the memory response to OVA/IFA secondary immunization by impairing the re-entry of MBCs into the GC and the rapid differentiation of plasma cells from MBCs (**Figure 4.8**). However, the specific mechanisms remain unknown. One of the possible reasons is related to the maintenance of MBCs. There are several factors needed to ensure their survival, functionality, and readiness to respond to future infections. For example, cytokines including IL-4 and IL-21, as well as B cell-activating factor (BAFF), are crucial for the long-term survival of MBCs<sup>238-241</sup>. Moreover, low-level or periodic re-exposure to the antigen, and periodic interaction with FDCs can both help maintain MBCs by providing necessary stimulation without full-blown activation. Transcription factors and signaling pathways, including B cell lymphoma (Bcl)-2 family proteins, Bcl-6, and Paired Box 5 (Pax5), are also involved in maintaining the identity and function of MBCs<sup>242-246</sup>. Last but not least, MBCs have the ability to undergo low-level homeostatic proliferation, which helps maintain their numbers over time without exhausting the pool<sup>247</sup>. The maintenance of MBCs is a complex process that has the potential to be regulated by insulin signaling. Thus, future

experiments will focus on the impact of insulin signaling on the maintenance and functionality of MBCs during memory responses.

In addition to modulating the efficiency of vaccination, IR has also been reported to increase mortality after infection. Thus, I also tested whether B cell-intrinsic IR affects B cell-mediated anti-viral immunity. By using an H1N1/PR8 influenza infection model in WT and B cell-specific InsR-deficient mice, I observed that B cell-intrinsic IR increased the disease severity after infection (**Figure 4.9**). To further investigate the mechanisms underlying the impairment in anti-viral immunity in B cell-specific InsR-deficient mice, I next measured the changes in antibody levels in sera and BALs, as well as H1N1/PR8 influenza virus-induced GC reactions. As shown, similar to OVA/CFA immunization model, B cell-intrinsic IR altered the antibody production and impaired the GC reactions respond to H1N1/PR8 influenza virus infection (**Figure 4.10-4.11**). The impairment in GC reactions under this setting may be associated with the loss of help from CD4<sup>+</sup> T cells and T<sub>FH</sub> cells (**Figure 4.12-4.13**).

I also tested the effect of B cell-intrinsic IR on immune dominant T cell responses within the context of H1N1/PR8 influenza virus infection. One of the interesting observations is that B cell-specific InsR-deficient mice showed a decrease in the frequency and number of GC B cells in both spleens and mLNs on day 14 post-PR8/H1N1 influenza virus infection. However, the frequency and number of antigen-specific CD8<sup>+</sup> T cells showed no difference in all tissues on day 14 post-infection, and the decrease in the frequency and number of antigen-specific CD4<sup>+</sup> T cells only showed in the spleens. The reasons causing such a difference may be associated with the difference in the time required for T cell activation and GC maturation. The activation of T cells generally occurs within a few days following antigen recognition<sup>248</sup>. The recognition of specific antigens by T cells happens within minutes to hours, while the activation and proliferation typically start within 24-48 hours and activated T cells start to perform their effector function by day 5-7<sup>248</sup>. However, the formation and maturation of GC is a much longer process, which needs around 14 days to finish the maturation phase and become more organized<sup>249, 250</sup>. Therefore, optimal time points for

assessing the GC response may be too long for assessments on T cells. Thus, I measured the influenza-specific CD4<sup>+</sup> and CD8<sup>+</sup> T cells in all tissues on day 8 post-influenza virus infection. I observed a significant decrease in the frequency of influenza-specific CD4<sup>+</sup> and CD8<sup>+</sup> T cells in the mLNs on day 8 post-infection (**Figure 4.12 D-E, Figure 4.14 D-E**). Moreover, the frequency of influenza-specific CD8<sup>+</sup> T cells also showed a decrease in the lungs on day 8 post-infection (**Figure 4.14 D-E**). Thus, T cell defects precede GC defects, suggesting that IR in B cells also dampen their function as APCs to induce T cell activation and effector differentiation.

Taken together, I reported that DIO induced IR and B cell-intrinsic IR both impaired the B cell antibody production and GC reaction during the OVA/CFA-induced primary immune response. Moreover, B cell-intrinsic IR impaired B cell-mediated memory responses during a secondary challenge with the same antigen. In the context of influenza virus infection, B cell-intrinsic IR impaired B cell-mediated anti-viral immunity by altering antibody production, impairing GC reactions, and impairing immune dominant T cell responses. All data in this chapter suggest that immunomodulation targeting B cell IR may improve the efficiency of vaccines and reduce mortality upon virus infection in obese individuals as well as individuals with IR.

#### **4.4 Contributions**

The H1N1/PR8 virus was generously provided by the Dr. Kevin Kane (Department of Medical Microbiology and Immunology, University of Alberta). The PCR and gel electrophoresis used for confirming the genotypes of mice were all completed by Dr. Masoud Akbari. The euthanasia of influenza-infected mice and tissue processing were completed with the help of Megan Lee and Kevin Chu. All other experiments mentioned in this chapter were completed by me.

## Chapter 5: Discussion

### 5.1 Conclusion

In this thesis, I explored the impact of insulin signaling and IR on B cell activation, metabolism, and function within the context of OVA/CFA/IFA immunization and H1N1/PR8 influenza virus infection. Using the DIO mouse model and mouse model with InsR ablation in B cells, I measured B cell activation, antibody production, GC reaction, and metabolism, as well as changes in the helper signals from T cells after exposure to OVA proteins or H1N1/PR8 virus. My results suggested that IR impaired B cell-mediated immune responses against vaccine and virus infection by reducing helper signals from T cells and regulating B cell metabolism.

#### *5.1.1 The impact of insulin signaling and IR on B cell activation and metabolism*

Previously, we and others have described that all development stages of B cells express *Insr*. According to the preliminary Western blot data from our lab (Unpublished data), insulin stimulation induced the activation of insulin signaling in B cells, and DIO impaired the insulin signaling in B cells, which all have been confirmed by Phospho-flow analysis in this thesis (**Figure 3.1, 3.3**). IR is associated with metabolic disturbances and chronic inflammation, which can directly or indirectly affect immune function. However, existing studies have not shown clear evidence linking the IR directly to impaired B cell development and function. Using a mouse model with B cell-specific InsR ablation, our lab previously demonstrated that B cell-intrinsic IR had no impact on the proportions of B cell precursors in the BM, suggesting IR had no impact on B cell development. However, the modulation of Insulin signaling and IR on B cell activation remains unexplored.

Upon encountering antigens, B cells rapidly proliferate and activate, followed by the energy-consuming blasting, and differentiate into effector cells. All these processes are metabolically regulated by the coordinated actions of mTORC1 and mTORC2 downstream of BCR and CD40

signaling<sup>251, 252</sup>. mTORC1 and mTORC2 are also downstream of insulin signaling. Based on preliminary data, I hypothesized that insulin signaling plays an important role in modulating B cell activation by regulating metabolism. Using a mouse model with B cell-specific InsR ablation, I observed insulin stimulation and B cell-intrinsic IR both had no effect on the expression level of co-stimulatory molecules and MHC class II in LPS- or CpG-stimulated B cells (**Figure 3.4-3.6**). Interestingly, Seahorse metabolic flux data showed that insulin stimulation, DIO-induced IR, and B cell-intrinsic IR all had the capacity to regulate the aerobic glucose metabolism and mitochondrial respiration in LPS- or CpG-stimulated B cells (**Figure 3.7-3.12**). These data together suggested that insulin signaling regulated B cell metabolism, but this process did not alter B cell activation *in vitro*. This observation contradicts my hypothesis.

To explain the discrepancy between the hypothesis and experimental results, I envision several alternative possibilities. Firstly, B cells may utilize alternative metabolic pathways to maintain activation despite regulated metabolism. For example, even though the glycolysis and OXPHOS pathways are all impaired, they may increase FAO to generate necessary energy, which was not measured in this thesis and will be the next step for this project. Moreover, the signaling pathways responsible for B cell activation are robust and can often compensate for metabolic changes. Activation through receptors such as the TLRs can still propagate effectively even if metabolic pathways are altered. It has already been reported that there is a crosstalk between TLRs and PI3K/AKT signaling pathways which are important for the activation of B cells<sup>253</sup>. Lastly, the regulation of metabolism may occur over a different timescale compared with activation. Activation could be a rapid process, whereas the regulation of metabolism may happen more gradually, allowing B cells to adjust without immediate effects on activation. For all the experiments in this thesis, B cells were stimulated using a high concentration of activating agents for 48 hours, which may make the effects of insulin signaling or IR. Thus, future experiments will consider stimulating the cells using activating agents with or without insulin for shorter or longer time and using a titration of activating agents. Additionally, in this thesis, only the expression levels of co-stimulatory molecules and MHC class II were used as indicators of B cell activation, future

experiments will also focus on the proliferation, cytokine production, and associated transcription factor expression of B cells.

### **5.1.2 The role of IR on B cell-mediated adaptive immunity elicited by vaccine and infection**

B cells contribute significantly to adaptive immunity elicited by vaccination and infection<sup>131-133</sup>, and insulin signaling has been demonstrated to occupy an important position in mediating cell function. Therefore, I hypothesized that B cell-intrinsic IR impairs B cell-mediated immune response against vaccines and viral infections, thereby, decreasing the efficiency of vaccination and increasing the mortality following viral infection.

By using a DIO mouse model and OVA/CFA immunization, I observed that DIO induced IR impaired the antibody production and GC reaction of B cells in response to primary immunization (**Figure 4.1-4.2**). Considering the difference between systemic IR and B cell-intrinsic IR, I next used a mouse model with InsR ablation in B cells to investigate the effect of B cell-intrinsic IR on B cell-mediated immune responses during the OVA/CFA primary immunization. Consistent with my hypothesis, B cell-intrinsic IR impaired the antibody production and GC reaction of B cells during the OVA/CFA primary immunization, which may result from the defect in help from antigen-specific CD4<sup>+</sup> T cell and T<sub>FH</sub> cells as well as metabolism regulation (**Figure 4.3-4.6**). B cell-mediated memory responses are important for vaccination strategies. By using an OVA/CFA/IFA-induced prime/boost mouse model, I tested the effect of B cell-intrinsic IR on B cell-mediated memory responses and observed a negative regulation of B cell-intrinsic IR on the antibody production by B cells, the GC re-entry of MBCs, and rapid differentiation of plasma cells from MBCs (**Figure 4.7-4.8**). However, the mechanisms by which B cell-intrinsic IR affects B cell-mediated memory responses are unclear. One of the possible reasons is that B cell-intrinsic IR impairs the maintenance, migration, and reactivation speed of MBCs, which need further investigation.

Regarding the impact of B cell-intrinsic IR on B cell-mediated anti-viral immunity, I utilized an intranasal H1N1/PR8 influenza virus infection model and observed that B cell-intrinsic IR impaired the antibody production and GC reaction of B cells, further increasing the disease severity (**Figure 4.9-4.11**). Similar to the results from the OVA/CFA-induced immunization model, the impairment in GC reaction within the context of influenza virus infection may result from the defect in help from antigen-specific CD4<sup>+</sup> T cells and T<sub>FH</sub> cells (**Figure 4.12-4.13**). Moreover, B cell-intrinsic IR impaired the function of B cells to modulate other immune cells such as T cells, since the percentage of antigen-specific CD8<sup>+</sup> T cells and the cytokine production of T cells showed a decrease in B cell-specific InsR-deficient mice after influenza virus infection (**Figure 4.14-4.16**). These data suggest that B cell-intrinsic IR may impair its antigen presentation function, leading to the dysregulation of cognate T cells upon an influenza virus infection. Besides, B cells can produce a large number of cytokines, including pro-inflammatory cytokines, contributing to chronic inflammation conditions and recruiting immune cells to infiltrate into the infected sites and function to clear the virus, which can be impaired by B cell-intrinsic IR, and further experiments are needed to assess this possibility.

One of the major differences between the OVA/CFA/IFA immunization model and the H1N1/PR8 influenza virus infection model is the mouse strain used. I used B cell-specific InsR-deficient mice triggered by *mb1* promoter for OVA/CFA/IFA immunization mode. Meanwhile, the B cell-specific InsR-deficient mice triggered by *CD19* promoter were used for the H1N1/PR8 influenza virus infection model. These two mouse models were used for both experiments at the beginning. However, a difference was observed between them. Specifically, these two models exhibited similar results in OVA/CFA/IFA immunization experiments, while *mb1*-triggered mice showed higher mortality rates after infection with influenza virus and hindered the progress of the experiments. It may be associated with the deletion of InsR at a very early stage of B cell development and indicates a potential research direction.

As mentioned above, both insulin signaling and BCR signaling activate the downstream cascades through mTOR, which is an essential metabolic sensor involved in multiple aspects of B cell metabolism and function. The resetting of mTOR may restore the functional capacity of B cells with IR. Metformin is a commonly prescribed medication for T2D and has been demonstrated to exert effects by indirectly inhibiting mTOR through activation of the AMPK<sup>254</sup>. Moreover, metformin has been showed to improve influenza vaccine response in T2D patients<sup>255</sup>. Thus, this project will further use metformin as a model drug to investigate whether IR-linked B cell dysfunction can be reversed by resetting mTOR.

## **5.2 Significance**

Obesity is accompanied by impaired adaptive immunity and predisposes to IR, and B cells contribute significantly to adaptive immunity. This thesis aims to establish mechanistic connections between IR and B cell function. The data generated suggested that the impairment in insulin signaling in B cells could be used to explain the reduced effectiveness of vaccines and the increased severity of respiratory infections in individuals with IR. Ultimately, targeting insulin signaling in B cells could pave the way for novel vaccine adjuvant strategies to enhance protective immunity in populations affected by obesity-associated IR.

## Reference

1. Haase, C., Schnecke, V. & Eriksen, K. in European Congress on Obesity, Vol. 28 2019-2001 (2019).
2. Klein, S., Gastaldelli, A., Yki-Järvinen, H. & Scherer, P.E. Why does obesity cause diabetes? *Cell Metab* **34**, 11-20 (2022).
3. Paich, H.A. *et al.* Overweight and obese adult humans have a defective cellular immune response to pandemic H1N1 influenza A virus. *Obesity (Silver Spring)* **21**, 2377-2386 (2013).
4. Cortes-Telles, A., Ortiz-Farias, D.L., Pou-Aguilar, Y.N., Almeida-de-la-Cruz, L. & Perez-Padilla, J.R. Clinical impact of obesity on respiratory diseases: A real-life study. *Lung India* **38**, 321-325 (2021).
5. Van Gaal, L.F., Mertens, I.L. & De Block, C.E. Mechanisms linking obesity with cardiovascular disease. *Nature* **444**, 875-880 (2006).
6. Ritchie, S.A. & Connell, J.M. The link between abdominal obesity, metabolic syndrome and cardiovascular disease. *Nutr Metab Cardiovasc Dis* **17**, 319-326 (2007).
7. Akil, L. & Ahmad, H.A. Relationships between obesity and cardiovascular diseases in four southern states and Colorado. *J Health Care Poor Underserved* **22**, 61-72 (2011).
8. Kenchaiah, S. *et al.* Body mass index and prognosis in patients with chronic heart failure: insights from the Candesartan in Heart failure: Assessment of Reduction in Mortality and morbidity (CHARM) program. *Circulation* **116**, 627-636 (2007).
9. Romero-Corral, A., Caples, S.M., Lopez-Jimenez, F. & Somers, V.K. Interactions between obesity and obstructive sleep apnea: implications for treatment. *Chest* **137**, 711-719 (2010).
10. Durán, J., Esnaola, S., Rubio, R. & Iztueta, A. Obstructive sleep apnea-hypopnea and related clinical features in a population-based sample of subjects aged 30 to 70 yr. *Am J Respir Crit Care Med* **163**, 685-689 (2001).
11. Peppard, P.E., Young, T., Palta, M., Dempsey, J. & Skatrud, J. Longitudinal study of moderate weight change and sleep-disordered breathing. *Jama* **284**, 3015-3021 (2000).

12. Mitchell, A.B. *et al.* Obesity increases risk of ischemic stroke in young adults. *Stroke* **46**, 1690-1692 (2015).
  13. Rexrode, K.M. *et al.* A prospective study of body mass index, weight change, and risk of stroke in women. *Jama* **277**, 1539-1545 (1997).
  14. Ni Mhurchu, C., Rodgers, A., Pan, W.H., Gu, D.F. & Woodward, M. Body mass index and cardiovascular disease in the Asia-Pacific Region: an overview of 33 cohorts involving 310 000 participants. *Int J Epidemiol* **33**, 751-758 (2004).
  15. Kurth, T. *et al.* Body mass index and the risk of stroke in men. *Arch Intern Med* **162**, 2557-2562 (2002).
  16. Pati, S., Irfan, W., Jameel, A., Ahmed, S. & Shahid, R.K. Obesity and Cancer: A Current Overview of Epidemiology, Pathogenesis, Outcomes, and Management. *Cancers (Basel)* **15** (2023).
  17. Wondmkun, Y.T. Obesity, Insulin Resistance, and Type 2 Diabetes: Associations and Therapeutic Implications. *Diabetes Metab Syndr Obes* **13**, 3611-3616 (2020).
  18. Kahn, B.B. & Flier, J.S. Obesity and insulin resistance. *J Clin Invest* **106**, 473-481 (2000).
  19. Qatanani, M. & Lazar, M.A. Mechanisms of obesity-associated insulin resistance: many choices on the menu. *Genes Dev* **21**, 1443-1455 (2007).
  20. Jiang, J. *et al.* Relationship of obesity to adipose tissue insulin resistance. *BMJ Open Diabetes Res Care* **8** (2020).
  21. Blüher, M. Obesity: global epidemiology and pathogenesis. *Nat Rev Endocrinol* **15**, 288-298 (2019).
  22. Purnell, J.Q. Definitions, Classification, and Epidemiology of Obesity, in *Endotext*. (eds. K.R. Feingold *et al.*) (MDText.com, Inc.
- Copyright © 2000-2024, MDText.com, Inc., South Dartmouth (MA); 2000).
23. WHO (2024).
  24. Serra-Majem, L. & Bautista-Castaño, I. Etiology of obesity: two "key issues" and other emerging factors. *Nutr Hosp* **28 Suppl 5**, 32-43 (2013).

25. Pigeyre, M., Yazdi, F.T., Kaur, Y. & Meyre, D. Recent progress in genetics, epigenetics and metagenomics unveils the pathophysiology of human obesity. *Clin Sci (Lond)* **130**, 943-986 (2016).
26. Monteiro, R. & Azevedo, I. Chronic Inflammation in Obesity and the Metabolic Syndrome. *Mediators of Inflammation* **2010**, 289645 (2010).
27. Khanna, D., Khanna, S., Khanna, P., Kahar, P. & Patel, B.M. Obesity: A Chronic Low-Grade Inflammation and Its Markers. *Cureus* **14**, e22711 (2022).
28. Verboven, K. *et al.* Abdominal subcutaneous and visceral adipocyte size, lipolysis and inflammation relate to insulin resistance in male obese humans. *Scientific Reports* **8**, 4677 (2018).
29. Mraz, M. & Haluzik, M. The role of adipose tissue immune cells in obesity and low-grade inflammation. *J Endocrinol* **222**, R113-127 (2014).
30. Ghazarian, M., Luck, H., Revelo, X., Winer, S. & Winer, D. Immunopathology of Adipose Tissue during Metabolic Syndrome. *Turk patoloji dergisi* **31 Suppl 1**, 172-180 (2015).
31. Atawia, R.T., Bunch, K.L., Toque, H.A., Caldwell, R.B. & Caldwell, R.W. Mechanisms of obesity-induced metabolic and vascular dysfunctions. *Front Biosci (Landmark Ed)* **24**, 890-934 (2019).
32. Kershaw, E.E. & Flier, J.S. Adipose tissue as an endocrine organ. *J Clin Endocrinol Metab* **89**, 2548-2556 (2004).
33. Choe, S.S., Huh, J.Y., Hwang, I.J., Kim, J.I. & Kim, J.B. Adipose Tissue Remodeling: Its Role in Energy Metabolism and Metabolic Disorders. *Front Endocrinol (Lausanne)* **7**, 30 (2016).
34. Frontini, A. & Cinti, S. Distribution and development of brown adipocytes in the murine and human adipose organ. *Cell Metab* **11**, 253-256 (2010).
35. Rosen, E.D. & Spiegelman, B.M. What we talk about when we talk about fat. *Cell* **156**, 20-44 (2014).

36. Fedorenko, A., Lishko, P.V. & Kirichok, Y. Mechanism of fatty-acid-dependent UCP1 uncoupling in brown fat mitochondria. *Cell* **151**, 400-413 (2012).
37. Ricquier, D. Uncoupling protein 1 of brown adipocytes, the only uncoupler: a historical perspective. *Front Endocrinol (Lausanne)* **2**, 85 (2011).
38. Bond, L.M., Burhans, M.S. & Ntambi, J.M. Uncoupling protein-1 deficiency promotes brown adipose tissue inflammation and ER stress. *PLoS One* **13**, e0205726 (2018).
39. Leitner, B.P. *et al.* Mapping of human brown adipose tissue in lean and obese young men. *Proc Natl Acad Sci U S A* **114**, 8649-8654 (2017).
40. Kulterer, O.C. *et al.* Brown Adipose Tissue Prevalence Is Lower in Obesity but Its Metabolic Activity Is Intact. *Front Endocrinol (Lausanne)* **13**, 858417 (2022).
41. Herz, C.T. *et al.* Active Brown Adipose Tissue is Associated With a Healthier Metabolic Phenotype in Obesity. *Diabetes* (2021).
42. Jurado-Fasoli, L. *et al.* Adults with metabolically healthy overweight or obesity present more brown adipose tissue and higher thermogenesis than their metabolically unhealthy counterparts. *EBioMedicine* **100**, 104948 (2024).
43. Liu, X., Zhang, Z., Song, Y., Xie, H. & Dong, M. An update on brown adipose tissue and obesity intervention: Function, regulation and therapeutic implications. *Front Endocrinol (Lausanne)* **13**, 1065263 (2022).
44. Iacobini, C., Vitale, M., Haxhi, J., Menini, S. & Pugliese, G. Impaired Remodeling of White Adipose Tissue in Obesity and Aging: From Defective Adipogenesis to Adipose Organ Dysfunction. *Cells* **13** (2024).
45. Chait, A. & den Hartigh, L.J. Adipose Tissue Distribution, Inflammation and Its Metabolic Consequences, Including Diabetes and Cardiovascular Disease. *Front Cardiovasc Med* **7**, 22 (2020).
46. Kirichenko, T.V. *et al.* The Role of Adipokines in Inflammatory Mechanisms of Obesity. *Int J Mol Sci* **23** (2022).

47. Luong, Q., Huang, J. & Lee, K.Y. Deciphering White Adipose Tissue Heterogeneity. *Biology (Basel)* **8** (2019).
48. Ibrahim, M.M. Subcutaneous and visceral adipose tissue: structural and functional differences. *Obes Rev* **11**, 11-18 (2010).
49. Kovsan, J. *et al.* Altered autophagy in human adipose tissues in obesity. *J Clin Endocrinol Metab* **96**, E268-277 (2011).
50. Hardy, O.T. *et al.* Body mass index-independent inflammation in omental adipose tissue associated with insulin resistance in morbid obesity. *Surg Obes Relat Dis* **7**, 60-67 (2011).
51. Martyniak, K. & Masternak, M.M. Changes in adipose tissue cellular composition during obesity and aging as a cause of metabolic dysregulation. *Exp Gerontol* **94**, 59-63 (2017).
52. Blaszcak, A.M., Jalilvand, A. & Hsueh, W.A. Adipocytes, Innate Immunity and Obesity: A Mini-Review. *Front Immunol* **12**, 650768 (2021).
53. Weisberg, S.P. *et al.* Obesity is associated with macrophage accumulation in adipose tissue. *J Clin Invest* **112**, 1796-1808 (2003).
54. Harman-Boehm, I. *et al.* Macrophage infiltration into omental versus subcutaneous fat across different populations: effect of regional adiposity and the comorbidities of obesity. *J Clin Endocrinol Metab* **92**, 2240-2247 (2007).
55. Chawla, A., Nguyen, K.D. & Goh, Y.P. Macrophage-mediated inflammation in metabolic disease. *Nat Rev Immunol* **11**, 738-749 (2011).
56. Lumeng, C.N., Deyoung, S.M., Bodzin, J.L. & Saltiel, A.R. Increased inflammatory properties of adipose tissue macrophages recruited during diet-induced obesity. *Diabetes* **56**, 16-23 (2007).
57. Lumeng, C.N., DelProposto, J.B., Westcott, D.J. & Saltiel, A.R. Phenotypic switching of adipose tissue macrophages with obesity is generated by spatiotemporal differences in macrophage subtypes. *Diabetes* **57**, 3239-3246 (2008).
58. Patsouris, D. *et al.* Ablation of CD11c-positive cells normalizes insulin sensitivity in obese insulin resistant animals. *Cell Metab* **8**, 301-309 (2008).

59. Lumeng, C.N., Bodzin, J.L. & Saltiel, A.R. Obesity induces a phenotypic switch in adipose tissue macrophage polarization. *J Clin Invest* **117**, 175-184 (2007).
60. Sallusto, F. & Lanzavecchia, A. The instructive role of dendritic cells on T-cell responses. *Arthritis Research & Therapy* **4**, S127 (2002).
61. Lee, B.C. & Lee, J. Cellular and molecular players in adipose tissue inflammation in the development of obesity-induced insulin resistance. *Biochim Biophys Acta* **1842**, 446-462 (2014).
62. Bertola, A. *et al.* Identification of adipose tissue dendritic cells correlated with obesity-associated insulin-resistance and inducing Th17 responses in mice and patients. *Diabetes* **61**, 2238-2247 (2012).
63. Bajaj, M. & Ibrahim, S. Resistance of the Body to Infection: I. Leukocytes, Granulocytes, the Monocyte-Macrophage System, and Inflammation, 594-608 (2005).
64. Galli, S.J. *et al.* Mast cells as "tunable" effector and immunoregulatory cells: recent advances. *Annu Rev Immunol* **23**, 749-786 (2005).
65. Liu, J. *et al.* Genetic deficiency and pharmacological stabilization of mast cells reduce diet-induced obesity and diabetes in mice. *Nat Med* **15**, 940-945 (2009).
66. Yabut, J.M. *et al.* Genetic deletion of mast cell serotonin synthesis prevents the development of obesity and insulin resistance. *Nature Communications* **11**, 463 (2020).
67. Fine, N., Tasevski, N., McCulloch, C.A., Tenenbaum, H.C. & Glogauer, M. The Neutrophil: Constant Defender and First Responder. *Front Immunol* **11**, 571085 (2020).
68. Elgazar-Carmon, V., Rudich, A., Hadad, N. & Levy, R. Neutrophils transiently infiltrate intra-abdominal fat early in the course of high-fat feeding. *J Lipid Res* **49**, 1894-1903 (2008).
69. Nijhuis, J. *et al.* Neutrophil activation in morbid obesity, chronic activation of acute inflammation. *Obesity (Silver Spring)* **17**, 2014-2018 (2009).
70. Talukdar, S. *et al.* Neutrophils mediate insulin resistance in mice fed a high-fat diet through secreted elastase. *Nat Med* **18**, 1407-1412 (2012).

71. Spencer, L.A. & Weller, P.F. Eosinophils and Th2 immunity: contemporary insights. *Immunol Cell Biol* **88**, 250-256 (2010).
72. LI, T. *et al.* 2006-P: The Role of Adipose Tissue-Resident Eosinophils in Adipocyte Metabolism and Whole-Body Energy Homeostasis. *Diabetes* **68** (2019).
73. Wu, D. *et al.* Eosinophils sustain adipose alternatively activated macrophages associated with glucose homeostasis. *Science* **332**, 243-247 (2011).
74. Abel, A.M., Yang, C., Thakar, M.S. & Malarkannan, S. Natural Killer Cells: Development, Maturation, and Clinical Utilization. *Front Immunol* **9**, 1869 (2018).
75. Wensveen, F.M. *et al.* NK cells link obesity-induced adipose stress to inflammation and insulin resistance. *Nat Immunol* **16**, 376-385 (2015).
76. Lee, B.C. *et al.* Adipose Natural Killer Cells Regulate Adipose Tissue Macrophages to Promote Insulin Resistance in Obesity. *Cell Metab* **23**, 685-698 (2016).
77. Winer, S. *et al.* Normalization of obesity-associated insulin resistance through immunotherapy. *Nature Medicine* **15**, 921-929 (2009).
78. Wu, H. *et al.* T-cell accumulation and regulated on activation, normal T cell expressed and secreted upregulation in adipose tissue in obesity. *Circulation* **115**, 1029-1038 (2007).
79. Winer, S. *et al.* Normalization of obesity-associated insulin resistance through immunotherapy. *Nat Med* **15**, 921-929 (2009).
80. Rocha, V.Z. *et al.* Interferon-gamma, a Th1 cytokine, regulates fat inflammation: a role for adaptive immunity in obesity. *Circ Res* **103**, 467-476 (2008).
81. Winer, S. *et al.* Obesity predisposes to Th17 bias. *Eur J Immunol* **39**, 2629-2635 (2009).
82. McLaughlin, T. *et al.* T-cell profile in adipose tissue is associated with insulin resistance and systemic inflammation in humans. *Arterioscler Thromb Vasc Biol* **34**, 2637-2643 (2014).
83. Feuerer, M. *et al.* Lean, but not obese, fat is enriched for a unique population of regulatory T cells that affect metabolic parameters. *Nat Med* **15**, 930-939 (2009).

84. Yang, H. *et al.* Obesity Increases the Production of Proinflammatory Mediators from Adipose Tissue T Cells and Compromises TCR Repertoire Diversity: Implications for Systemic Inflammation and Insulin Resistance. *Journal of immunology (Baltimore, Md. : 1950)* **185**, 1836-1845 (2010).
85. Nishimura, S. *et al.* CD8<sup>+</sup> effector T cells contribute to macrophage recruitment and adipose tissue inflammation in obesity. *Nat Med* **15**, 914-920 (2009).
86. Hiéronimus, L. & Huaux, F. B-1 cells in immunotoxicology: Mechanisms underlying their response to chemicals and particles. *Front Toxicol* **5**, 960861 (2023).
87. Chekol Abebe, E. *et al.* The Role of Regulatory B Cells in Health and Diseases: A Systemic Review. *J Inflamm Res* **14**, 75-84 (2021).
88. Nishimura, S. *et al.* Adipose Natural Regulatory B Cells Negatively Control Adipose Tissue Inflammation. *Cell Metab* **18**, 759-766 (2013).
89. Winer, D.A. *et al.* B cells promote insulin resistance through modulation of T cells and production of pathogenic IgG antibodies. *Nat Med* **17**, 610-617 (2011).
90. DeFuria, J. *et al.* B cells promote inflammation in obesity and type 2 diabetes through regulation of T-cell function and an inflammatory cytokine profile. *Proc Natl Acad Sci U S A* **110**, 5133-5138 (2013).
91. Wilcox, G. Insulin and insulin resistance. *Clin Biochem Rev* **26**, 19-39 (2005).
92. Cefalu, W.T. Insulin resistance: cellular and clinical concepts. *Exp Biol Med (Maywood)* **226**, 13-26 (2001).
93. Rahman, M.S. *et al.* Role of Insulin in Health and Disease: An Update. *Int J Mol Sci* **22** (2021).
94. Haeusler, R.A., McGraw, T.E. & Accili, D. Biochemical and cellular properties of insulin receptor signalling. *Nat Rev Mol Cell Biol* **19**, 31-44 (2018).
95. Manning, B.D. & Cantley, L.C. AKT/PKB Signaling: Navigating Downstream. *Cell* **129**, 1261-1274 (2007).

96. Yoon, M.-S. & Choi, C.S. The role of amino acid-induced mammalian target of rapamycin complex 1(mTORC1) signaling in insulin resistance. *Experimental & Molecular Medicine* **48**, e201-e201 (2016).
97. Yoon, M.S. The Role of Mammalian Target of Rapamycin (mTOR) in Insulin Signaling. *Nutrients* **9** (2017).
98. Minton, K. Role for mTORC2 in insulin resistance. *Nature Reviews Molecular Cell Biology* **14**, 67-67 (2013).
99. Yadav, A., Jyoti, P., Jain, S.K. & Bhattacharjee, J. Correlation of adiponectin and leptin with insulin resistance: a pilot study in healthy north Indian population. *Indian J Clin Biochem* **26**, 193-196 (2011).
100. Izquierdo, A.G., Crujeiras, A.B., Casanueva, F.F. & Carreira, M.C. Leptin, Obesity, and Leptin Resistance: Where Are We 25 Years Later? *Nutrients* **11** (2019).
101. Evans, M.C., Lord, R.A. & Anderson, G.M. Multiple Leptin Signalling Pathways in the Control of Metabolism and Fertility: A Means to Different Ends? *Int J Mol Sci* **22** (2021).
102. Genchi, V.A. *et al.* Impaired Leptin Signalling in Obesity: Is Leptin a New Thermolipokine? *Int J Mol Sci* **22** (2021).
103. Filippidis, G. *et al.* Resistin serum levels are increased but not correlated with insulin resistance in chronic hemodialysis patients. *Blood Purif* **23**, 421-428 (2005).
104. Lee, J.H. *et al.* Circulating resistin levels are not associated with obesity or insulin resistance in humans and are not regulated by fasting or leptin administration: cross-sectional and interventional studies in normal, insulin-resistant, and diabetic subjects. *J Clin Endocrinol Metab* **88**, 4848-4856 (2003).
105. Arita, Y. *et al.* Paradoxical decrease of an adipose-specific protein, adiponectin, in obesity. 1999. *Biochem Biophys Res Commun* **425**, 560-564 (2012).
106. Hotta, K. *et al.* Plasma concentrations of a novel, adipose-specific protein, adiponectin, in type 2 diabetic patients. *Arterioscler Thromb Vasc Biol* **20**, 1595-1599 (2000).

107. Yang, Q. *et al.* Serum retinol binding protein 4 contributes to insulin resistance in obesity and type 2 diabetes. *Nature* **436**, 356-362 (2005).
108. Fan, J. & Hu, J. Retinol binding protein 4 and type 2 diabetes: from insulin resistance to pancreatic  $\beta$ -cell function. *Endocrine* (2024).
109. Wu, H. & Ballantyne, C.M. Metabolic Inflammation and Insulin Resistance in Obesity. *Circulation Research* **126**, 1549-1564 (2020).
110. Moller, D.E. Potential role of TNF-alpha in the pathogenesis of insulin resistance and type 2 diabetes. *Trends Endocrinol Metab* **11**, 212-217 (2000).
111. Chen, L., Chen, R., Wang, H. & Liang, F. Mechanisms Linking Inflammation to Insulin Resistance. *Int J Endocrinol* **2015**, 508409 (2015).
112. Hotamisligil, G.S. *et al.* IRS-1-mediated inhibition of insulin receptor tyrosine kinase activity in TNF-alpha- and obesity-induced insulin resistance. *Science* **271**, 665-668 (1996).
113. Čolak, E. & Pap, D. The role of oxidative stress in the development of obesity and obesity-related metabolic disorders. *J Med Biochem* **40**, 1-9 (2021).
114. Fonseca-Alaniz, M.H., Takada, J., Alonso-Vale, M.I. & Lima, F.B. Adipose tissue as an endocrine organ: from theory to practice. *J Pediatr (Rio J)* **83**, S192-203 (2007).
115. Stephens, J.M., Lee, J. & Pilch, P.F. Tumor Necrosis Factor- $\alpha$ -induced Insulin Resistance in 3T3-L1 Adipocytes Is Accompanied by a Loss of Insulin Receptor Substrate-1 and GLUT4 Expression without a Loss of Insulin Receptor-mediated Signal Transduction\*. *Journal of Biological Chemistry* **272**, 971-976 (1997).
116. Hotamisligil, G.S., Murray, D.L., Choy, L.N. & Spiegelman, B.M. Tumor necrosis factor alpha inhibits signaling from the insulin receptor. *Proc Natl Acad Sci U S A* **91**, 4854-4858 (1994).
117. Jager, J., Grémeaux, T., Cormont, M., Le Marchand-Brustel, Y. & Tanti, J.F. Interleukin-1beta-induced insulin resistance in adipocytes through down-regulation of insulin receptor substrate-1 expression. *Endocrinology* **148**, 241-251 (2007).

118. Yu, H. *et al.* Tumor necrosis factor- $\alpha$  reduces adiponectin production by decreasing transcriptional activity of peroxisome proliferator-activated receptor- $\gamma$  in calf adipocytes. *Journal of Dairy Science* **106**, 5182-5195 (2023).
119. Nguyen, M.T. *et al.* JNK and tumor necrosis factor-alpha mediate free fatty acid-induced insulin resistance in 3T3-L1 adipocytes. *J Biol Chem* **280**, 35361-35371 (2005).
120. Gurzov, E.N., Stanley, W.J., Pappas, E.G., Thomas, H.E. & Gough, D.J. The JAK/STAT pathway in obesity and diabetes. *Febs j* **283**, 3002-3015 (2016).
121. Trøseid, M. *et al.* Plasma lipopolysaccharide is closely associated with glycemic control and abdominal obesity: evidence from bariatric surgery. *Diabetes Care* **36**, 3627-3632 (2013).
122. Hersoug, L.-G., Møller, P. & Loft, S. Role of microbiota-derived lipopolysaccharide in adipose tissue inflammation, adipocyte size and pyroptosis during obesity. *Nutrition Research Reviews* **31**, 153-163 (2018).
123. Liang, H., Hussey, S.E., Sanchez-Avila, A., Tantiwong, P. & Musi, N. Effect of lipopolysaccharide on inflammation and insulin action in human muscle. *PLoS One* **8**, e63983 (2013).
124. Xin, Y. *et al.* Elevated free fatty acid level is associated with insulin-resistant state in nondiabetic Chinese people. *Diabetes Metab Syndr Obes* **12**, 139-147 (2019).
125. Karpe, F., Dickmann, J.R. & Frayn, K.N. Fatty Acids, Obesity, and Insulin Resistance: Time for a Reevaluation. *Diabetes* **60**, 2441-2449 (2011).
126. Petersen, K.F. & Shulman, G.I. Etiology of Insulin Resistance. *The American Journal of Medicine* **119**, S10-S16 (2006).
127. Gordon, E.S. LIPID METABOLISM, DIABETES MELLITUS, AND OBESITY. *Adv Intern Med* **12**, 66-102 (1964).
128. Brand, M.D., Orr, A.L., Perevoshchikova, I.V. & Quinlan, C.L. The role of mitochondrial function and cellular bioenergetics in ageing and disease. *Br J Dermatol* **169 Suppl 2**, 1-8 (2013).

129. Bournat, J.C. & Brown, C.W. Mitochondrial dysfunction in obesity. *Curr Opin Endocrinol Diabetes Obes* **17**, 446-452 (2010).
130. Petersen, K.F., Dufour, S., Befroy, D., Garcia, R. & Shulman, G.I. Impaired Mitochondrial Activity in the Insulin-Resistant Offspring of Patients with Type 2 Diabetes. *New England Journal of Medicine* **350**, 664-671 (2004).
131. Sheridan, P.A. *et al.* Obesity is associated with impaired immune response to influenza vaccination in humans. *Int J Obes (Lond)* **36**, 1072-1077 (2012).
132. Pozzilli, P. *et al.* The immune response to influenza vaccination in diabetic patients. *Diabetologia* **29**, 850-854 (1986).
133. Rojas-Osornio, S.A., Cruz-Hernández, T.R., Drago-Serrano, M.E. & Campos-Rodríguez, R. Immunity to influenza: Impact of obesity. *Obes Res Clin Pract* **13**, 419-429 (2019).
134. Karlsson, E.A., Sheridan, P.A. & Beck, M.A. Diet-induced obesity impairs the T cell memory response to influenza virus infection. *J Immunol* **184**, 3127-3133 (2010).
135. Milner, J.J. *et al.* Diet-induced obese mice exhibit altered heterologous immunity during a secondary 2009 pandemic H1N1 infection. *J Immunol* **191**, 2474-2485 (2013).
136. Milner, J.J. *et al.* Obesity Increases Mortality and Modulates the Lung Metabolome during Pandemic H1N1 Influenza Virus Infection in Mice. *J Immunol* **194**, 4846-4859 (2015).
137. Selvaraj, U.M., Poinatte, K., Torres, V., Ortega, S.B. & Stowe, A.M. Heterogeneity of B Cell Functions in Stroke-Related Risk, Prevention, Injury, and Repair. *Neurotherapeutics* **13**, 729-747 (2016).
138. von Büdingen, H.C., Palanichamy, A., Lehmann-Horn, K., Michel, B.A. & Zamvil, S.S. Update on the autoimmune pathology of multiple sclerosis: B-cells as disease-drivers and therapeutic targets. *Eur Neurol* **73**, 238-246 (2015).
139. LeBien, T.W. & Tedder, T.F. B lymphocytes: how they develop and function. *Blood* **112**, 1570-1580 (2008).

140. Ramírez, J., Lukin, K. & Hagman, J. From hematopoietic progenitors to B cells: mechanisms of lineage restriction and commitment. *Curr Opin Immunol* **22**, 177-184 (2010).
141. Dias, S., Silva, H., Jr., Cumano, A. & Vieira, P. Interleukin-7 is necessary to maintain the B cell potential in common lymphoid progenitors. *J Exp Med* **201**, 971-979 (2005).
142. Vilagos, B. *et al.* Essential role of EBF1 in the generation and function of distinct mature B cell types. *J Exp Med* **209**, 775-792 (2012).
143. Györy, I. *et al.* Transcription factor Ebf1 regulates differentiation stage-specific signaling, proliferation, and survival of B cells. *Genes Dev* **26**, 668-682 (2012).
144. Tonegawa, S. Somatic generation of antibody diversity. *Nature* **302**, 575-581 (1983).
145. Nemazee, D. Mechanisms of central tolerance for B cells. *Nature Reviews Immunology* **17**, 281-294 (2017).
146. Tsubata, T. B-cell tolerance and autoimmunity. *F1000Res* **6**, 391 (2017).
147. Geisberger, R., Lamers, M. & Achatz, G. The riddle of the dual expression of IgM and IgD. *Immunology* **118**, 429-437 (2006).
148. Cerutti, A., Cols, M. & Puga, I. Marginal zone B cells: virtues of innate-like antibody-producing lymphocytes. *Nat Rev Immunol* **13**, 118-132 (2013).
149. Nera, K.-P., Kyläniemi, M.K. & Lassila, O. Regulation of B Cell to Plasma Cell Transition within the Follicular B Cell Response. *Scandinavian Journal of Immunology* **82**, 225-234 (2015).
150. Nutt, S.L. & Tarlinton, D.M. Germinal center B and follicular helper T cells: siblings, cousins or just good friends? *Nat Immunol* **12**, 472-477 (2011).
151. Klein, U. & Dalla-Favera, R. Germinal centres: role in B-cell physiology and malignancy. *Nature Reviews Immunology* **8**, 22-33 (2008).
152. Nakagawa, R. & Calado, D.P. Positive Selection in the Light Zone of Germinal Centers. *Front Immunol* **12**, 661678 (2021).

153. Guan, S.G. & Qi, A.S. Contributions of memory B cells to secondary immune response. *Bull Math Biol* **57**, 713-731 (1995).
154. Pollard, A.J. & Bijker, E.M. A guide to vaccinology: from basic principles to new developments. *Nature Reviews Immunology* **21**, 83-100 (2021).
155. Akkaya, M., Kwak, K. & Pierce, S.K. B cell memory: building two walls of protection against pathogens. *Nature Reviews Immunology* **20**, 229-238 (2020).
156. Cyster, J.G. & Allen, C.D.C. B Cell Responses: Cell Interaction Dynamics and Decisions. *Cell* **177**, 524-540 (2019).
157. Dogan, I. *et al.* Multiple layers of B cell memory with different effector functions. *Nature Immunology* **10**, 1292-1299 (2009).
158. Weisel, F. & Shlomchik, M. Memory B Cells of Mice and Humans. *Annual Review of Immunology* **35**, 255-284 (2017).
159. Forthall, D.N. Functions of Antibodies. *Microbiol Spectr* **2**, 1-17 (2014).
160. Lu, L.L., Suscovich, T.J., Fortune, S.M. & Alter, G. Beyond binding: antibody effector functions in infectious diseases. *Nature Reviews Immunology* **18**, 46-61 (2018).
161. Schroeder, H.W., Jr. & Cavacini, L. Structure and function of immunoglobulins. *J Allergy Clin Immunol* **125**, S41-52 (2010).
162. Lund, F.E. Cytokine-producing B lymphocytes-key regulators of immunity. *Curr Opin Immunol* **20**, 332-338 (2008).
163. Riedel, R. *et al.* Discrete populations of isotype-switched memory B lymphocytes are maintained in murine spleen and bone marrow. *Nature Communications* **11**, 2570 (2020).
164. Rastogi, I. *et al.* Role of B cells as antigen presenting cells. *Front Immunol* **13**, 954936 (2022).
165. Chen, X. & Jensen, P.E. The role of B lymphocytes as antigen-presenting cells. *Arch Immunol Ther Exp (Warsz)* **56**, 77-83 (2008).
166. Raposo, G. *et al.* B lymphocytes secrete antigen-presenting vesicles. *J Exp Med* **183**, 1161-1172 (1996).

167. Hong, S. *et al.* B Cells Are the Dominant Antigen-Presenting Cells that Activate Naive CD4(+) T Cells upon Immunization with a Virus-Derived Nanoparticle Antigen. *Immunity* **49**, 695-708.e694 (2018).
168. Hua, Z. & Hou, B. The role of B cell antigen presentation in the initiation of CD4+ T cell response. *Immunol Rev* **296**, 24-35 (2020).
169. Mathieu, M. *et al.* CD40-activated B cells can efficiently prime antigen-specific naïve CD8+ T cells to generate effector but not memory T cells. *PLoS One* **7**, e30139 (2012).
170. Akkaya, M. & Pierce, S.K. From zero to sixty and back to zero again: the metabolic life of B cells. *Curr Opin Immunol* **57**, 1-7 (2019).
171. Simon-Molas, H., Del Prete, R. & Kabanova, A. Glucose metabolism in B cell malignancies: a focus on glycolysis branching pathways. *Molecular Oncology* **18**, 1777-1794 (2024).
172. Nsiah-Sefaa, A. & McKenzie, M. Combined defects in oxidative phosphorylation and fatty acid  $\beta$ -oxidation in mitochondrial disease. *Biosci Rep* **36** (2016).
173. Jin, L., Alesi, G.N. & Kang, S. Glutaminolysis as a target for cancer therapy. *Oncogene* **35**, 3619-3625 (2016).
174. Martínez-Reyes, I. & Chandel, N.S. Mitochondrial TCA cycle metabolites control physiology and disease. *Nature Communications* **11**, 102 (2020).
175. Tessaro, F.H.G., Ayala, T.S., Nolasco, E.L., Bella, L.M. & Martins, J.O. Insulin Influences LPS-Induced TNF- $\alpha$  and IL-6 Release Through Distinct Pathways in Mouse Macrophages from Different Compartments. *Cell Physiol Biochem* **42**, 2093-2104 (2017).
176. Ratter, J.M. *et al.* Insulin acutely activates metabolism of primary human monocytes and promotes a proinflammatory phenotype. *J Leukoc Biol* **110**, 885-891 (2021).
177. Lu, H. *et al.* Insulin enhances dendritic cell maturation and scavenger receptor-mediated uptake of oxidised low-density lipoprotein. *J Diabetes Complications* **29**, 465-471 (2015).
178. Himpe, E., Degallier, C., Coppens, A. & Kooijman, R. Insulin-like growth factor-1 delays Fas-mediated apoptosis in human neutrophils through the phosphatidylinositol-3 kinase pathway. *J Endocrinol* **199**, 69-80 (2008).

179. Han, J.M., Patterson, S.J., Speck, M., Ehses, J.A. & Levings, M.K. Insulin inhibits IL-10-mediated regulatory T cell function: implications for obesity. *J Immunol* **192**, 623-629 (2014).
180. Tsai, S. *et al.* Insulin Receptor-Mediated Stimulation Boosts T Cell Immunity during Inflammation and Infection. *Cell Metab* **28**, 922-934.e924 (2018).
181. Baudler, S. *et al.* Insulin-like growth factor-1 controls type 2 T cell-independent B cell response. *J Immunol* **174**, 5516-5525 (2005).
182. Posner, B.I. Insulin Signalling: The Inside Story. *Can J Diabetes* **41**, 108-113 (2017).
183. Savova, M.S., Mihaylova, L.V., Tews, D., Wabitsch, M. & Georgiev, M.I. Targeting PI3K/AKT signaling pathway in obesity. *Biomedicine & Pharmacotherapy* **159**, 114244 (2023).
184. Saxton, R.A. & Sabatini, D.M. mTOR Signaling in Growth, Metabolism, and Disease. *Cell* **168**, 960-976 (2017).
185. Keating, R. *et al.* The kinase mTOR modulates the antibody response to provide cross-protective immunity to lethal infection with influenza virus. *Nat Immunol* **14**, 1266-1276 (2013).
186. Iwata, T.N., Ramírez-Komo, J.A., Park, H. & Iritani, B.M. Control of B lymphocyte development and functions by the mTOR signaling pathways. *Cytokine Growth Factor Rev* **35**, 47-62 (2017).
187. Iwata, T.N. *et al.* Conditional Disruption of Raptor Reveals an Essential Role for mTORC1 in B Cell Development, Survival, and Metabolism. *J Immunol* **197**, 2250-2260 (2016).
188. Raybuck, A.L. *et al.* B Cell - Intrinsic mTORC1 Promotes Germinal Center-Defining Transcription Factor Gene Expression, Somatic Hypermutation, and Memory B Cell Generation in Humoral Immunity. *The Journal of Immunology* **200**, 2627-2639 (2018).
189. de Baat, A., Trinh, B., Ellingsgaard, H. & Donath, M.Y. Physiological role of cytokines in the regulation of mammalian metabolism. *Trends in Immunology* **44**, 613-627 (2023).

190. Cain, D., Kondo, M., Chen, H. & Kelsoe, G. Effects of acute and chronic inflammation on B-cell development and differentiation. *J Invest Dermatol* **129**, 266-277 (2009).
191. Kawai, T., Autieri, M.V. & Scalia, R. Adipose tissue inflammation and metabolic dysfunction in obesity. *Am J Physiol Cell Physiol* **320**, C375-c391 (2021).
192. Gaborit, B. *et al.* Early humoral response to COVID-19 vaccination in patients living with obesity and diabetes in France. The COVPOP OBEDIAB study with results from the ANRS0001S COV-POPART cohort. *Metabolism* **142**, 155412 (2023).
193. O'Meara, T.R. *et al.* Reduced SARS-CoV-2 mRNA vaccine immunogenicity and protection in mice with diet-induced obesity and insulin resistance. *J Allergy Clin Immunol* **152**, 1107-1120.e1106 (2023).
194. Jayawardena, R., Jeyakumar, D.T., Misra, A., Hills, A.P. & Ranasinghe, P. Obesity: A potential risk factor for infection and mortality in the current COVID-19 epidemic. *Diabetes Metab Syndr* **14**, 2199-2203 (2020).
195. Hobeika, E. *et al.* Testing gene function early in the B cell lineage in mb1-cre mice. *Proc Natl Acad Sci U S A* **103**, 13789-13794 (2006).
196. Ai, W., Li, H., Song, N., Li, L. & Chen, H. Optimal method to stimulate cytokine production and its use in immunotoxicity assessment. *Int J Environ Res Public Health* **10**, 3834-3842 (2013).
197. Hossain, M., Giver, C.R. & Waller, N. Short-Term Ionomycin Exposure Activates Naive Murine T-Cells and Induces a Rapid Phenotypic Shift to Memory T-Cell Status: Potential for Use as a Method To Reduce GvHD Activity of Allogeneic T-Cells. *Blood* **110**, 2182-2182 (2007).
198. Fujiwara, T., Oda, K., Yokota, S., Takatsuki, A. & Ikehara, Y. Brefeldin A causes disassembly of the Golgi complex and accumulation of secretory proteins in the endoplasmic reticulum. *J Biol Chem* **263**, 18545-18552 (1988).
199. Traba, J., Miozzo, P., Akkaya, B., Pierce, S.K. & Akkaya, M. An Optimized Protocol to Analyze Glycolysis and Mitochondrial Respiration in Lymphocytes. *J Vis Exp* (2016).

200. Venkataraman, C., Shankar, G., Sen, G. & Bondada, S. Bacterial lipopolysaccharide induced B cell activation is mediated via a phosphatidylinositol 3-kinase dependent signaling pathway. *Immunol Lett* **69**, 233-238 (1999).
201. Klinman, D.M. Immunotherapeutic uses of CpG oligodeoxynucleotides. *Nature Reviews Immunology* **4**, 249-259 (2004).
202. Petersen, M.C. & Shulman, G.I. Mechanisms of Insulin Action and Insulin Resistance. *Physiol Rev* **98**, 2133-2223 (2018).
203. Lee, D.Y. *et al.* Review of the Current Research on Fetal Bovine Serum and the Development of Cultured Meat. *Food Sci Anim Resour* **42**, 775-799 (2022).
204. An, W. *et al.* Activation of the insulin receptor by insulin-like growth factor 2. *Nature Communications* **15**, 2609 (2024).
205. Brand, M.D. & Nicholls, D.G. Assessing mitochondrial dysfunction in cells. *Biochem J* **435**, 297-312 (2011).
206. Hill, B.G. *et al.* Integration of cellular bioenergetics with mitochondrial quality control and autophagy. *Biol Chem* **393**, 1485-1512 (2012).
207. Adeva-Andany, M.M. *et al.* Interferon Upregulation Associates with Insulin Resistance in Humans. *Curr Diabetes Rev* (2024).
208. Wada, T. *et al.* Both type I and II IFN induce insulin resistance by inducing different isoforms of SOCS expression in 3T3-L1 adipocytes. *American Journal of Physiology-Endocrinology and Metabolism* **300**, E1112-E1123 (2011).
209. Huang, L.Y., Chiu, C.J., Hsing, C.H. & Hsu, Y.H. Interferon Family Cytokines in Obesity and Insulin Sensitivity. *Cells* **11** (2022).
210. Chen, S. *et al.* The role of B cells in COVID-19 infection and vaccination. *Front Immunol* **13**, 988536 (2022).
211. Pettini, E., Medaglini, D. & Ciabattini, A. Profiling the B cell immune response elicited by vaccination against the respiratory virus SARS-CoV-2. *Front Immunol* **13**, 1058748 (2022).

212. Lapuente, D., Winkler, T.H. & Tenbusch, M. B-cell and antibody responses to SARS-CoV-2: infection, vaccination, and hybrid immunity. *Cellular & Molecular Immunology* **21**, 144-158 (2024).
213. Govender, N., Khaliq, O.P., Moodley, J. & Naicker, T. Insulin resistance in COVID-19 and diabetes. *Prim Care Diabetes* **15**, 629-634 (2021).
214. Sagun, G. *et al.* The relation between insulin resistance and lung function: a cross sectional study. *BMC Pulm Med* **15**, 139 (2015).
215. Al-Sayyar, A. *et al.* Respiratory Tract Infections in Diabetes - Lessons From Tuberculosis and Influenza to Guide Understanding of COVID-19 Severity. *Front Endocrinol (Lausanne)* **13**, 919223 (2022).
216. Park, Y.H. *et al.* Insulin resistance mediates high-fat diet-induced pulmonary fibrosis and airway hyperresponsiveness through the TGF- $\beta$ 1 pathway. *Experimental & Molecular Medicine* **51**, 1-12 (2019).
217. Ohno, M. *et al.* Influenza virus infection affects insulin signaling, fatty acid-metabolizing enzyme expressions, and the tricarboxylic acid cycle in mice. *Scientific Reports* **10**, 10879 (2020).
218. Luzi, L. & Radaelli, M.G. Influenza and obesity: its odd relationship and the lessons for COVID-19 pandemic. *Acta Diabetologica* **57**, 759-764 (2020).
219. Hui, J.M. *et al.* Insulin resistance is associated with chronic hepatitis C virus infection and fibrosis progression [corrected]. *Gastroenterology* **125**, 1695-1704 (2003).
220. Pedro, M.N. *et al.* Insulin Resistance in HIV-Patients: Causes and Consequences. *Front Endocrinol (Lausanne)* **9**, 514 (2018).
221. Tiozzo, E. *et al.* The Relationship between HIV Duration, Insulin Resistance and Diabetes Risk. *Int J Environ Res Public Health* **18** (2021).
222. Høgh, J. *et al.* Insulin resistance in people living with HIV is associated with exposure to thymidine analogues and/or didanosine and prior immunodeficiency. *BMC Infectious Diseases* **22**, 503 (2022).

223. Wang, X., Chen, J., Cao, Z. & Yu, X. Associations between human cytomegalovirus infection and type 2 diabetes mellitus: a systematic review and meta-analysis. *BMJ Open* **13**, e071934 (2023).
224. Hjelmæsæth, J. *et al.* Asymptomatic cytomegalovirus infection is associated with increased risk of new-onset diabetes mellitus and impaired insulin release after renal transplantation. *Diabetologia* **47**, 1550-1556 (2004).
225. Singh, M. & O'Hagan, D.T. Recent advances in veterinary vaccine adjuvants. *International Journal for Parasitology* **33**, 469-478 (2003).
226. Fontes, J.A. *et al.* Complete Freund's adjuvant induces experimental autoimmune myocarditis by enhancing IL-6 production during initiation of the immune response. *Immun Inflamm Dis* **5**, 163-176 (2017).
227. Gould, H.J. & Sutton, B.J. IgE in allergy and asthma today. *Nature Reviews Immunology* **8**, 205-217 (2008).
228. Zhang, X. *et al.* IgE Contributes to Atherosclerosis and Obesity by Affecting Macrophage Polarization, Macrophage Protein Network, and Foam Cell Formation. *Arteriosclerosis, Thrombosis, and Vascular Biology* **40**, 597-610 (2020).
229. Lee, S.E., Baek, J.Y., Han, K. & Koh, E.H. Insulin Resistance Increases Serum Immunoglobulin E Sensitization in Premenopausal Women. *Diabetes Metab J* **45**, 175-182 (2021).
230. Liu, Y., Wang, X. & Liu, Y. Association of serum total IgE and allergen-specific IgE with insulin resistance in adolescents: an analysis of the NHANES database. *BMC Pediatrics* **24**, 332 (2024).
231. Kim, M.K. *et al.* House dust mite and Cockroach specific Immunoglobulin E sensitization is associated with diabetes mellitus in the adult Korean population. *Scientific Reports* **8**, 2614 (2018).

232. Dolovich, J., Schnatz, J.D., Reisman, R.E., Yagi, Y. & Arbesman, C.E. Insulin allergy and insulin resistance: Case report with immunologic studies. *Journal of Allergy* **46**, 127-137 (1970).
233. Wang, Z. *et al.* Immunoglobulin E and Mast Cell Proteases Are Potential Risk Factors of Human Pre-Diabetes and Diabetes Mellitus. *PLOS ONE* **6**, e28962 (2011).
234. Petersen, K.-G., Khalaf, A., Naithani, V., Gattner, H. & Kerp, L. IgE antibodies to insulin and related peptides, a result of insulin treatment? *Diabetes Research and Clinical Practice* **7**, 41-46 (1989).
235. Engeroff, P. & Vogel, M. The role of CD23 in the regulation of allergic responses. *Allergy* **76**, 1981-1989 (2021).
236. Deenick, E.K., Hasbold, J. & Hodgkin, P.D. Decision criteria for resolving isotype switching conflicts by B cells. *Eur J Immunol* **35**, 2949-2955 (2005).
237. Olatunde, A.C., Hale, J.S. & Lamb, T.J. Cytokine-skewed Tfh cells: functional consequences for B cell help. *Trends Immunol* **42**, 536-550 (2021).
238. Johnson, J.T. *et al.* CD4 T Cell-Derived IL-21 Is Critical for Sustaining Plasmodium Infection-Induced Germinal Center Responses and Promoting the Selection of Memory B Cells with Recall Potential. *The Journal of Immunology* **212**, 1467-1478 (2024).
239. Chakma, C.R. & Good-Jacobson, K.L. Requirements of IL-4 during the Generation of B Cell Memory. *The Journal of Immunology* **210**, 1853-1860 (2023).
240. Rasheed, M.A. *et al.* Interleukin-21 is a critical cytokine for the generation of virus-specific long-lived plasma cells. *J Virol* **87**, 7737-7746 (2013).
241. Rankin, A. *et al.* IL-21 Receptor Is Critical for the Development of Memory B Cell Responses. *Journal of immunology (Baltimore, Md. : 1950)* **186**, 667-674 (2011).
242. Nuñez, G., Hockenbery, D., McDonnell, T.J., Sorensen, C.M. & Korsmeyer, S.J. Bcl-2 maintains B cell memory. *Nature* **353**, 71-73 (1991).

243. del Pino Molina, L. *et al.* Defective Bcl-2 expression in memory B cells from common variable immunodeficiency patients. *Clinical & Experimental Immunology* **203**, 341-350 (2021).
244. Laidlaw, B.J. & Cyster, J.G. Transcriptional regulation of memory B cell differentiation. *Nature Reviews Immunology* **21**, 209-220 (2021).
245. Kuo, T.C. *et al.* Repression of BCL-6 is required for the formation of human memory B cells in vitro. *J Exp Med* **204**, 819-830 (2007).
246. Syeda, M.Z., Hong, T., Huang, C., Huang, W. & Mu, Q. B cell memory: from generation to reactivation: a multipronged defense wall against pathogens. *Cell Death Discovery* **10**, 117 (2024).
247. Luckey, C.J. *et al.* Memory T and memory B cells share a transcriptional program of self-renewal with long-term hematopoietic stem cells. *Proc Natl Acad Sci U S A* **103**, 3304-3309 (2006).
248. Iezzi, G., Karjalainen, K. & Lanzavecchia, A. The duration of antigenic stimulation determines the fate of naive and effector T cells. *Immunity* **8**, 89-95 (1998).
249. De Silva, N.S. & Klein, U. Dynamics of B cells in germinal centres. *Nat Rev Immunol* **15**, 137-148 (2015).
250. Lee, J.H. *et al.* Long-primed germinal centres with enduring affinity maturation and clonal migration. *Nature* **609**, 998-1004 (2022).
251. Yam-Puc, J.C., Zhang, L., Zhang, Y. & Toellner, K.M. Role of B-cell receptors for B-cell development and antigen-induced differentiation. *Fl000Res* **7**, 429 (2018).
252. Elgueta, R. *et al.* Molecular mechanism and function of CD40/CD40L engagement in the immune system. *Immunol Rev* **229**, 152-172 (2009).
253. Kao, R., Browder, W. & Li, C. Cellular Cardiomyoplasty: What Have We Learned? *Asian cardiovascular & thoracic annals* **17**, 89-101 (2009).
254. Howell, J.J. *et al.* Metformin Inhibits Hepatic mTORC1 Signaling via Dose-Dependent Mechanisms Involving AMPK and the TSC Complex. *Cell Metab* **25**, 463-471 (2017).

255. Diaz, A. *et al.* Metformin improves in vivo and in vitro B cell function in individuals with obesity and Type-2 Diabetes. *Vaccine* **35**, 2694-2700 (2017).